UNIVERSIDADE FEDERAL DE MINAS GERAIS
Instituto de Ciências Exatas
Programa de Pós-Graduação em Ciência da Computação

Rodrigo Otávio Gonçalves Chaves

Oriented quantum walks

Belo Horizonte
2023

Rodrigo Otávio Gonçalves Chaves

Oriented quantum walks

Versão Final

Tese apresentada ao Programa de Pós-Graduação em Ciência da Computação da Universidade Federal de Minas Gerais, como requisito parcial à obtenção do título de Doutor em Ciência da Computação.

Orientador: Gabriel de Morais Coutinho
Coorientador: Bruno de Oliveira Chagas

Belo Horizonte
2023

Rodrigo Otávio Gonçalves Chaves

Passeios Quânticos em grafos orientados

Final Version

Dissertation presented to the Graduate Program in Computer Science of the Federal University of Minas Gerais in partial fulfillment of the requirements for the degree of Doctor in Computer Science.

Advisor: Gabriel de Morais Coutinho
Co-Advisor: Bruno de Oliveira Chagas

Belo Horizonte
2023

Chaves, Rodrigo Otávio Gonçalves.

C512o Oriented quantum walks [recurso eletrônico] / Rodrigo Otávio Gonçalves Chaves – 2023.
1 recurso online (93 f. il, color.) : pdf.

Orientador: Gabriel de Morais Coutinho.
Coorientador: Bruno de Oliveira Chagas.

Tese (Doutorado) - Universidade Federal de Minas Gerais, Instituto de Ciências Exatas, Departamento de Ciências da Computação.
Referências: f.87-93

1. Computação – Teses. 2. Teoria dos grafos – Teses. 3. Computação quântica – Teses. 4. Informação quântica – Teses. 5. Passeios quânticos – Teses. I. Coutinho, Gabriel de Morais. II. Chagas, Bruno de Oliveira. III. Universidade Federal de Minas Gerais, Instituto de Ciências Exatas, Departamento de Computação. IV.Título.

CDU 519.6*71(043)

Ficha catalográfica elaborada pela bibliotecária Irenquer Vismeg Lucas Cruz
CRB 6/819 - Universidade Federal de Minas Gerais - ICEx

UNIVERSIDADE FEDERAL DE MINAS GERAIS
INSTITUTO DE CIÊNCIAS EXATAS
DEPARTAMENTO DE CIÊNCIA DA COMPUTAÇÃO
PROGRAMA DE PÓS-GRADUAÇÃO EM CIÊNCIA DA COMPUTAÇÃO

FOLHA DE APROVAÇÃO

ORIENTED QUANTUM WALKS

RODRIGO OTÁVIO GONÇALVES CHAVES

Tese defendida e aprovada pela banca examinadora constituída pelos Senhores:

Prof. Gabriel de Morais Coutinho - Orientador
Departamento de Ciência da Computação - UFMG

Dr. Bruno de Oliveira Chagas - Coorientador
Mastercad

Prof. Vinicius Fernandes dos Santos
Departamento de Ciência da Computação - UFMG

Prof. Guilherme de Castro Mendes Gomes
Departamento de Ciência da Computação - UFMG

Prof. Franklin de Lima Marquezino
Engenharia de Sistemas e Ciência da Computação - COPPE - UFRJ

Prof. Wandearley da Silva Dias
Instituto de Física - UFAL

Belo Horizonte, 26 de abril de 2023.

Documento assinado eletronicamente por **Gabriel de Morais Coutinho**, **Professor do Magistério Superior**, em 10/05/2023, às 13:16, conforme horário oficial de Brasília, com fundamento no art. 5º do Decreto nº 10.543, de 13 de novembro de 2020.

Documento assinado eletronicamente por **Vinicius Fernandes dos Santos**, **Professor do Magistério Superior**, em 10/05/2023, às 14:20, conforme horário oficial de Brasília, com fundamento no art. 5º do Decreto nº 10.543, de 13 de novembro de 2020.

Documento assinado eletronicamente por **Guilherme de Castro Mendes Gomes**, **Professor do Magistério Superior**, em 16/05/2023, às 11:11, conforme horário oficial de Brasília, com fundamento no art. 5º do Decreto nº 10.543, de 13 de novembro de 2020.

Documento assinado eletronicamente por **Wandearley da Silva Dias**, **Usuário Externo**, em 29/05/2023, às 13:41, conforme horário oficial de Brasília, com fundamento no art. 5º do Decreto nº 10.543, de 13 de novembro de 2020.

Documento assinado eletronicamente por **Franklin de Lima Marquezino**, **Usuário Externo**, em 30/05/2023, às 22:36, conforme horário oficial de Brasília, com fundamento no art. 5º do Decreto nº 10.543, de 13 de novembro de 2020.

Documento assinado eletronicamente por **Bruno de Oliveira Chagas**, **Usuário Externo**, em 21/10/2024, às 12:52, conforme horário oficial de Brasília, com fundamento no art. 5º do Decreto nº 10.543, de 13 de novembro de 2020.

A autenticidade deste documento pode ser conferida no site https://sei.ufmg.br/sei/controlador_externo.php?acao=documento_conferir&id_orgao_acesso_externo=0, informando o código verificador **2251180** e o código CRC **09454DA3**.

Referência: Processo nº 23072.224271/2023-13 SEI nº 2251180

Acknowledgments

Agradeço a todos que se mostraram essenciais na conclusão desse objetivo. Primeiramente, ao incentivo da minha família na concretização desse sonho. Durante o percurso, diferentes tipos de apoio são necessários para se chegar na reta final desse grande objetivo e minha família sempre esteve presente em todos eles. Agradeço também aos excelentes orientadores que tive: Gabriel e Bruno. Sempre lutaram para que eu obtivesse as melhoras oportunidades e sempre se mostraram disponíveis em todas as dificuldades que encontrei. Até mesmo após ter postergado a escrita dessa tese o máximo que eu consegui.

Não menos importante são os amigos que se conquistam durante a jornada. Celebro todos os doteiros do Brasil que me permitiram xingá-los em momentos de frustração e, em especial, meus amigos André e Lucas. Apesar de eu não ter conseguido ensiná-los nada sobre como ser bons jogadores de Dota2, mantivemos uma rotina insalubre de jogatina que faria inveja em qualquer viciado em drogas. Não só de Dota2 vive o homem, então Daniel, João, Samuel, e Gus foram essenciais para desbravar a culinária de Belo Horizonte enquanto temas importantíssimos eram discutidos como o perfil de Tinder ideal.

A jornada numa nova área foi desafiadora, mas me deparei com pessoas incríveis no laboratório que me motivaram a dar o meu máximo para que eu tivesse perfis de excelência para almejar. Rafael, Juliana, e Matheus não são só mentes brilhantes, mas pessoas incríveis que, inquestionavelmente, obterão um sucesso tremendo em qualquer empreitada que colocarem sua mente e coração.

Lidar com a vida é também ter que lidar com fins e recomeços. Pessoas marcantes não se fazem mais presentes, mas não deixam de ter impacto inexplicável quando estiveram presentes. Mithyzi foi um presente que obtive durante a vida e que a distância não abalou a força que nos conecta. Se alguém se sentiu esquecido, me manda uma mensagem que eu dou um abraço e peço desculpas depois.

Resumo

Passeios quânticos surgiram como um proposta de expansão de passeios aleatórios para sistemas exclusivamente quânticos. Esse trabalho tem como objetivo demonstrar como implementar um passeio quânticos em computadores quânticos de maneira mais eficiente para certos tipos de grafos ao utilizar a versão truncada da tranformada de Fourier quântica. Também demonstraremos alguns resultados relacionados com a adição de pesos complexos nas aretas de grafos dentre eles como a dinâmica do passeio se altera para certos grafos como árvores e caminhos. Adicionalmente provaremos a existência de uma família de grafos que possuem vértices no qual é impossível encontrar o caminhante neles para qualquer tempo t do passeio. Provaremos a conexão desse fenômeno nessa família com a degenerescência dos autovalores do Hamiltoniano associado ao grafo o que nos permite trilhar um caminho para uma possível compreensão de uma formato geral para os tipos de grafo que exibem esse fenômeno.

Palavras-chave: passeios quânticos; informação quântica; teoria algébrica de grafos.

Abstract

Quantum walks were initially proposed as a natural expansion from random walks for quantum systems. The junction between graph theory and quantum information showed itself crucial to investigate and explain phenomena like state transfer and the velocity that information spreads in a quantum system described by a graph. show how to implement more efficient quantum walk time evolution in a quantum computer using a truncated version of the quantum Fourier transform. We will also show the addition of complex weights in the graph edges can change the dynamics of certain types of graphs like trees and paths and we compare those changes with the non-weighted cases. The addition of complex weights can create vertices with zero probability of finding a walker during any time t of the quantum walk, also called zero transfer, for certain graphs. In this work we present a family of graphs with zero transfer and we show that there is a connection of the phenomena with the degeneracy of the eigenvalues of the Hamiltonian which paves a way for a general understanding of the phenomena.

Keywords: quantum walks; quantum information; algebraic graph theory.

Contents

Chapter 1

Introduction

Suppose Gabriel had one too many at a conference dinner and has to walk back to his hotel. Every n meters he walks, there is a probability of turning an arbitrary angle and walking another n meters. Well, when will Gabriel reach his hotel? Random walks were first defined to answer a similar problem proposed by Pearson [57] in 1905. As a response, they were associated with random processes that occur in a succession of random steps in a mathematical space. Since conception, they have been used in a wide range of problems. From physics, in the mathematical model of Brownian motion [78], to the classification of web pages on the internet [37]. A quantum mechanical counterpart proposed by Aharonov *et al.* [94] resulted in two initial models: continuous-time quantum walk and discrete-time quantum walk. Clearly, from their names, the former has time as a continuous variable; meanwhile, time is discrete in the latter.

Quantum walks have many applications in the field of quantum computing and it is the main topic of many research papers in the literature. One of the first applications of quantum walks was the relation between Grover's search algorithm and discrete-time quantum walks [74]. As we will see, the coined model of discrete-time quantum walks uses a coin to estimate if the walker will jump from one vertex to another. The model can start with two coins: one for a marked vertex and another for all other vertices. In this way, discrete-time quantum walks have a natural way to implement Grover's algorithm for graphs and the algorithm showed a quadratic speedup compared to classical algorithms in hypercubes [71], square lattices [3], and the search for triangles in graphs [36]. Decision trees are an essential tool for operations research and machine learning [80] and a natural classical algorithm is to run a random walk, starting at the root, to find a marked vertex. Farhi and Gutmann found a family of graphs in which the quantum walk succeeds in polynomial time while its classical counterpart takes exponential time [33]. Childs *et al.* proved that it is possible to achieve universal computation using quantum walks [23]. Although it allowed the creation of a new theoretical architecture for quantum computers, no company created a quantum walk computer.

Another interest point when studying quantum walks is its information transport properties and the discrepancies compared with the classical counterpart. Likewise the algorithmic case, the quantum model shows an improvement in the hitting time [59, 58],

which is the time a walker takes to hit a marked vertex, with a quadratic speedup over the classical case. Continuous-time quantum walks, a model where time is continuous, can be applied in the context of state transfers. One of the most known results in quantum theory is the impossibility of constructing a quantum repeater by cloning. Hence it is still an open problem how to reliably transmit quantum information over long distances. State transfer tries to tackle this problem by transporting an arbitrary state between two vertices in a graph with high probability. The expectation was that the transfer would occur in continuous-time quantum walks with the right choice of Hamiltonian. Initially, state transfer in path graphs [64] was considered to lead to promising results, although not for undirected graphs. Then the concept was extended to other types of graphs [43] and it ushered a characterization of perfect state transfer, which occurs when the probability of transfering the state between vertices to be equal to one, for undirected graphs [25]. Despite all the knowledge about perfect state transfer in undirected graphs, a complete characterization for the oriented case and when the transfer probability is not one is still absent.

Another quantum walk phenomenon related to state transfer is zero transfer, defined by the impossibility of finding the walker on a given vertex of the graph at any time. One application of this phenomenon could be an indirect measure of the interaction between a quantum system and the environment [13]. Zero transfer is closely related to the addition of weights in a graph since it is impossible to occur in an undirected when only connected graphs are considered. However, it is not understood what properties the graph must have to be possible to observe zero transfer. This phenomenon is part of chiral quantum walks [96] or graphs with complex roots of unity as weights. They are also called unit gain graphs and there is an increased interest in order to understand how the information transport changes when compared to weightless graphs.

Despite the extensive literature on the subject, the interest for oriented graphs is quite recent. The introduction of imaginary weights of modulus one was essential to obtain new transport phenomena that would be inaccessible otherwise. This work aims to expand the knowledge related to four themes:

1. It is known that noisy quantum computers cannot efficiently simulate quantum walks due to the number of multi-controlled gates required. Is it possible to use algebraic graph theory to make the simulation less prone to errors in noisy quantum computers?

2. Are there graphs for which the addition of orientation does not change the quantum system's dynamics?

3. Even though the weights have modulus 1, can the addition of orientation be enough to change the velocity in which the information is spread through the graph?

4. Can algebraic graph theory explain known phenomena in the literature and offer new perspectives to phenomena closely related to the addition of orientation?

These four questions are the stepping stone of all the work presented here that culminated in interesting results. This work improves the current knowledge of quantum walks with roots of unity as weights and how information transport is affected by direction. It will be shown how complex weights do not change the quantum walk dynamics for trees and infinite path graphs for certain initial conditions. With the goal of generalizating zero transfer and pave the way to its complete characterization, we used old graph theorems to indicate the importance of degenerate eigenvalues for the occurrence of the phenomenon [76]. This was done in the hopes that zero transfer can be fully described in the future. Another result is the possibility of decomposing circulant graphs with Fourier matrices leading to an efficient way to implement them in NISQ computers using the Quantum Fourier Algorithm [77].

In Chapter 2, we will give the basics of quantum mechanics that will be necessary to the understanding of other chapters. We will see how to represent states in quantum mechanics, how to measure quantum states, and how to construct spaces of higher dimensions. Chapter 3 will be dedicated to classical and quantum walks, where it will be defined and it will be given the differences when dealing with discrete or continuous time. Also, state transfer will be determined and characterized for graphs without orientation. Following those definitions, it will be seen in Chapter 4 how the addition of orientation creates, in certain graphs, new phenomena like perfect state transfer and zero transfer for all time t.

Chapter 2

Basics of quantum mechanics

2.1 Introduction

Quantum mechanics was built on a set of postulates during the 20th century. Initially, it was created to explain a deviation in the emitted light of heated bodies, also referred to as black body radiation. Planck heuristically derived a formula for the observed spectrum of light by assuming that the changes in energy of an electrically charged oscillator are discrete and not continuous, as was previously thought. A lot of mathematical formalism and physics came from that breakthrough thought in the 1900s. The theory was tested through trial and error using experiments in solid-state physics as guidance to distinguish between what was wrong and what was right. Eventually, physicists arrived at the postulates that we will see in this chapter. They allowed us to understand superconductors, semiconductors, how to describe phase transitions, chemical reactions, and many other applications.

In the 1960s, the work of Gordon [44] and Helstrom [52] was crucial for the foundation of quantum information. While the former proposed a formulation of communication using quantum mechanics, the latter proposed strategies to distinguish between states of a quantum system. Those strategies allowed physicists to notice that one could get different kinds of results from the measurement of the system depending on which strategies were used. Then, quantum mechanical analogs to Shannon's work were created and, consequentially, a new research subfield. Quantum information followed quantum mechanics in its ascension in popularity due to its applicability: new cryptography protocols, teleportation, transference of information, and quantum computation.

The goal of this chapter is to give an introduction to the basics of quantum information that will be used later in this work and can be found in any graduate textbook [16, 63]. Throughout the chapter, we will use the bra-ket notation for vectors, unless stated otherwise. Also, we define the inner product for matrices M and N of size $n \times n$ as

$$\langle M, N \rangle = \mathrm{Tr}\big(M^T N\big). \tag{2.1}$$

2.2 State space

The first postulate of quantum mechanics goes as follows:

Postulate 1: Associated to any isolated physical system is a complex vector space with a defined inner product, also referred to as a Hilbert space ($\mathcal{H}$), known as the state space of the system. The space can have finite or infinite dimensions.

Obtaining the state space that best describes a system is, usually, not an easy task. We can notice that the postulate and quantum mechanics do not give a way to find that out. In spite of that, physicists were able to create a different number of rules to solve the problem. For example, quantum electrodynamics (QED) serves this purpose since it was created to explain interactions between light and atoms. Another example would be the Fock space and Fock states which are constantly being used in condensed matter physics and photonics.

Since we will be dealing with qubits, our state space is a two-dimensional complex space, $\mathbb{C}^2$. State vectors, or simply states, are one-dimesional subspaces, typically represented by unit vectors. Let $|0\rangle$ and $|1\rangle$ be the orthonormal basis for $\mathbb{C}^2$, then the most general state for the qubit will be given by

$$|\psi\rangle = \cos\frac{\theta}{2}|0\rangle + e^{i\phi}\sin\frac{\theta}{2}|1\rangle\,. \tag{2.2}$$

The similarities between bits and qubits are not only in name. While the former describes a classical system with two possible instances, the latter will do the same for all two-levels quantum systems. Since the usage of bits is so diverse, it is also considered a unit of information. Likewise, due to analogous characteristics, the qubit is also a unit of information for quantum systems. When dealing with bits, one must always represent the different states of the system by choosing one element in the set $\{0, 1\}$, while in quantum mechanics a state can be represented in infinitely many ways using $|0\rangle$ and $|1\rangle$ as the basis, as we saw in equation 2.2.

A natural question arises then: is it possible to get more than one bit of information from a quantum state? The quick answer is no. Later in this chapter, we will see how quantum measurements work and we will be able to get an intuition on the reason why it is impossible to get more than one bit of information. A more formal approach, known as Holevo's bound [11], will not be discussed here due to the necessity of explaining theories that are not within our scope. Nevertheless, there are indeed ways, through quantum mechanics, to communicate a certain number of bits of information using a smaller number of qubits. The superdense coding protocol [21] does just that, but it uses a resource exclusive to quantum mechanics referred to as entanglement. Later on, we will see what entanglement is with more precision.

Quantum systems evolve and this is described by the second postulate:

Postulate 2: The evolution of a closed system is described by a unitary transformation, i.e. there is an operator U that

$$|\psi(t)\rangle = U(t)\,|\psi(0)\rangle\,, \tag{2.3}$$

where $|\psi(0)\rangle$ is the initial state of the system.

When we are dealing with continuous-time transformations, there is a well-known way to find the matrix $U(t)$ through Schrödinger's equation:

$$i\hbar\frac{d\,|\psi(t)\rangle}{dt} = H\,|\psi(t)\rangle\,, \tag{2.4}$$

where H is a time-independent matrix that is referred to as the Hamiltonian of the system. The $\hbar$ is Planck's constant and from now on, we will use $\hbar = 1$ since the constant is only a scaling factor. A system is closed when it does not interact with any other system outside and energy is conserved. The Hamiltonian H gives the many possible transformations that energy goes through and that is why it plays a central role in Schrödinger's equation. In our case, we will not be concerned in that discussion of finding the physical description of the Hamiltonian for a particular physical system. Since our problems are always an abstraction that can be applied to numerous similar problems, the Hamiltonian will always be given as a starting point without trying to physically justify it.

The solution to equation 2.4 gives that our time evolution operator must be

$$U(t) = e^{-itH}. \tag{2.5}$$

Equation 2.5 elucidates an important characteristic of a Hamiltonian which is hermiticity to preserve unitarity of $U(t)$. Assuming from now on that our systems are finite-dimensional unless stated otherwise, Hermitian matrices have a spectral decomposition of H given by

$$H = \sum_n \lambda_n\,|\psi_n\rangle\langle\psi_n|\,, \tag{2.6}$$

where λ_n is the eigenvalue corresponding to the n-th eigenvector. Notice that the eigenspaces in the spectral decomposition in equation 2.6 are considered to be one dimensional, in other words, the matrix H has simple eigenvalues. Although physicists prefer to deal with cases like that, we will face eigenspaces of dimensions higher than one. The spectral decomposition remains the same, but we will have a rank-d projection matrix instead of a rank-1 projection.

The suitability of spectral decomposition in quantum mechanics is its relation to the application of functions in matrices. Let $f(x)$ be a function defined in terms of a power series, then, for Hermitian matrices, we have that

$$f(H) = \sum_n f(\lambda_n)\,|\psi_n\rangle\langle\psi_n|\,. \tag{2.7}$$

We now have an operator that describes the evolution in time of a quantum state and how it can be applied to our Hamiltonians. This will be used extensively throughout this work, in particular

$$e^{-itH} = \sum_n e^{-it\lambda_n} |\psi_n\rangle\langle\psi_n| \tag{2.8}$$

2.2.1 Density matrices

So far, we have explained quantum mechanics in the state vector formalism. Another alternative formulation is possible using density operators or density matrices. This new way of representing the state space makes some problems easier to solve while being mathematically equivalent to state vectors.

The qubit state is represented by a positive semidefinite matrix with trace one referred to as the density matrix. Let $|\psi\rangle$ be a state of the state space, then the density matrix ρ associated to $|\psi\rangle$ will be

$$\rho = |\psi\rangle\langle\psi| \,. \tag{2.9}$$

In this case, ρ is a rank-1 projector and it is referred to as a pure state. Suppose we have a particle that has a probability p_i of being prepared in any of its possible states, $\{|\psi\rangle_i\}$. However, we do not have the knowledge of which state the particle will have at the time of the measurement. Then, how do we describe the state of the particle right before measurement? While representing this would be an intricate problem using state vectors, the density matrix formalism offers a handy way to deal with it. The density operator for this system would be

$$\rho = \sum_i p_i |\psi_i\rangle\langle\psi_i| \,. \tag{2.10}$$

Here, ρ is not a rank-1 projector anymore, hence it is referred to as a mixed state. It is possible to show that a density matrix satisfies $\mathrm{Tr}(\rho^2) \leq 1$ with equality if and only if the state is pure, which is the usual criterion for checking the purity of density matrices.

In view of this new formalism, we can also transform the previous state vector of a qubit into a density matrix representation and we will get an interesting geometrical intuition while doing it. Let $\mathcal{H}$ be the real vector space of 2×2 Hermitian matrices and Ψ be an isomorphism such that $\Psi : \mathbb{R}^4 \to \mathcal{H}$ by acting as follows

$$v = \begin{pmatrix} w \\ x \\ y \\ z \end{pmatrix}, \tag{2.11}$$

then

$$\Psi(v) = \begin{pmatrix} w+z & x-iy \\ x+iy & w-z \end{pmatrix}. \tag{2.12}$$

If we set $\{e_i\}_{i=1}^4$ to be the canonical basis of $\mathbb{R}^4$, then this isomorphism gives matrices that are known as the Pauli matrices

$$I = \begin{pmatrix} 1 & 0 \\ 0 & 1 \end{pmatrix}, \qquad \sigma_x = \begin{pmatrix} 0 & 1 \\ 1 & 0 \end{pmatrix}, \qquad \sigma_y = \begin{pmatrix} 0 & -i \\ i & 0 \end{pmatrix}, \qquad \sigma_z = \begin{pmatrix} 1 & 0 \\ 0 & -1 \end{pmatrix}. \tag{2.13}$$

Pauli matrices can also be written as I, X, Y, and Z which is the usual notation for quantum computation. It is apparent that the Pauli matrices are linearly independent and that they are the basis for the space of 2×2 Hermitian matrices relative to our inner product of matrices. Before we move on, Define two matrices $P, Q \in \mathbb{R}^{n \times n}$, then the commutator of two matrices is defined as

$$[P, Q] = PQ - QP. \tag{2.14}$$

This is an important relation between matrices, since it is known that two matrices share the same set of basis vector if their commutator equals zero. For the Pauli matrices, their commutator relations is defined as $[\sigma_j, \sigma_k] = 2i\varepsilon_{jkl}\sigma_k$, where ε_{jkl} is the Levi-Civita symbol defined as

$$\varepsilon_{jkl} = \begin{cases} +1 & \text{if } (j,k,l) \text{ is } (1,2,3),\ (2,3,1), \text{ or } (3,1,2); \\ -1 & \text{if } (j,k,l) \text{ is } (3,2,1),\ (1,3,2), \text{ or } (2,1,3); \\ 0 & \text{if } j = k,\ k = l, \text{ or } l = j \end{cases}. \tag{2.15}$$

Suppose that our qubit state is $\rho = \Psi(v)$, then

$$\mathrm{Tr}(\rho) = \mathrm{Tr}(\Psi(v)) = 2w. \tag{2.16}$$

As a consequence, for ρ to be a valid density matrix $w = 1/2$. The density matrix ρ must also be positive semidefinite, so we get the following lemma

Lemma 2.0.1. *If ρ is a 2×2 Hermitian matrix, then it is positive semidefinite if, and only if,* $\mathrm{Tr}(\rho) \geq 0$ *and* $\det(\rho) \geq 0$.

Proof. If ρ is positive semidefinite, then all of its eigenvalues are non-negative. So, $\mathrm{Tr}(\rho)$ and $\det(\rho)$ are also non-negative. For the converse, if $\mathrm{Tr}(\rho) \geq 0$, then $w > 0$. The expression for $\det(\rho)$ will be given by

$$\det(\rho) = w^2 - x^2 - y^2 - z^2. \tag{2.17}$$

Then, if $\det(\rho) \geq 0$, $w^2 > z^2$ and the diagonal terms of ρ are non-negative. Hence, both the diagonal terms and the determinant of ρ are non-zero and it must be positive semidefinite. □

We can represent any state of a qubit, pure or mixed, in a three-dimensional space in $\mathbb{R}^3$ given by

$$\rho = \frac{I + \langle r, \vec{\sigma} \rangle}{2}, \tag{2.18}$$

where $\mathbf{r}$ is a vector inside a sphere of radius 1 and $\vec{\sigma} = (\sigma_x, \sigma_y, \sigma_z)$. The figure 2.1 is a geometric visualization of such a representation that is also referred to as the Bloch sphere. Points on the surface of the sphere are pure states while points inside are mixed states.

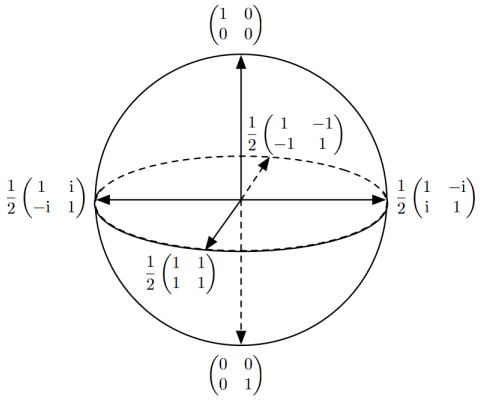

Figure 2.1: Figure representing the Bloch sphere and six pure states obtained from [39].

2.2.2 Composition of state spaces

We hear about improvements in quantum computers from IBM or Google and how the numbers of qubits in their quantum computers have improved from a certain number to a new threshold. Yet, we only managed to talk about $\mathbb{C}^2$ as state spaces, then how do we get state spaces of higher dimensions? To explain this, we encounter another postulate of quantum mechanics:

> **Postulate 3**: The state space of a composite physical system is the tensor product of the state spaces of each component. In other words, if we have n systems and the system i is prepared in the $|\psi_i\rangle$ state, then the joint state of the total system is $|\psi_1\rangle \otimes \cdots \otimes |\psi_i\rangle \otimes \cdots \otimes |\psi_n\rangle$.

Ergo, for a system with d qubits, the state space will be simply $(\mathbb{C}^2)^{\otimes d}$. This composition is the core of IBM's, Google's, or any other organization's quantum computer. Throughout this work we will consider, for simplicity, that $|\psi\rangle\,|\psi'\rangle$ or $|\psi\psi'\rangle$ equals $|\psi\rangle \otimes |\psi'\rangle$.

2.3 Measurement

Heretofore, we have discussed the mathematical intricacies of quantum mechanics and now we will see how it translates to physical experiments. The following postulate was created to define what can be observed in an experiment and it goes as follows:

> **Postulate 4**: The observables of a quantum system with a state space $\mathcal{H}$ are the self-adjoint operators acting on the system, that is, they correspond to Hermitian matrices.

This means that for every physical quantity, like position or momentum, we need a Hermitian operator associated with it.

Notice that the postulate does not give us a way to measure such quantities, but only how to mathematically represent them. First, the set of measurement operators $\{M_i\}$ is a finite set of elements where each one is a positive semidefinite matrix that acts on a finite-dimensional Hilbert space. They must obey the completeness relation

$$\sum_i M_i = I. \tag{2.19}$$

So to solve that problem, physicists came to the following postulate:

> **Postulate 5**: Quantum measurements are described by a set $\{M_m\}$ of measurement operators that act on the state space of the system being measured. The index m refers to possible measurement outcomes of the experiment. Let $|\psi\rangle$ be the state that the quantum system is prepared, then the probability that the result m occurs, $p(m)$, is given by the following rule
>
> $$p(m) = \langle\psi| M_m^\dagger M_m |\psi\rangle \tag{2.20}$$
>
> and the state of the system after the measurement is
>
> $$\frac{M_m |\psi\rangle}{\sqrt{\langle\psi| M_m^\dagger M_m |\psi\rangle}}. \tag{2.21}$$

There are two kinds of measurement operators: projective measurement and positive operator-valued measure (POVM). The former occurs when M_m is a rank-1 projection matrix for all m, i.e. $M_m M_n = \delta_{mn} M_m$, while matrices in the latter do not need to be orthogonal between each other.

As a direct consequence of Postule 4, we can describe how to measure observables and predict the results of their measurement. Suppose we have an observable H that has the following spectral decomposition

$$H = \sum_{k=1}^{n} \lambda_k F_k. \tag{2.22}$$

Let ρ be the pure state in which our system was prepared. Then, after carrying a projective measurement with respect to the observable H,

(i) the result of the measurement is λ_r with probability $\langle \rho, F_r \rangle$ (this is also known as Born's rule);

(ii) if the result of the measurement is r, then the state of the system afterward will be

$$\frac{1}{\langle \rho, F_r \rangle} F_r \rho F_r. \tag{2.23}$$

From now on, we will assume that the orthogonal basis of $\mathbb{C}^2$ is the standard basis for our state space unless stated otherwise.

Now, as was previously assured, we have the tools to get an intuition about why the qubit cannot carry more than one bit of information. Suppose we prepare our qubit in an arbitrary state given by

$$|\psi\rangle = a\,|0\rangle + b\,|1\rangle\,, \tag{2.24}$$

where $a, b \in \mathbb{C}$ and $|a|^2 + |b|^2 = 1$. Then, to have access to any information we will need to build a measurement device that will have $M_0 = |0\rangle\langle 0|$ and $M_1 = |1\rangle\langle 1|$ as components. Hence, after the measurement, we get $|0\rangle$ or $|1\rangle$ with the first having probability given by

$$p(0) = \langle\psi|\, M_0^\dagger M_0\, |\psi\rangle = |a|^2, \tag{2.25}$$

and the second with probability given by

$$p(1) = \langle\psi|\, M_1^\dagger M_1\, |\psi\rangle = |b|^2. \tag{2.26}$$

So we see that even though we have infinite ways to prepare the state of a qubit, we can only get a binary answer in a measurement.

Notice that the measurement never gives the "true" state of the system, instead, it always imposes a state on the system. Because of this, there are fields of quantum mechanics that deal exactly with the problem of finding out the "true" state of the system, like quantum state tomography [4], and distinguishing between states in the same state space. The last problem created numerous protocols depending on what kind of information you want to obtain [22, 83].

2.4 Phase

Phase plays an important role in quantum mechanics, however it encapsulates many different meanings depending on the context. Hence, we will dedicate this section

to discussing some of that in detail. Consider the state $e^{i\theta}|\psi\rangle$ where $|\psi\rangle$ is a state vector and θ a real number. We say that $e^{i\theta}|\psi\rangle$ is equal to $|\psi\rangle$ up to a global phase factor $e^{i\theta}$. An interesting fact is that the global phase factor does not change the statistics of the measurement. Let M_m be a measurement operator associated with some state space. Note that the probability of outcome m will be

$$\langle\psi| e^{-i\theta} M_m^\dagger M_m e^{i\theta} |\psi\rangle = \langle\psi| M_m^\dagger M_m |\psi\rangle . \tag{2.27}$$

Therefore, from an observational point of view, $|\psi\rangle$ and $e^{i\theta}|\psi\rangle$ give the same statistics. From now on, we will ignore global phase factors since they do not interfere with the physical properties of the systems.

On the other hand, consider the states

$$a|0\rangle - b|1\rangle , \qquad a|0\rangle + b|1\rangle . \tag{2.28}$$

The first state has $-b$ as the amplitude for $|1\rangle$, while the second has b. The magnitude for each amplitude is the same, but they change in sign. Then the relative phase occurs when two amplitudes b and b' differ by $b' = e^{i\theta}b$. Different from the global phase, the relative phase changes the statistics of the measurement and is an important characteristic of quantum mechanics.

2.5 No-cloning Theorem

There is an important theorem relating broadcasting of states in quantum mechanics. Classically, if we want to transmit information through numerous channels or many different recipients, all that we have to do is to copy the bit and send it. The No-cloning Theorem [30, 89] says that it is impossible to do the same in quantum mechanics.

Suppose we have a unitary operator U: $\mathcal{H}_1 \otimes \mathcal{H}_2 \to \mathcal{H}_1 \otimes \mathcal{H}_2$ that does the following

$$U(|\psi\rangle|i\rangle) = e^{i\alpha(\psi,e)}|\psi\rangle|\psi\rangle . \tag{2.29}$$

Then, the operator will act as a quantum copying machine that will take any state in $\mathcal{H}_1$ and make a copy of it in the space $\mathcal{H}_2$. Since we saw that the global phase is not relevant, the copy can have a scaling factor of $e^{i\alpha(\psi,e)}$ that depends on the chosen states that were initially chosen and $\alpha(\psi, e) \in \mathbb{R}$. Now, let $|\psi\rangle$ and $|\phi\rangle$ be two arbitrary states in $\mathcal{H}_1$, then

$$\langle\phi|\psi\rangle = \langle\phi|\psi\rangle\langle i|i\rangle = \langle\phi|\langle i|\ |\psi\rangle|i\rangle = \langle\phi|\langle i|U^\dagger U|\psi\rangle|i\rangle = e^{i(\alpha(\phi,i)-\alpha(\psi,i))}\langle\phi|\psi\rangle^2 . \tag{2.30}$$

Therefore,

$$|\langle\phi|\psi\rangle| = |\langle\phi|\psi\rangle|^2, \tag{2.31}$$

and it can only be the case if $|\langle\phi|\psi\rangle| = 0$ or $|\langle\phi|\psi\rangle| = 1$. As a consequence of Cauchy-Schwarz inequality, $|\psi\rangle$ is orthogonal or parallel to $|\phi\rangle$, which is a contradiction to our initial assumption. Hence, it is impossible to find a global unitary operator in quantum mechanics that emulates a copying machine for arbitrary states.

This theorem was proven with the assumption that our states were pure. Therefore, a natural question is what happens when we deal with mixed states. Is there a machine in such a case? Well, unfortunately, the answer is still no. Barnum *et al.* [48] generalized this result for noncommuting mixed states and it received the name of the no-broadcast theorem.

2.6 Entanglement

A well-known phenomenon in quantum mechanics is entanglement. The fact that there is no classic counterpart draws much curiosity to it. In this section, we will define what entanglement is and its basic properties.

Consider two state spaces $\mathbb{C}^k$ and $\mathbb{C}^n$ with their composition being $\mathbb{C}^k \otimes \mathbb{C}^n$. A density matrix ρ in that space has dimension $kn \times kn$ and it represents a quantum state. The state ρ is referred to as entangled if there are no $\rho_k \in \mathbb{C}^k$ and $\rho_n \in \mathbb{C}^n$ such that

$$\rho = \rho_k \otimes \rho_n. \tag{2.32}$$

As an example, let the state space by $\mathbb{C}^2 \otimes \mathbb{C}^2$ and we have the state

$$\rho = |\Psi\rangle\langle\Psi|\,, \tag{2.33}$$

where

$$|\Psi\rangle = \frac{|01\rangle + |10\rangle}{\sqrt{2}}. \tag{2.34}$$

If we have the other two states given by

$$|\psi\rangle = a\,|0\rangle + b\,|1\rangle\,, \tag{2.35}$$

$$|\psi'\rangle = a'\,|0\rangle + b'\,|1\rangle\,, \tag{2.36}$$

then it is impossible to find values of $a, a', b, b' \in \mathbb{C}$ that makes

$$|\Psi\rangle = |\psi\rangle \otimes |\psi'\rangle\,. \tag{2.37}$$

Entanglement becomes interesting when measurement enters the field. Suppose we prepare our measurement as $M_0 \otimes I = |0\rangle\langle 0| \otimes I$ and $M_1 \otimes I = |1\rangle\langle 1| \otimes I$. Then, upon

measuring $|\Psi\rangle$, with probability 1/2 we will get 0 or 1. If we get 0 in our measurement, the state after it will be

$$\frac{M_0 \otimes I\,|\Psi\rangle}{\sqrt{\langle\Psi|\,M_0 \otimes I\,|\Psi\rangle}} = |01\rangle\,. \tag{2.38}$$

When we do the same for operator $M_1 \otimes I$, the state after measurement will be $|10\rangle$. Therefore, when we measure the second qubit with $I \otimes |0\rangle\langle 0|$ or $I \otimes |1\rangle\langle 1|$, we will always get anticorrelated results. In other words, the result $|1\rangle$ ($|0\rangle$) for the second only appears if the result for the first was $|0\rangle$ ($|1\rangle$).

So if it is possible to build classically correlated systems, what is so special about entanglement? The difference comes when we change the basis. Suppose now that we will measure the system in the state $|\Psi\rangle$ using $M_+ = |+\rangle\langle +|$ instead of M_0 and $M_- = |-\rangle\langle -|$ instead of M_1 where

$$|+\rangle = \frac{|0\rangle + |1\rangle}{\sqrt{2}}, \tag{2.39}$$

$$|-\rangle = \frac{|0\rangle - |1\rangle}{\sqrt{2}}. \tag{2.40}$$

Now, applying a change of basis to the state $|\Psi\rangle$ we see that

$$|\Psi\rangle = \frac{|+-\rangle + |-+\rangle}{\sqrt{2}}. \tag{2.41}$$

As a consequence, correlations remain even when we change the basis of our measurement. Suppose there is a classical machine trying to emulate entanglement, then it would send anti-correlated particles prepared in $|0\rangle$ and $|1\rangle$. However, whenever one of the parties decided to change the basis of measurement, the correlations would disappear differently from what we just saw for entanglement. Hence, this phenomenon has no classical analogue and that is why it is so remarkable. There are numerous protocols, such as teleportation, that could not exist without entanglement.

2.7 Quantum Computing

One of our results is related to the simulation of quantum walks in quantum computers. The aim of this section is to give a quick description of how the gate model of quantum computers works and, hopefully, it will be sufficient to understand our results.

The dream of a quantum computer to describe quantum systems started with the work of Benioff [17] where he showed how to describe Turing machines using Schrödinger's equation. This motives the creation of a new field, since it was believed that simulation of quantum systems, like quantum chemistry problems, would be way easier in a computer

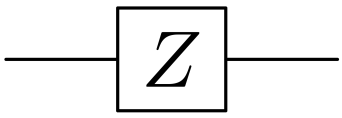

Figure 2.2: Circuit representation of a Pauli Z.

that is quantum by itself. However, in 1992, David Deutsch and Richard Jozsa [29] showed in a toy problem that a quantum computer could solve classical problems faster than a classical computer. This was the start for the current run for a fault-tolerant quantum computer.

Different architectures were proposed: superconductors [95], ion-traps [85], neutral atoms [60], photonic quantum computers [8] Each one of them have their own set of advantages and challenges, however most of them are constructed with an abstraction in mind referred to as the gate model of quantum computing. The gate has similar role when compared to classical computing which is to create logical blocks to perform the computation. It is mainly an abstraction to describe a circuit which is a sequence of unitary operators that are the building blocks of algorithm.

The gate model for quantum computation names each unitary acting on a qubit as a gate. A Pauli Z matrix, for example, would be referred to as a one qubit gate and written as it is shown in figure 2.2. Each line represents a qubit and gates that act on only one qubits are referred to as 1-qubit gates.

It is possible to construct gates that act on more than one qubit. A famous 2-qubit gate is referred to as the SWAP gate defined as

$$SWAP = \begin{bmatrix} 1 & 0 & 0 & 0 \\ 0 & 0 & 1 & 0 \\ 0 & 1 & 0 & 0 \\ 0 & 0 & 0 & 1 \end{bmatrix}. \tag{2.42}$$

The SWAP gate, as the name suggests, swaps the state of two qubits and, in circuit notation, is represented by the figure 2.3. 2.2. In the set of 2-qubit gates, there are also

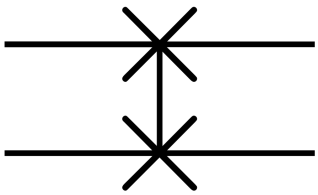

Figure 2.3: Circuit representation of a SWAP gate.

controlled gates. In short, they apply a unitary on one of the qubits based on the state of the control qubit. We will define a general controlled-U (or CU) as

$$CU = |0\rangle\langle 0| \otimes I + |1\rangle\langle 1| \otimes U. \tag{2.43}$$

Figure 2.4 gives the circuit representation of a controlled-U with the top qubit being used as a control and the U unitary being applied on the bottom qubit.

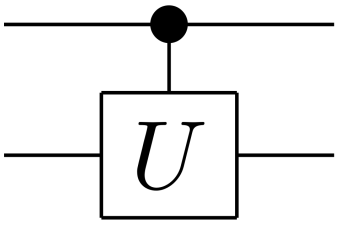

Figure 2.4: Circuit representation of a controlled-U gate.

One thing to notice is that controlled gates can use k qubits as the control and are not restricted to only one. In this case, they are referred to as multi-controlled qubit gates and one of the most famous multi-controlled qubit gate is the Toffoli gate (or CCNOT) [86] that can be defined as

$$CCNOT = \begin{bmatrix} 1 & 0 & 0 & 0 & 0 & 0 & 0 & 0 \\ 0 & 1 & 0 & 0 & 0 & 0 & 0 & 0 \\ 0 & 0 & 1 & 0 & 0 & 0 & 0 & 0 \\ 0 & 0 & 0 & 1 & 0 & 0 & 0 & 0 \\ 0 & 0 & 0 & 0 & 1 & 0 & 0 & 0 \\ 0 & 0 & 0 & 0 & 0 & 1 & 0 & 0 \\ 0 & 0 & 0 & 0 & 0 & 0 & 0 & 1 \\ 0 & 0 & 0 & 0 & 0 & 0 & 1 & 0 \end{bmatrix}. \tag{2.44}$$

Its circuit representation of a Toffoli gate can be seen in figure 2.5.

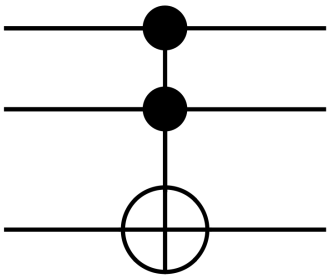

Figure 2.5: Circuit representation of a Toffoli gate.

Although we can express a wide range of unitary matrices with circuits, quantum computers do not have the same freedom. They have a limited set of operators that can be executed by the processor and all unitaries in the circuit are decomposed by the compiler into the basis set of gates. One of the challenges of current quantum computers is how to efficiently decompose a circuit to make it as short as possible. This challenge is related to the coherence time of quantum computers. It is difficult for them to keep the

qubits in the same state without introducing errors, so the circuit must have a limited number of gates otherwise the results become increasingly unreliable.

Controlled gates have widespread use in quantum computing. Since they are the one responsible for qubit interactions, they are the main source of entanglement during quantum computation. They are also essentials for the simulation of quantum walks [35] as expected due to the interaction between numerous vertices in a quantum walk, as we will see. This is also one of the challenges with current computers. Although we can represent any type of interaction between qubits in circuits, every quantum processor has its own topology. Oxford Quantum Circuits' Lucy, for example, has a ring topology[1] similar to the graph represented in figure 2.6.

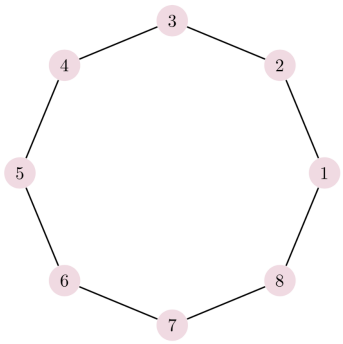

Figure 2.6: Topology of OQC's Lucy.

If an algorithm or a simulated quantum walk requires the action of 2-qubit gates associated with non-neighbours qubits, then numerous SWAP gates are added during the compilation process. This increases the number of gates associated with the circuit and might extrapolate the coherence time of the processor. That is why simulation of certain quantum walks is a hard task for quantum computers and ways to simplify the simulation are of great interest in the general community.

[1]Information provided by Amazon Braket at https://aws.amazon.com/braket/quantum-computers/oqc/

Chapter 3

Quantum walks

3.1 Introduction

The previous chapter gave a brief overview on how to describe a quantum state, a closed quantum system, and how it evolves in time. These are fundamental concepts required to completely understand quantum walks. Both random walks and quantum walks have numerous models to define them, however we will limit ourselves to continuous-time and discrete-time quantum and random walks. In this chapter, we will see how the description of those models and how quantum mechanics creates new phenomena that would be impossible in a classical scenario.

Our focus in this work is to use quantum walks in the context of state transfer and how the properties of the transfers are associated with the algebraic structure of the graph. However it is import to notice the multitude of applications associated with quantum walks. For example, it was shown that a quantum model can be used to explain the transport of particles in protein complexes associates with photosynthesis [68, 69, 40]. Another example is the in the three-qubit liquid-state nuclear-magnetic-resonance quantum-information processor [19] where the quantum interference was even observed experimentally.

Quantum walks can be applied to physical phenomena, like the examples we saw previously, so it raises the question if it was every observed in a controlled experiment and what are required from the limits of the classical random walks when compared to its quantum counterpart. Quantum walks have been demonstrated using nuclear magnetic resonance [19], phase [50], and position [67] space of trapped ions, the frequency space of an optical resonator [28], single photons in bulk [14] and fibre [12] optics, and the scattering of light in coupled waveguide arrays [47]. The realisations have been limited to single particle quantum walks, which have an exact mapping to classical wave phenomena [73], and do not provide any advantage from quantum effects. That is why single particle quantum walks have been observed using classical light [47, 31]. Classical theory no longer provides a sufficient description for quantum walks of more than one indistinguishable

particle, since quantum theory predicts that probability amplitudes interfere leading to distinctly non-classical correlations [72]. The major challenge associated with realising quantum walks of correlated particles is the need for a low decoherence system that preserves their non-classical features. Recent advances in technology were required, but quantum walk of two correlated particles was observed in a photonics scenario leading to violations to the classical limit [7]. All of this suggest the robustness of quantum walks to describe natural phenomena.

In the first part of this chapter, we will define classical random walks in systems without memory which can also be named Markov chains. This model has numerous applications and has been central to important discoveries in various fields like physics and computer science. Although we will not dive into all of those results, we will define Markov chains and give some simple examples to show the contrast between them and the quantum mechanical counterpart.

Quantum walks will be the central theme of the last half of the chapter. First, coined discrete-time quantum walks will be presented to show how it contrasts with the discrete-time classical model. Also, it offers a concrete application of the model: Grover's search algorithm. The algorithm was one of the first to show a quadratic speedup compared to classical counterparts. Although the algorithm was not first described as a quantum walk, you will see that it is easy to describe it as one.

The main focus is continuous-time quantum walks and the possibility of describing those systems with graphs and defining different transport properties. Some known results from literature will be presented and they will be crucial to understand our work and how the addition of complex weights change transport properties on graphs.

All the content of this chapter is widely known and it can be found in any standard textbook about the theme [74, 27].

3.2 Classical discrete-time Markov chains

A classical random walk is a stochastic process that can be associated with graphs. A walker starts in a vertex of a graph G and it has a probability to move from one vertex to another. In other words, the process is a sequence of random variables $x_0, x_1, \ldots$ denoted by $\{x_t : t \in \mathbb{N}\}$. We call X_t the state at time t and the state space is denoted as $\mathcal{S}$, which can be $\mathbb{Z}^n$, $\mathbb{N}^n$ or $\mathbb{R}^n$. The probability of moving to another vertex is not associated with the path that the walker took. Therefore, the probabilities in future time obey the

following

$$\text{Prob}(x_{t+1} = j | x_t = i_n, x_{t-1} = i_{n-1}, \ldots, x_0 = i_0) = \text{Prob}(x_{t+1} = j | x_t = i), \tag{3.1}$$

for all $t \geq 0$ and $i_0, \ldots, i, j \in \mathcal{S}$. Then this process is usually called memoryless and can be generalized by a Markov chain.

The Markov chain will have an associated probability distribution for every time step. Our state space will be $\mathbb{R}^n$ and our random variables will be represented by vector x with $\langle x, \mathbb{1} \rangle = 1$, where $\mathbb{1}$ is the all ones vector. Let G be a graph with n vertices and an edge set $E(G)$, then the vector x will be

$$x(t) = \begin{pmatrix} p_1(t) \\ \vdots \\ p_n(t) \end{pmatrix}, \tag{3.2}$$

where $p_i(t)$ is the probability of finding the walker on vertex i at time t. We cannot tell precisely where the walker will be in future steps, but there is a way to evolve the distribution of probabilities through time. That is done with what is called the transition matrix M also called the probability matrix or stochastic matrix.

Let $x(0)$ be the probability distribution at time 0, then the time evolution will be given by

$$x(t) = M^t x(0). \tag{3.3}$$

The equation above shows two crucial properties of the matrix M: it is a $\mathbb{R}^{n \times n}$ matrix and all of its columns sum to one. Clearly, this is a discrete-time walk since the system evolves by sequential application of M to the initial condition.

With this in mind, we are now ready to deal with an interesting example. Set our graph G to be the complete graph with n vertices and also the walker to have an equal probability to move to any adjacent vertex. Then we can set M to be

$$M_{ij} = \begin{cases} 0 & \text{if } i = j \\ \frac{1}{n-1} & \text{if } i \neq j \end{cases}. \tag{3.4}$$

We could also define the transition matrix employing the adjacency matrix of the graph (A). In such a case, the transition matrix would simply be

$$M_{ij} = \frac{A_{ij}}{d_j}, \tag{3.5}$$

where d_j is the number of neighbors of the vertex j.

Now we can write explicitly the matrix M

$$M = \frac{1}{n-1} \begin{pmatrix} 0 & 1 & 1 & \ldots & 1 \\ 1 & 0 & 1 & \ldots & 1 \\ 1 & 1 & 0 & \ldots & 1 \\ \vdots & \vdots & \vdots & \ddots & \vdots \\ 1 & 1 & 1 & \ldots & 0 \end{pmatrix}. \tag{3.6}$$

Suppose our walker starts at the vertex 1, then its probability distribution will be

$$x(0) = \begin{pmatrix} 1 \\ 0 \\ \vdots \\ 0 \end{pmatrix}. \tag{3.7}$$

Using the time evolution as was defined we get

$$x(1) = \frac{1}{n-1} \begin{pmatrix} 0 \\ 1 \\ \vdots \\ 1 \end{pmatrix}, \tag{3.8}$$

$$x(2) = \frac{1}{(n-1)^2} \begin{pmatrix} n-1 \\ n-2 \\ \vdots \\ n-2 \end{pmatrix}, \tag{3.9}$$

$$x(3) = \frac{1}{(n-1)^3} \begin{pmatrix} (n-1)(n-2) \\ (n-2)^2 \\ \vdots \\ (n-2)^2 \end{pmatrix}. \tag{3.10}$$

We can clearly see that $p_2(t) = p_3(t) = \cdots = p_n(t)$ and $p_1(t) = p_2(t-1)$. Hence, using the fact that we are dealing with vectors that sum to one we get

$$p_2(t) = \frac{1 - p_2(t-1)}{n-1}, \tag{3.11}$$

which gives

$$p_2(1) = \frac{1}{n-1}, \tag{3.12}$$

$$p_2(2) = \frac{1}{n-1} - \frac{1}{(n-1)^2}, \tag{3.13}$$

$$p_2(3) = \frac{1}{n-1} - \frac{1}{(n-1)^2} + \frac{1}{(n-1)^3}, \tag{3.14}$$

$$p_2(4) = \frac{1}{n-1} - \frac{1}{(n-1)^2} + \frac{1}{(n-1)^3} - \frac{1}{(n-1)^4}. \tag{3.15}$$

Then we can write $p_2(t)$ as

$$p_2(t) = \sum_{k=1}^{t} \frac{(-1)^{k+1}}{(n-1)^k} = -\sum_{k=1}^{t} \frac{1}{(1-n)^k} = \frac{1}{n}\left(1 - \frac{1}{(1-n)^t}\right), \tag{3.16}$$

where the last expression was obtained by noticing that $p_2(t)$ is a geometric series.

It is possible to see from 3.16 that when $t \to \infty$ the observer will have an equal probability to find the walker in any vertex of the graph. We will see later the difference between this result and the one found in quantum walks.

3.3 Classical continuous-time Markov chains

The previous model assumed time to be a discrete parameter with transitions happening in steps. We will see now that we can consider continuous-time Markov chains as discrete-time Markov chains with the transitions happening at any time.

Similarly to what was exhibited, we will have a state space $\mathcal{S}$ that satisfies the Markov property. That is, let $\mathcal{F}_{X(t)}$ denote all the information about the history of X up to time t. If we move time by an infinitesimal value ϵ and setting $X_i, X_j \in \mathcal{S}$ then

$$\text{Prob}\{X(t+\epsilon) = i | \mathcal{F}_{X(t)=j}\} = \text{Prob}\{X(t+\epsilon) = i | X(t) = j\}. \tag{3.17}$$

Another property that we will consider is time homogeneity which is defined as

$$\text{Prob}\{X(t+\epsilon) = i | X(t) = j\} = \text{Prob}\{X(\epsilon) = i | X(0) = j\}. \tag{3.18}$$

We can imagine this process as a slow evolution in time of the probability densities. The walker will be in a certain vertex and the chance of it moving to another vertex increases in time. Once again, we will have a transition matrix describing the evolution in time of the process. Suppose that our walker is in vertex j, so it will have a probability of moving to vertex i given by a transition rate denoted as γ. In this case, during an infinitesimal amount of time ϵ, the probability of moving to another vertex will be $\gamma\epsilon$. While the probability of staying in the same vertex will be $1 - d_j\gamma\epsilon$, where d_j is the degree of j. From this, we can define the transition matrix $M(t)$ as

$$M_{ij}(t) = \begin{cases} 1 - d_j\gamma t + \mathcal{O}(t^2) & \text{if } i = j, \\ \gamma t + \mathcal{O}(t^2) & \text{if } i \neq j \text{ and } (ij) \in E(G), \\ 0 & \text{otherwise.} \end{cases} \tag{3.19}$$

Let us also define the generating matrix H:

$$H_{ij} = \begin{cases} d_j\gamma & \text{if } i = j, \\ -\gamma & \text{if } i \neq j \text{ and } (ij) \in E(G), \\ 0 & \text{otherwise.} \end{cases} \tag{3.20}$$

Notice that so far, we have the same rate γ for every vertex, but that is not a rule. We could have rates $\gamma(i, j)$ dependent on what vertex the walker is on or which neighbor he has. We would not describe the graph as undirected, but as a oriented one with different weights on each arc.

The transition matrix obeys the following property

$$M(t+\epsilon) = M(t)M(\epsilon), \tag{3.21}$$

for $t, \epsilon \geq 0$, which can be proven using time homogeneity in Equation 3.18 and the Markov property in Equation 3.17. From it, we get that

$$M(t+\epsilon)_{ij} = \sum_k M(t)_{ik} M(\epsilon)_{kj}. \tag{3.22}$$

By isolating the diagonals terms we get

$$\begin{aligned} M(t+\epsilon)_{ij} &= M(t)_{ij} M(\epsilon)_{jj} + \sum_{k \neq j} M(t)_{ik} M(\epsilon)_{kj} \\ &= M(t)_{ij}(1 - \epsilon H_{jj}) - \epsilon \sum_{k \neq j} M(t)_{ik} H_{kj}. \end{aligned} \tag{3.23}$$

If we move the first term of the right to the left, divide by ϵ, and make $\epsilon \to 0$, then

$$\frac{d}{dt} M(t)_{ij} = -\sum_k M(t)_{ik} H_{kj}. \tag{3.24}$$

The solution to this differential equation with initial condition $M_{ij}(0) = \delta_{ij}$ is

$$M(t) = e^{-Ht}. \tag{3.25}$$

Since we now know how the transition matrix is described, we can find the evolution in time of the probability distribution. Let $x(0)$ be the initial probability distribution, then after some time t it will be

$$x(t) = M(t)x(0). \tag{3.26}$$

Both definitions of random walks allow us to compare them with their quantum mechanical counterparts. We will see with this comparison how quantum mechanics changes some properties of random walks.

3.4 Discrete-time quantum walks

Discrete-time random walks use the stochastic matrix to turn time into a discrete parameter by applying the matrix t times to the initial state. However in quantum mechanics, the time evolution is dictated by a continuous operator on time and it is impossible to apply the time evolution operator t times and get discrete time steps. To circumvent this problem, physicists constructed numerous models for discrete-time and one of them is coined quantum walks and it consists of writing the state space as $\mathcal{H} = \mathcal{H}_P \otimes \mathcal{H}_C$, i.e. the composition of a space that dictates the position of the walker with another that tells when the transition occurs from one vertex to another.

The state space $\mathcal{H}_P$ will be defined as $\mathbb{C}^n$, where n is the number of vertices in the graph, and it has basis states, $\{|k\rangle\}$, that span the whole space. For example, if we are dealing with a path graph P_n then $i \in \{0, 1, \ldots, n\}$, but if we use a cycle graph, C_n, then $i \in \mathbb{Z}/n\mathbb{Z}$. The state space $\mathcal{H}_P$ will be related to the position of the walker on a graph with $|i\rangle$ associated with the vertex i of the graph. We have a way to describe the walk, but we still lack how to define a move from one vertex to another. That is why we need the state space $\mathcal{H}_C$ that will be our "coin" to define when a move is going to happen. The coin space will be $\mathbb{C}^d$ where d is the highest degree of the graph. One example would be paths or cycles where the coin space can be defined with $\mathbb{C}^2$ and it has $\{|0\rangle, |1\rangle\}$ as basis. Physically, there is no problem with the definition of $\mathcal{H}$ and we can see that by supposing that we have an electron walking on a chain of atoms [93]. It will have its position in the chain and a spin. Then we can create a unitary, for example, that will move the electron forward if its spin is up or backward otherwise. Physically, the coin is responsible for giving momentum to the walker so that its position evolves as time passes. While, from a mathematical perspective, the coin gives reversibility, since it is a way to track the last position of the walker.

Following the previous definition, we define the shift matrix S that acts on $\mathcal{H}$ as

$$S|0\rangle|k\rangle = |0\rangle|k+1\rangle, \tag{3.27}$$

$$S|1\rangle|k\rangle = |1\rangle|k-1\rangle. \tag{3.28}$$

Since we know how S acts on the states, we can define it as

$$S = |0\rangle\langle 0| \otimes \sum_k |k+1\rangle\langle k| + |1\rangle\langle 1| \otimes \sum_k |k-1\rangle\langle k|. \tag{3.29}$$

Now, we can define the unitary that describes the walk as

$$U = S(C \otimes I), \tag{3.30}$$

where C will be our "coin-flip" that applies a rotation in the coin space. Notice that we can have numerous choices of the unitary C and each one of them gives a different family of walks. Usually, when the comparison between classical and quantum is desired, we choose balanced coins that give an equal probability for the walker to move forward or backward.

The Hadamard coin is an example of a frequently used coin and it is defined as

$$C = \frac{1}{\sqrt{2}} \begin{pmatrix} 1 & 1 \\ 1 & -1 \end{pmatrix}. \tag{3.31}$$

We check that it is indeed balanced. Suppose we have a graph G and the state $|k\rangle$ to be the localization of a particle at the vertex k. If the walker starts at the state $|0\rangle$, then

$$|0\rangle|0\rangle \xrightarrow{\text{C}} \frac{1}{\sqrt{2}}(|0\rangle + |1\rangle)|0\rangle \xrightarrow{\text{S}} \frac{1}{\sqrt{2}}(|0\rangle|1\rangle + |1\rangle|-1\rangle). \tag{3.32}$$

Notice that a measurement performed using the basis of the state space, would result in $|0\rangle|1\rangle$ with probability 1/2 or $|0\rangle|-1\rangle$ with probability 1/2.

This definition presented makes the walker behave as expected: each time U acts on the state, the particle will jump between the vertices of the graph with some probability. However, the Hadamard coin makes the walk asymmetric as we will see now. Let $|0\rangle|0\rangle$ be the initial state of the particle, then

$$\begin{aligned} |0\rangle|0\rangle &\xrightarrow{U} \frac{1}{\sqrt{2}}(|0\rangle|1\rangle + |1\rangle|-1\rangle) \\ &\xrightarrow{U} \frac{1}{2}(|0\rangle|2\rangle - |0\rangle|0\rangle + |1\rangle|0\rangle + |1\rangle|-2\rangle) \\ &\xrightarrow{U} \frac{1}{2\sqrt{2}}(|0\rangle|3\rangle + |0\rangle|-1\rangle + |1\rangle|1\rangle - 2|1\rangle|-1\rangle - |1\rangle|-3\rangle). \end{aligned} \tag{3.33}$$

What Equation 3.33 is showing us is that the walk starts to drift to the left as time goes by. It can be attributed to the element -1 in the coin operator. When applying U multiple times, the element $C_{2,2}$ subtracts some terms that would increase the probability of the walker going to the right. It is possible to define a more symmetrical coin like

$$C = \frac{1}{\sqrt{2}}\begin{pmatrix} 1 & i \\ i & 1 \end{pmatrix}, \tag{3.34}$$

that makes the walker go to both sides with equal probability. The discussion above is always restricted to the initial condition of the quantum walk. If the walker starts with a state given by

$$|\psi\rangle = \frac{1}{\sqrt{2}}\big(|0\rangle + i|1\rangle\big)|0\rangle, \tag{3.35}$$

then the Hadamard will be the balanced coin in this case.

The study comparing the discrete-time quantum walk and the classical case gives numerous results showing improvement in the quantum case. An example is the spread velocity of the walker where the quantum case reaches other vertices faster than the classical case. Since those results are out of the scope of this work, we will leave the references [26, 59, 58, 2, 74] for the interested reader.

3.4.1 Grover's search algorithm

Grover's search algorithm [46] is one of the most impactful algorithms in quantum computing and, as we will see, there is a very natural way of implementing it using discrete-time quantum walks (DTQW). Suppose there is an unsorted database and we want to find a marked element $|w\rangle$, notice that all elements in the database are defined

labelled with the basis states of the computational basis. Then the algorithm starts by defining an oracle operator, U_w, that will add a negative phase to the marked element:

$$U_w |i\rangle = \begin{cases} |i\rangle & \text{if } i \neq w \\ -|i\rangle & \text{if } i = w \end{cases}. \tag{3.36}$$

It is easy to see that U_w is a diagonal matrix and can be expressed as $U_w = I - 2|w\rangle\langle w|$, where I is the identity.

The other step of the algorithm is to apply amplitude amplification. The system will be initialized in a uniform superposition

$$|s\rangle = \frac{1}{\sqrt{n}} \sum_{i=0}^{n-1} |i\rangle . \tag{3.37}$$

Then the algorithm applies sequential reflections on $|s\rangle$ to rotate it, in each step, closer to $|w\rangle$. The procedure uses two reflections U_w that was presented previously and $U_s = 2|s\rangle\langle s| - I$ which is a reflection through $|s\rangle$. Notice that all reflections are done on the plane of $|w\rangle$ and $|s'\rangle$ with $\langle w|s'\rangle = 0$. Figure 3.1 shows one iteration of the algorithm and the resulting state.

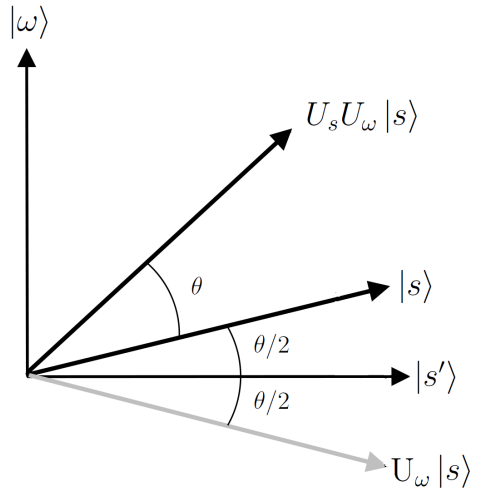

Figure 3.1: Figure representing the amplitude amplification procedure transforming the state $|s\rangle$ to $U_s U_w |s\rangle$ with one iteration of the Grover's algorithm.

The state $|s\rangle$ can be written as

$$|s\rangle = \sin\theta |w\rangle + \cos\theta |s'\rangle , \tag{3.38}$$

and after the application of $U_s U_w$ the resulting state is rotated by $\theta = 2 \arcsin \frac{1}{\sqrt{n}}$. Therefore, with enough iterations, we can rotate the state $|s\rangle$ to a state closer to $|w\rangle$ and improve the probability of finding the marked element. After r iterations, the probability of finding $|w\rangle$ will be

$$|\langle w| U_s U_w |s\rangle|^2 = \sin^2\left(\left(r + \frac{1}{2}\right)\theta\right), \tag{3.39}$$

and the near-optimal measurement will be with $r \approx \pi\sqrt{n}/4$.

Wong [91], Shenvi *et al.* [71], and Ambainis *et al.* [3] results characterize ways to implement Grover's algorithm as a DTQW for the complete graph, the hypercube, and periodic square lattices, respectively. We will focus on complete graphs and we start by setting our Hilbert space $\mathcal{H}$ which is the composition of space $\mathbb{C}^n$ associated with the vertices of the graph, with n being the number of vertices, and the space $\mathbb{C}^d$ associated with the coin. As previously, the coin space is associated with the edges of the graph and, in this algorithm, we will add one self-loop in each vertex. Notice that the complete Hilbert space will be described by $\mathcal{H} = \mathbb{C}^n \otimes \mathbb{C}^n$, since each vertex of the complete graph will have n edges. Now we define the flip-flop shift operator $S : \mathcal{H} \to \mathcal{H}$ as

$$S\left|i\right\rangle \otimes \left|j\right\rangle = \left|j\right\rangle \otimes \left|i\right\rangle . \tag{3.40}$$

As usual, we will start with the initial state being a uniform superposition of the whole Hilbert space:

$$\left|\psi\right\rangle = \left|s\right\rangle \otimes \left|s\right\rangle . \tag{3.41}$$

The quantum walk is defined by repeated applications of

$$U_0 = S(I \otimes C_0), \tag{3.42}$$

were C_0 is the Grover diffusion coin

$$C_0 = 2\left|s\right\rangle\!\left\langle s\right| - I = U_s. \tag{3.43}$$

The cautious reader will notice that $\left|\psi\right\rangle$ is an eigenvector of U_0, so to turn into a search algorithm, we need to introduce a new coin C_1 that is associated only with the marked vertex. The search operator is now

$$U = S[(I - \left|w\right\rangle\!\left\langle w\right|) \otimes U_s + \left|w\right\rangle\!\left\langle w\right| \otimes C_1]. \tag{3.44}$$

Multiple coins can be associated with C_1, but, in our case, we will choose $C_1 = -U_s$ and, as a consequence,

$$\begin{aligned} U &= S[(I - 2\left|w\right\rangle\!\left\langle w\right|) \otimes U_s] \\ &= S[(I \otimes U_s)][(I - 2\left|w\right\rangle\!\left\langle w\right|) \otimes I] && (3.45) \\ &= S(U_w \otimes U_s). && (3.46) \end{aligned}$$

Remembering that we start our algorithm with $\left|\psi\right\rangle = \left|s\right\rangle \otimes \left|s\right\rangle$,

$$\begin{aligned} U^2\left|\psi\right\rangle &= US(U_w \otimes U_s)\left|\psi\right\rangle = U(U_s\left|s\right\rangle \otimes U_w\left|s\right\rangle) \\ &= (U_wU_s)\left|s\right\rangle \otimes (U_sU_w)\left|s\right\rangle . \end{aligned} \tag{3.47}$$

We defined Grover's search with r iterations as $(U_wU_s)^r\left|s\right\rangle$ and we can see that we arrive at the same result with $2r$ steps of the DTQW and a measurement on the space associated with the vertices.

3.5 Continuous-time quantum walks

Unlike the discrete-time case, the Hilbert space associated with a continuous-time quantum walk, $\mathcal{H}$, does not have a state space for a coin. We start by defining an Hermitian matrix H associated with the adjacency or Laplacian matrix of a graph. As we saw in the previous chapter, the time evolution will be given by

$$U(t) = e^{-iHt}, \tag{3.48}$$

that acts as

$$|\psi(t)\rangle = U\,|\psi(0)\rangle\,. \tag{3.49}$$

The probability distribution will then be

$$p_i = |\langle i|\psi(t)\rangle|^2, \tag{3.50}$$

where i is a vertex label and $|i\rangle$ is the basis vector with 1 in the i-th entry.

The time evolution dictated by quantum mechanics provides numerous results that distinguish a classical walk from a quantum walk. One of the differences arises when analyzing the expected hitting time of the walk, which is the time it takes for the walker to reach a target. It was shown [33, 6] that quantum walks hit the target exponentially faster than classical walks. Algorithms in quantum computing use this fact to improve complexity of classical algorithms using quantum walks. Farhi *et al.* were able to show speed-ups for search in certain types of binary trees [33] and Montanaro [70] proved a quadratic speedup for a Monte Carlo algorithm using quantum walks. Other properties of quantum walks can be found in references to other works of Childs *et al.* [6], Kempe *et al.* [59], and Portugal [74].

The probability distribution associated with the continuous-time quantum walk is not equal to the classical case, similarly to the discrete-time model. In 2010, Whitfield *et al.* [54] proposed a new type of quantum walk called Quantum Stochastic Walk that generalizes both continuous-time classical and quantum walks. The model is defined using open quantum systems and the time evolution is dictated by a different set of rules that were defined for closed systems. The amount of decoherence, which is the loss of quantumness in a system, makes the system behave similar to a classical one. Since this is not the scope of this work, the interested reader will find more in the references [54, 59].

As promised, we will show the different behavior of the quantum walks in complete graphs. Remember that the adjacency matrix of a graph G, A, has a spectral decomposition given by

$$A = \sum_{r=1}^{n} \theta_r E_r. \tag{3.51}$$

Then, we start with the following lemma:

Lemma 3.0.1 ([39]). *Let A be the adjacency matrix of a graph with eigenvalues θ_r and $a, b \in V(G)$, then*

$$|U(t)_{ab}| \leq \sum_{r=0}^{n} |(E_r)_{ab}|, \tag{3.52}$$

where E_r are the idempotents of A.

Proof. The time evolution operator is given by

$$U(t) = \sum_{r=0}^{n} e^{it\theta_r} E_r. \tag{3.53}$$

Then,

$$|U(t)_{ab}| = \left| \sum_{r=0}^{n} e^{it\theta_r} (E_r)_{ab} \right| \leq \sum_{r=0}^{n} \left| e^{it\theta_r} (E_r)_{ab} \right| = \sum_{r=0}^{n} |(E_r)_{ab}|, \tag{3.54}$$

where the triangle inequality was used and the fact that all the eigenvalues have norm 1. □

The above lemma is all we need to prove the claim.

Theorem 3.1 ([39]). *In a continuous-time quantum walk, it is impossible to find a time t in which there is an equal probability of finding the walker at any vertex of a complete graph, K_n, with n vertices and $n > 4$.*

Proof. The first step is noticing that the adjacency matrix of complete graphs can be written as $A = J - I$, where J is the all ones matrix. Then, they have two eigenvalues: $n-1$ and -1, with the latter having a multiplicity of $n-1$. The corresponding idempotents are

$$\frac{1}{n} J, \qquad I - \frac{1}{n} J. \tag{3.55}$$

The time evolution operator will then be

$$U(t) = e^{i(n-1)t} \frac{1}{n} J + e^{-it} \left(I - \frac{1}{n} J \right). \tag{3.56}$$

Let a, b be two vertices in the graph and $|a\rangle, |b\rangle$ their characteristic vectors, i.e. the vectors with 1 in the entry a (or b, respectively) and zero elsewhere. The probability of finding the walker that started in a at the vertex b is given by

$$|\langle b| U(t) |a\rangle|^2 = |U(t)_{ab}|^2. \tag{3.57}$$

When we apply the previous lemma, we get

$$|U(t)_{ab}|^2 \leq \left(\frac{|J_{ab}|}{n} + \frac{|-J_{ab}|}{n} \right)^2 = \frac{4}{n^2}. \tag{3.58}$$

If we want an equal probability of finding the walker in any vertex, then every entry of $U(t)$ must be equal to $1/\sqrt{n}$, therefore

$$\frac{1}{n} \leq \frac{4}{n^2}. \tag{3.59}$$

This is only possible if $n \leq 4$ and the claim is proved. □

3.5.1 Graphs and nature

Previously, the time evolution operator was created using the adjacency matrix of a graph as the Hamiltonian of the system. Although this is completely valid from a mathematical perspective, a natural question arises: can we do the other way around, i.e., can we start from a known physical model and check that it is indeed described by the adjacency matrix of a graph? The answer is obtained from a known result in quantum walks [39]. First denote our state space as $(\mathbb{C}^2)^{\otimes n}$ and $|0\rangle, |1\rangle$ our standard basis for $\mathbb{C}^2$. Then, the basis for $(\mathbb{C}^2)^{\otimes n}$ will be given by

$$|f_S\rangle = |i_1\rangle \otimes |i_2\rangle \otimes \cdots \otimes |i_n\rangle , \tag{3.60}$$

where S is a subset of $\{1, \ldots, n\}$ and $i_r = 1$ if $r \in S$ (otherwise is zero). If S has k elements, then the vector $|f_S\rangle$ spans a subspace of the state space which is called k-excitation subspace.

Now, we define the edge-Hamiltonian H_{xy} as

$$H_{xy} = \frac{1}{2} \sum_{i,j \in E(G)} X_i X_j + Y_i Y_j, \tag{3.61}$$

where X_i is the Pauli matrix X acting on the ith state vector and identity elsewhere and analogously for Y_i. Recall that

$$X|0\rangle = |1\rangle , \tag{3.62}$$

$$X|1\rangle = |0\rangle , \tag{3.63}$$

and

$$Y|0\rangle = i|1\rangle , \tag{3.64}$$

$$Y|1\rangle = -i|0\rangle . \tag{3.65}$$

Hence, if $S \oplus T$ denotes the symmetric difference between subsets,

$$X_i X_j |f_S\rangle = \left|f_{S \oplus \{i,j\}}\right\rangle , \tag{3.66}$$

while

$$Y_i Y_j |f_S\rangle = -(-1)^{|S \cap \{i,j\}|} \left|f_{S \oplus \{i.j\}}\right\rangle . \tag{3.67}$$

Therefore,

$$\begin{aligned} H_{xy}(ij)|f_S\rangle &= \frac{1}{2}\left(1 - (-1)^{|S \cap \{i,j\}|}\right) \left|f_{S \oplus \{i,j\}}\right\rangle \\ &= \begin{cases} \left|f_{S \oplus \{i,j\}}\right\rangle , & \text{when } |S \cap \{i,j\}| \text{ is even;} \\ 0, & \text{otherwise} \end{cases} . \end{aligned} \tag{3.68}$$

As a consequence, the Hamiltonian $H_{xy}(ij)$ maps the k-excitation subspace to itself. Another Hamiltonian called the XY-Hamiltonian is defined as

$$H_{xy} = \sum_{ij \in E(G)} X_i X_j + Y_i Y_j. \tag{3.69}$$

It is the first model proposed by physicists of antiferromagnetic spin chains [34] that was solvable. It is easy to see that the k-excitation subspace is also invariant by the action of H_{xy}. As we defined that the evolution of time of quantum systems is given by

$$e^{-itH_{xy}}, \tag{3.70}$$

by a simple Taylor series expansion, we see that the subspace will also be invariant for any time t. If we restrict the quantum system to the 1-excitation subspace, then the adjacency matrix A of the graph G, as a consequence of Equation 3.68, can be used to describe the system. Then,

$$U(t) = e^{-itA}, \tag{3.71}$$

will be a block of $e^{-itH_{xy}}$.

The k-symmetrical power $G^{\{k\}}$ of a graph G has the k-subsets of $V(G)$ as vertices, where two k-subsets are adjacent if their symmetric difference is an edge of G. With this at hand, we get the following theorem

Theorem 3.2 ([39]). *The matrix that represents the action of H_{xy} on the span of the vectors $|f_S\rangle$ where $|S| = k$ is the adjacency matrix of the k-th symmetrical power of the graph X.*

Proof. We have

$$H_{xy} |f_S\rangle = \sum_{ij \in E(G)} H_{xy}(ij) |f_S\rangle = \sum_{T : S \oplus T \in E(G)} |f_T\rangle . \tag{3.72}$$

And the last sum is over the neighbors of S in $G^{\{k\}}$. □

This result gives us a description of the XY-Hamiltonian and its composition of blocks of k-excitation subspaces. All of those subspaces can be associated with a graph.

3.5.2 Perfect state transfer

As previously illustrated, it is impossible to clone a quantum state which makes long-distance communication a challenge, since it is not possible to build repeaters similar to what we have in classical communication. Christandl *et al.* [64] were one of the first

groups to investigate a solution with a property called state transfer. Their solution is based on the idea that it is possible to construct a system that is related to a graph, and has an initial arbitrary state associated with a vertex. A simple time evolution of the system is in charge of transferring the state from its initial vertex to any other vertex of the graph. What they discovered is that a graph with this property is uncommon, which led to numerous works connecting algebraic graph theory and quantum walks in search of graphs with this property.

In the previous subsection, we saw that it is possible to write certain Hamiltonians as a block matrix with each block corresponding to the excitation space it represents. When we are dealing with a 1-excitation space, the matrix $U(t) = \exp(-itA)$ will represent the operator that evolves the initial state to time t. If we start with an excitation in a particle located at the vertex a with characteristic vector $|a\rangle$, then a perfect state transfer (PST) from a to b occurs at time t when

$$|\langle b| U(t) |a\rangle| = 1. \tag{3.73}$$

The spectral decomposition of $U(t)$ gives that

$$U(t)_{ab} = \sum_{r=0}^{d} e^{-it\theta_r} (E_r)_{ab}, \tag{3.74}$$

and from it, we get the following chain of inequalities

$$\begin{aligned} |U(t)_{ab}| &\leq \sum_{r=0}^{d} |(E_r)_{ab}| && (3.75)\\ &\leq \sum_{r=0}^{d} \sqrt{(E_r)_{aa}}\sqrt{(E_r)_{bb}} && (3.76)\\ &\leq \sqrt{\sum_r (E_r)_{aa} \sum_r (E_r)_{bb}} && (3.77)\\ &= 1. && (3.78) \end{aligned}$$

This set of inequalities will reveal why algebraic graph theory can be useful to explain quantum information phenomena. The analysis of the idempotent matrices characteristics can provide valuable insights in understanding what family of graphs can have PST. We will now see three lemmas that dives deeper in this idea.

Lemma 3.2.1 ([39]). *In Equation 3.75, equality only holds if and only if there is a complex number γ such that $e^{-it\theta_r} = \gamma\nu_r$, where ν_r is the sign of $(E_r)_{ab}$, whenever $(E_r)_{ab} \neq 0$.*

Proof. The proof comes directly from the triangle inequality and equality holds if and only if the stated condition holds. □

Lemma 3.2.2 ([39]). *Equality in 3.76 holds if and only if $E_r |a\rangle$ and $E_r |b\rangle$ are parallel.*

Proof. Let

$$\langle a| E_r |a\rangle\langle b| E_r |b\rangle - (\langle a| E_r |b\rangle)^2 = \langle a| E_r E_r |a\rangle\langle b| E_r E_r |b\rangle - (\langle a| E_r E_r |b\rangle)^2, \tag{3.79}$$

where it was used the fact that E_r is idempotent. Then defining $E_r |a\rangle = |v\rangle$ and $E_r |b\rangle = |u\rangle$,

$$\langle a| E_r E_r |a\rangle\langle b| E_r E_r |b\rangle - (\langle a| E_r E_r |b\rangle)^2 = \langle v|v\rangle \langle u|u\rangle - \langle u|v\rangle^2, \tag{3.80}$$

Using the Cauchy-Schwarz inequality

$$\langle v|v\rangle \langle u|u\rangle - \langle u|v\rangle^2 \geq 0. \tag{3.81}$$

In the previous inequality, equality occurs if and only if $|u\rangle = E_r |a\rangle$ and $|v\rangle = E_r |b\rangle$ are parallel. □

Lemma 3.2.3. *[39] Equality in 3.77 holds if and only if a and b are cospectral.*

Proof. Using Cauchy-Schwarz to the vectors $\sqrt{(E_r)_{aa}}$ and $\sqrt{(E_r)_{bb}}$ for each r we get that

$$\sum_r \sqrt{(E_r)_{aa}}\sqrt{(E_r)_{bb}} \leq \sqrt{\sum_r (E_r)_{aa}}\sqrt{\sum_r (E_r)_{bb}}, \tag{3.82}$$

and equality holds if and only if $(E_r)_{aa} = (E_r)_{bb}$ for all r. □

Let A be an adjacency matrix of a graph G and E_r its corresponding idempotents, then vertices a and b of G are cospectral if $(E_r)_{aa} = (E_r)_{bb}$ for all r. We can also define strongly cospectral vertices when vertices a and b are cospectral and also $E_r |a\rangle$ and $E_r |b\rangle$ are parallel.

It is possible to prove that if we have PST from vertex a to b, then there is PST from b to a. It is a direct consequence of lemma 3.2.1, the fact that γ is a complex number of modulus 1, and that $U(-t)$ is the inverse of $U(t)$. Also, the previous fact leads to periodicity, in other words, if PST occurs between a and b, then at time $2t$ the excited state can be found at vertex a again with probability 1. This leads directly to the following lemma:

Lemma 3.2.4 ([43]). *A graph G is periodic at the vertex a if and only if the ratio condition holds, which is the following*

$$\frac{\theta_r - \theta_s}{\theta_k - \theta_l} \in \mathbb{Q}, \tag{3.83}$$

where $\theta_r, \theta_s, \theta_k, \theta_l$ are eigenvalues in the eigenvalue support of a with $\theta_k \neq \theta_l$.

Proof. Since periodicity is a consequence of PST, if we apply it to lemma 3.2.1 we get that $e^{-it\theta_r}$ must be constant for all r, due to the fact that all $(E_r)_{aa} \neq 0$ must sum up to 1. Then

$$e^{it(\theta_r-\theta_s)} = 1, \tag{3.84}$$

and for that to happen

$$t(\theta_r - \theta_s) = 2m_{rs}\pi \tag{3.85}$$

where m_{rs} is an integer. As a consequence,

$$\frac{\theta_r - \theta_s}{\theta_k - \theta_l} = \frac{m_{rs}}{m_{kl}} \in \mathbb{Q}. \tag{3.86}$$

Therefore, if the graph is periodic then the ratio condition holds. Now for the converse, suppose the ratio condition holds

$$m_{rs} = \frac{m_{kl}}{(\theta_k - \theta_l)}(\theta_r - \theta_s) \in \mathbb{Z}, \tag{3.87}$$

then the graph is periodic at the time

$$t = 2\pi\frac{m_{kl}}{(\theta_k - \theta_l)}. \tag{3.88}$$

□

Given a rational m and a prime p, we can write $m = \frac{p^\alpha r}{s}$, where r and s are integers not divisible by p. Then the p-adic norm is defined by

$$|m|_p = p^{-\alpha}. \tag{3.89}$$

Thus, if m is an integer, its p-adic norms are inversely proportional to the power of p dividing m.

The eigenvalue support of a vertex a is defined as the set of eigenvalues $\{\theta_0, \ldots, \theta_k\}$ such that

$$E_r |a\rangle \neq 0. \tag{3.90}$$

Now, we are ready for the following description of PST in undirected graphs.

Theorem 3.3 ([25]). *Let a and b be vertices in a graph G, and assume the eigenvalue support of a consists of eigenvalues $S = \{\theta_0, \ldots, \theta_k\}$. There is a perfect state transfer between a and b if and only if:*

(a) Vertices a and b are strongly cospectral;

(b) The eigenvalues in S are either integers or a number that is a solution to any quadratic polynomial, and, moreover, there are integers c, Δ, d_0,..., d_k, with Δ positive and square-free, so that

$$\theta_r = \frac{1}{2}(c + d_r\sqrt{\Delta}); \tag{3.91}$$

(c) There is a non-negative integer α *so that*

- $(E_r)_{a,b} > 0$ *if and only if* $\left|(\theta_0 - \theta_r)/\sqrt{\Delta}\right|_2 < 2^\alpha$,
- $(E_r)_{a,b} < 0$ *if and only if* $\left|(\theta_0 - \theta_r)/\sqrt{\Delta}\right|_2 = 2^\alpha$.

If the above conditions hold and taking $\Delta = 1$ *if the eigenvalues are all integers, let*

$$g = \gcd\left\{\frac{\theta_0 - \theta_r}{\sqrt{\Delta}}\right\}_{\theta_r \in S}. \tag{3.92}$$

Then the minimum time we have perfect state transfer between a *and* b *is* $\tau = \frac{\pi}{g\sqrt{\Delta}}$ *and any other time it occurs is an odd multiple of* τ.

We will leave the proof aside since it dives into some algebraic number theory and it is out of the scope of this work, but the reader can find it in the references [43, 42, 39, 25].

3.5.3 Perfect state transfer in oriented graphs

We have seen continuous-time quantum walks only occurring when we are dealing with unweighted graphs. We will start to see how the addition of orientations creates some properties and change others. In particular, when we analyse perfect state transfer (PST) from this perspective, the phenomenon of universal perfect state transfer (UPST) appears which is state transfer between all vertices of a graph. All the results in this section are due to Lato and Godsil. [82]

From now on, all graphs can be considered to be orientated, do not have loops and every edge points to a unique direction. The adjacency matrix of the graph, A, is defined as

$$A_{ab} = \begin{cases} 1 & \text{if there is an edge from } a \text{ to } b \\ 0 & \text{otherwise} \end{cases}, \tag{3.93}$$

$$A_{ba} = \begin{cases} -1 & \text{if there is an edge from } a \text{ to } b \\ 0 & \text{otherwise} \end{cases}. \tag{3.94}$$

Notice that A, as above, disagrees with one of the postulates of quantum mechanics since it is not Hermitian. However, that can be solved by adding weights i to all edges, which gives a Hermitian matrix iA. This results in the time evolution operator being defined as

$$U(t) = e^{-tA}. \tag{3.95}$$

As before, perfect state transfer (PST) from vertex a to b at time τ is defined as

$$|\langle b| U(\tau) |a\rangle| = 1, \tag{3.96}$$

When we were dealing with undirected graphs the definition above meant that

$$U(\tau) |a\rangle = \gamma |b\rangle , \tag{3.97}$$

where $|\gamma| = 1$. Hence, γ can be any unitary number, but that is not the case for oriented graphs. In order to prove it, we need some properties of skew-symmetric matrices such as

Lemma 3.3.1 ([82]). *Let A be a skew-symmetric matrix with real entries. Then the real part of every eigenvalue of A is zero, and A has an orthonormal basis of eigenvectors.*

Proof. Let $|\lambda_r\rangle$ be the eigenvector of $-iA$ with eigenvalue λ_r, then

$$A |\lambda_r\rangle = (i\lambda_r) |\lambda_r\rangle . \tag{3.98}$$

Consequently, $i\lambda_r$ is an eigenvalue of A with eigenvector $|\lambda_r\rangle$. Since $-iA$ has an orthonormal basis of eigenvectors, the same applies to A. Remembering that all eigenvalues of Hermitian matrices are real, then all eigenvalues of A must be zero or imaginary. □

The other one is related to the symmetry of the eigenvalues

Lemma 3.3.2 ([82]). *Let G be an oriented graph with a skew-symmetric adjacency matrix A. If θ is an eigenvalue with idempotent E, then $-\theta$ is also an eigenvalue with corresponding idempotents $\bar{E}$.*

Proof. Since A has only real entries and θ_r no real part

$$A\bar{E} = \bar{AE} = \bar{\theta E} = \theta\bar{E}. \tag{3.99}$$

□

With that at hand, we get the result about γ that is

Lemma 3.3.3 ([82]). *If vertex a is either periodic or has perfect state transfer to vertex b, then $\gamma = \pm 1$.*

Proof. As defined, when perfect state transfer occurs from vertex a to b at time τ we have

$$\sum_r e^{\tau\theta_r} E_r |a\rangle = \gamma |b\rangle . \tag{3.100}$$

Taking the conjugate on both sides

$$\sum_r e^{-\tau\theta_r} \bar{E}_r |a\rangle = \bar{\gamma} |b\rangle . \tag{3.101}$$

As we saw before $-\theta_r$ is an eigenvalue for the idempotent $\bar{E}_r$, then

$$\bar{\gamma}\,|b\rangle = \sum_r e^{-\tau\theta_r}\bar{E}_r\,|a\rangle = \sum_r e^{\tau\theta_r}E_r\,|a\rangle = \gamma\,|b\rangle\,, \tag{3.102}$$

therefore $\gamma = \bar{\gamma}$, since $|\gamma| = 1$, then the only real number possible is $\gamma = \pm 1$. The reasoning is similar for periodicity, with the only difference being

$$\sum_r e^{\tau\theta_r}E_r\,|a\rangle = \gamma\,|a\rangle\,. \tag{3.103}$$

This gives the same conclusion that $\gamma = \pm 1$. □

In the undirected case, we saw how eigenvalues and idempotents must behave to obtain perfect state transfer. There is a similar description for oriented graphs and the first step is to prove strong cospectrality. We defined strong cospectrality between vertices a and b as vertices cospectral and parallel. As a consequence, we got the following relation

$$E_r\,|a\rangle = \pm E_r\,|b\rangle\,, \tag{3.104}$$

but we will see that Equation 3.104 is slightly different for oriented graphs. In section 3.5.2, we saw that vertices a and b are cospectral if and only if $(E_r)_{aa} = (E_r)_{bb}$, this gives the following lemma

Lemma 3.3.4 ([82]). *Vertices a and b are strongly cospectral if and only if, for all spectral idempotents E_r, there exists a complex scalar α_r with $|\alpha_r| = 1$ such that*

$$E_r\,|a\rangle = \alpha_r E_r\,|b\rangle\,. \tag{3.105}$$

Proof. For both directions, we will consider that there is an α_r such that

$$E_r\,|a\rangle = \alpha_r E_r\,|b\rangle\,. \tag{3.106}$$

Now, notice that

$$\begin{aligned}(E_r)_{aa} &= \langle a|\,E_r\,|a\rangle && (3.107)\\ &= \alpha_r\,\langle a|\,E_r\,|b\rangle && (3.108)\\ &= \alpha_r(\langle b|\,E_r^\dagger\,|a\rangle)^\dagger && (3.109)\\ & && (3.110)\end{aligned}$$

since $E_r^T = E_r$ and characteristic vectors of vertices only have real entries

$$\begin{aligned}(E_r)_{aa} &= \alpha_r(\langle \bar{b}|\,\bar{E}_r\,|\bar{a}\rangle)^T && (3.111)\\ &= \alpha_r\bar{\alpha}_r(\langle b|\,E_r\,|b\rangle) && (3.112)\\ &= |\alpha_r|(E_r)_{bb}. && (3.113)\end{aligned}$$

We saw that strongly cospectral vertices occurs if and only if $(E_r)_{aa} = (E_r)_{bb}$, then $|\alpha_r| = 1$. □

The Lemma 3.3.4 allows us to show that PST occurs for oriented graphs only between strongly cospectral vertices. The result is similar to what we know for the undirected case.

Lemma 3.3.5 ([82]). *Let G be an oriented graph with vertices a and b. If there is perfect state transfer from a to b, then a and b are strongly cospectral.*

Proof. Suppose there is perfect state transfer from a to b at time τ, then

$$\sum_r e^{\tau\theta_r} E_r \left|a\right\rangle = \pm \sum_r E_r \left|b\right\rangle , \tag{3.114}$$

or equivalently, for all r,

$$e^{\tau\theta_r} E_r \left|a\right\rangle = \pm E_r \left|b\right\rangle . \tag{3.115}$$

By multiplying both sides by $e^{-\tau\theta_r}$ we get

$$E_r \left|a\right\rangle = \pm e^{-\tau\theta_r} E_r \left|b\right\rangle = \alpha_r E_r \left|b\right\rangle , \tag{3.116}$$

where $\alpha_r = \pm e^{-\tau\theta_r}$ and, as a consequence, a and b are strongly cospectral. □

A direct consequence of the lemma above is the existence of a real number $q_r(a,b)$ that is

$$-1 \leq q_r(a,b) \leq 1, \tag{3.117}$$

and

$$E_r \left|a\right\rangle = e^{i\pi q_r(a,b)} E_r \left|b\right\rangle . \tag{3.118}$$

All the previous results allowed Lato to reach the following description for PST in oriented graphs:

Theorem 3.4 ([82]). *Let G be an oriented graph with vertices a and b. There is perfect state transfer from a to b if and only if:*

(i) Vertices a and b are strongly cospectral;

(ii) There exists some $\tau \in \mathbb{R}$ such that, for all θ_r that is in the eigenvalue support of a,

$$q_r(a,b) + \frac{i\tau\theta_r}{\pi} \tag{3.119}$$

is always an even integer or always an odd integer.

Proof. It was proved previously that perfect state transfer occurs only when the vertices are strongly cospectral, then (ii) is all that is left to prove. Perfect state transfer occurs if and only if there is some time $\tau \in \mathbb{R}$ and some phase factor ± 1 such that

$$e^{\tau\theta_r} E_r \left|a\right\rangle = \pm E_r \left|b\right\rangle = e^{i\pi q_r(a,b)} E_r \left|a\right\rangle . \tag{3.120}$$

If the phase factor is 1, this is equivalent to saying that for all θ_r in the eigenvalue support a,

$$e^{\tau\theta_r - i\pi q_r(a,b)} = 1. \tag{3.121}$$

As a consequence, there is an integer k_r such that

$$\tau\theta_r - i\pi q_r(a,b) = 2k_r i\pi. \tag{3.122}$$

Multiplying the above equation by $\frac{i}{\pi}$ shows that perfect state transfer can only occurs with phase factor 1 if and only if

$$\frac{i\tau\theta_r}{\pi} + q_r(a,b) \tag{3.123}$$

is always an even integer. A similar reasoning can be applied when the phase factor is equal to -1. In such a case, there is an integer k_r such that

$$\tau\theta_r - i\pi q_r(a,b) = (2k_r+1)i\pi, \tag{3.124}$$

or equivalently

$$\frac{i\tau\theta_r}{\pi} + q_r(a,b) \tag{3.125}$$

is always an odd integer. □

As we saw before, when PST occurs, periodicity is also present at time 2τ. Due to the difficulty of characterizing the former, it is convenient to do it for the latter since it applies to both. Therefore, Lato and Godsil proved the following theorem

Theorem 3.5 ([82]). *Let G be a connected graph with at least two vertices. Then the following are equivalent:*

(i) The vertex a is periodic;

(ii) For all r, s with θ_r, θ_s in the eigenvalue support of a and $\theta_s \neq 0$, the ratio $\frac{\theta_r}{\theta_s}$ is rational;

(iii) There exists a square-free positive integer Δ such that all eigenvalues in the eigenvalue support of a are in $\mathbb{Z}(\sqrt{-\Delta})$.

The proof of the above theorem requires some understanding of field theory and, since it was not introduced in this work, we will not exhibit here. The curious reader can find it in the reference [82].

3.5.4 Universal perfect state transfer

The addition of orientation makes it possible to find graphs that have PST between every pair of vertices. This property is called universal perfect state transfer (UPST) and all the results in this section come from the work of Connelly *et al.* and Cameron *et al.* [32, 81].

Before we characterize UPST, we will see an example of a graph that has such property. Consider the following Hamiltonian of a cycle with three vertices C_3:

$$C_3 = \begin{pmatrix} 0 & -i & i \\ i & 0 & -i \\ -i & i & 0 \end{pmatrix}. \tag{3.126}$$

Let $\omega = e^{\frac{2\pi i}{3}}$, then, since C_3 spectral decomposition is known [20] and it has eigenvalues $\lambda_0 = 0$, $\lambda_1 = \sqrt{3}$, $\lambda_2 = -\sqrt{3}$. Hence, we have that

$$e^{-itC_3} = \frac{1}{3}\begin{pmatrix} 1 & 1 & 1 \\ 1 & 1 & 1 \\ 1 & 1 & 1 \end{pmatrix} + \frac{e^{-it\sqrt{3}}}{3}\begin{pmatrix} 1 & \bar{\omega} & \omega \\ \omega & 1 & \bar{\omega} \\ \bar{\omega} & \omega & 1 \end{pmatrix} + \frac{e^{it\sqrt{3}}}{3}\begin{pmatrix} 1 & \omega & \bar{\omega} \\ \bar{\omega} & 1 & \omega \\ \omega & \bar{\omega} & 1 \end{pmatrix}. \tag{3.127}$$

If we start our walk at 0, the quantum walk will give

$$e^{-itC_3}|0\rangle = \frac{1}{3}\begin{pmatrix} 1 + 2\cos\left(t\sqrt{3}\right) \\ 1 + 2\cos\left(t\sqrt{3} - 2\pi/3\right) \\ 1 + 2\cos\left(t\sqrt{3} + 2\pi/3\right) \end{pmatrix}. \tag{3.128}$$

Therefore, we have PST from 0 to itself at time $t = 2\pi/\sqrt{3}$, from 0 to 1 at time $t = 8\pi/(3\sqrt{3})$, and from 0 to 2 at time $t = 4\pi/(3\sqrt{3})$. To give a glimpse of the results in the literature about UPST, we will introduce two preliminary concepts: circulant graphs and switching isomorphism.

Circulant graphs

A circulant graph is a graph whose adjacency matrix is circulant. A $n \times n$ circulant matrix $C = \mathrm{Circ}(v)$ defined by the sequence $v = \{a_0, \ldots, a_{n-1}\}$ is given by

$$C = \begin{pmatrix} a_0 & a_1 & a_2 & \ldots & a_{n-1} \\ a_{n-1} & a_0 & a_1 & \ldots & a_{n-2} \\ a_{n-2} & a_{n-1} & a_0 & \ldots & a_{n-3} \\ \vdots & \vdots & \vdots & \ldots & \vdots \\ a_1 & a_2 & a_3 & \ldots & a_0 \end{pmatrix}. \tag{3.129}$$

Notice that if we deal with Hermitian matrices in quantum mechanics, then an additional condition for all adjacency matrices is that $a_j = a_{n-j}$.

The usefulness of circulant matrices rests in the fact that its eigenvalues and eigenvectors can be easily found. Let $\Theta_n = \mathrm{Circ}(0, 0, \ldots, 1)$ denote the circulant matrix that represents the n-cycle permutation, then

$$\Theta_n = \begin{pmatrix} 0 & 0 & \ldots & 0 & 1 \\ 1 & 0 & \ldots & 0 & 0 \\ 0 & 1 & \ldots & 0 & 0 \\ \vdots & \vdots & \vdots & \vdots & \vdots \\ 0 & 0 & \ldots & 1 & 0 \end{pmatrix}. \tag{3.130}$$

It is possible to characterize circulant matrices by constructing polynomials with Θ_n. The circulant matrix C, for example, can be written as

$$C = \sum_{k=1}^{n} a_{n-k}\Theta_n^k. \tag{3.131}$$

Let $\omega_n = e^{\frac{i2\pi}{n}}$ be the principal n-th root of unity. The Fourier matrix, $\mathcal{F}_n$ of order n is a unitary matrix with its entries being $\langle j|\,\mathcal{F}_n\,|i\rangle = \omega_n^{ij}/\sqrt{n}$ for each $i, j \in \{0, 1, \ldots, n-1\}$. A known fact is that $\mathcal{F}_n$ diagonalizes any circulant C,

$$\mathcal{F}_n^\dagger A \mathcal{F} = \begin{pmatrix} \lambda_0 & 0 & \ldots & 0 \\ 0 & \lambda_1 & \ldots & 0 \\ \vdots & \vdots & \ldots & \vdots \\ 0 & 0 & \ldots & \lambda_{n-1} \end{pmatrix}. \tag{3.132}$$

By the equation above, we can write an expression for each eigenvalue of C as

$$\lambda_k = \sum_{j=0}^{n-1} a_j \omega_n^{kj}, \tag{3.133}$$

and eigenvectors given by

$$|\lambda_j\rangle = \frac{1}{\sqrt{n}}(1, w^j, w^{2j}, \ldots, w^{(n-1)j})^T, \tag{3.134}$$

for $j = 0, \ldots, n-1$.

More about circulant graphs can be found in Godsil and Royle [20].

Switching automorphism

A monomial matrix $n \times n$ is a product of a permutation matrix P_ν, where ν is a permutation of n elements and a complex diagonal matrix D of size n. If $\nu(j) = i$, then the

(i,j)-entry of the permutation matrix is given by $(P_\nu)_{ij} = i$ for each $i,j \in \{1,\dots,n\}$. It can be easily seen that any monomial matrix is a unitary matrix since

$$(P_\nu D)^\dagger = \bar{D}P_\nu^T = (P_\nu D)^{-1}, \tag{3.135}$$

where it was used the fact that $P_\nu^T = P_\nu^{-1}$. All eigenvalues of unitary matrices are complex numbers of modulus equal to 1 and this applies to the monomial matrices. From now on, we will not focus on D, since it is only a scaling matrix, and what will be important for us is the permutation action of ν. We will use $\tilde{P}_\nu = P_\nu D$ to simplify the notation.

It is clear that the identity is a monomial matrix and notice that the set of monomial matrices is closed under multiplication, as

$$\tilde{P}_{\nu_1}\tilde{P}_{\nu_2} = (P_{\nu_1}D_1)(P_{\nu_2}D_2) = P_{\nu_1}P_{\nu_2}\hat{D}_1 D_2 = \tilde{P}_{\nu_1\circ\nu_2}, \tag{3.136}$$

where the (j,j) entry of $\hat{D}_1$ is equal to the $(\nu_2(j),\nu_2(j))$ of D_1. Evidently, the set of monomial matrices form a group under multiplication.

Two Hermitian graphs, which are graphs that have a Hermitian adjacency matrix, G_1 and G_2 are switching isomorphic, or $G_1 \simeq G_2$, if there is a monomial matrix $\tilde{P}_\nu$, where ν is a permutation that sends a vertex from G_2 to G_1, with

$$A(G_2) = \tilde{P}_\nu^\dagger A(G_1)\tilde{P}_\nu = (P_\nu D)^\dagger A(G_1)(P_\nu D). \tag{3.137}$$

The group of switching automorphism, $\mathrm{SwAut}(G)$ is the group of monomial matrices that commutes with $A(G)$, i.e.

$$\mathrm{SwAut}(G) = \{\tilde{P}_\nu : A(G)\tilde{P}_\nu = \tilde{P}_\nu A(G)\}. \tag{3.138}$$

Note that if $P_\nu D_1$ and $P_\nu D_2$ are both in $\mathrm{SwAut}(G)$, then $D_1 = \gamma D_2$ for some $\gamma \in \mathbb{C}$.

Characterization of UPST

This subsection aims to give a characterization of graph properties that allow its occurrence. As we will see, there is a limit in the number of vertices and, also, the graphs must be switch isomorphic to circulant graphs. Although the former result comes from interesting graph properties, it limits the application of UPST in long-distance communication since the number of vertices cannot go over 11.

UPST is PST from a vertex a to all vertices of the graph [32]. Therefore, we will show two important lemmas that will be used to prove other theorems. The first lemma proves that USPT implies periodicity:

Lemma 3.5.1 ([81]). *Let G be a graph with universal perfect state transfer. Then, G is periodic.*

The second lemma is the relation between eigenvalues of the adjacency matrix of the graph that has UPST.

Lemma 3.5.2 ([43]). *Let G be a graph with universal perfect state transfer whose adjacency matrix $A(G)$ satisfies $\operatorname{Tr} A(G) = 0$. Then, for any eigenvalues $\lambda_j \neq \lambda_k$, with $\lambda_k \neq 0$, the ratio λ_j/λ_k is rational.*

The first step is to prove that whenever a graph G has PST from vertex a to vertex $\nu(a)$ for some automoprhism ν of G, then the unitary matrix e^{-itA} is equal to the monomial matrix $\tilde{P}_\nu$ up to scaling.

Lemma 3.5.3 ([81]). *Let G be an n-vertex graph with perfect state transfer from vertex a to vertex $\nu(a)$ at time t, for some switching automorphism $\tilde{P}_\nu \in SwAuto(G)$. Then*

$$e^{-itA(G)} = \gamma \tilde{P}_\nu, \tag{3.139}$$

for some $\gamma \in \mathbb{C}$.

Proof. Let $\lambda_1, \ldots, \lambda_n$ be the eigenvalues of A and $e^{i\theta_1}, \ldots, e^{i\theta_n}$ be the eigenvalues of $\tilde{P}_\nu$ for $\theta_k \in \mathbb{R}$, since it is a monomial matrix. Since $\tilde{P}_\nu \in \mathrm{SwAuto}(G)$, then A and $\tilde{P}_\nu$ commutes. As a consequence they share the same basis of eigenvectors $\{|x_1\rangle, \ldots, |x_n\rangle\}$. We get that

$$A = \sum_{k=1}^{n} \lambda_k |x_k\rangle\langle x_k|, \qquad \tilde{P}_\nu = \sum_{k=1}^{n} e^{i\theta_k} |x_k\rangle\langle x_k|. \tag{3.140}$$

Since G has perfect state transfer from a to $\nu(a)$ at time t, then

$$1 = \left|\langle a| \tilde{P}_\nu^\dagger e^{-itA} |a\rangle\right| = \left|\sum_{k=1}^{n} e^{-i(t\lambda_k+\theta_k)} \langle a|x_k\rangle \langle a|x_k\rangle\right| \leq \sum_{k=1}^{n} |\langle a|x_k\rangle|^2 = 1, \tag{3.141}$$

where the last equality comes from $\sum_{k=1}^{n} |x_k\rangle\langle x_k| = I$. Hence, there is a number $\alpha \in \mathbb{R}$ so that $e^{-i(t\lambda_k+\theta_k)} = e^{i\alpha}$, for each $k = 1, \ldots, n$. Thus we have

$$e^{-itA} = \sum_{k=1}^{n} e^{-it\lambda_k} |x_k\rangle\langle x_k| = e^{i\alpha} \sum_{k=1}^{n} e^{i\theta_k} |x_k\rangle\langle x_k| = e^{i\alpha} \tilde{P}_\nu. \tag{3.142}$$

□

Before we move on to some of the main theorems, we will see a lemma that is a result of Cameron *et al.* [81]. We will see proof that UPST only occurs at specific times, as we expected since it is the same for PST.

Lemma 3.5.4. *[81] Let G be a graph with universal perfect state transfer. Then, the set*

$$\Gamma = \{t \in \mathbb{R} : (\exists \phi \in SwAut(G))(\exists \gamma \in \mathbb{C})[e^{-itA} = \gamma \tilde{P}_\nu]\} \tag{3.143}$$

is a discrete additive subgroup of $\mathbb{R}$.

Now, we will see two theorems that describe the graph structures for UPST occurrence. The first one goes as follows

Theorem 3.6 ([81]). *Let G be a graph with universal perfect state transfer. Then, the switching automorphism group SwAut(G) is cyclic.*

Proof. Let G be a graph with Hermitian adjacency matrix A, as before Γ is the discrete subgroup of $\mathbb{R}$, and $\gamma_0, \gamma_1, \ldots$ are complex numbers of unit modulus. Consider that the last positive element of Γ is t^* and let $\tilde{P}\nu^* \in \mathrm{SwAut}(G)$ be the switching automorphism for which $e^{-it^*A} = \gamma_0 \tilde{P}_{\nu^*}$.

The first step is to prove that every element of Γ is an integer multiple of t^*. Suppose that $e^{-it_1A} = \gamma_1 \tilde{P}_\psi$ for some $\tilde{P}_\psi \in \mathrm{SwAut}(G)$ and $mt^* < t_1 < (m+1)t^*$ for some non-negative integer m. Then

$$e^{-i(t_1 - mt^*)A} = e^{-it_1A}(e^{-it^*A})^m \tag{3.144}$$
$$= \gamma_1 \tilde{P}_\psi (\gamma_0 \tilde{P}_{\nu^*})^m \tag{3.145}$$
$$= (\gamma_0^m \gamma_1) \tilde{P}_\psi \tilde{P}_{(\nu^*)^m} \tag{3.146}$$
$$= (\gamma_0^m \gamma_1 \gamma_2) \tilde{P}_{\psi \circ (\nu^*)^m}, \tag{3.147}$$

which is a contradiction since t^* was defined as the minimum of Γ and $t^* > t_1 - mt^*$.

Now, fix a vertex a of G and define $\psi(a) = b$ with $\tilde{P}_\psi |a\rangle = \gamma_3 |b\rangle$. Since G has universal perfect state transfer, there is a time t_2 that

$$e^{-it_2A} |a\rangle = \gamma_4 |b\rangle = (\gamma_3^{-1}\gamma_4) \tilde{P}_\psi |a\rangle = \gamma \tilde{P}_\psi |a\rangle . \tag{3.148}$$

Therefore, for each $\tilde{P}_\psi \in \mathrm{SwAut}(G)$, there is a time t_2 that is a multiple of t^* as it was proved before. As a consequence we have that

$$\gamma \tilde{P}_\psi = e^{-it_2A} = (e^{-it^*A})^m = \gamma_0^m \tilde{P}_{\nu^*}^m, \tag{3.149}$$

which shows that $\psi = (\nu^*)^m$ and $\mathrm{SwAut}(G) = \langle \nu^* \rangle$. □

It is possible to describe which graphs have universal perfect state transfer and it will be the following theorem.

Theorem 3.7 ([81]). *Let G be a n-vertex graph with universal perfect state transfer. Then, SwAut(G) is cyclic of order n if, and only if, G is switching isomorphic to a circulant.*

Proof. Suppose that $\mathrm{SwAut}(G)$ is cyclic of order n and A is the Hermitian adjacency matrix of the graph G. Let $\tilde{P}\nu^*$ be the generator of $\mathrm{SwAut}(G)$ then, since $\tilde{P}_{\nu^*}$ has no fixed point as it was proved by Cameron *et al.* [81] and has order n, its structure is of a n-cycle. Without loss of generality, we may assume $\nu^* = (1, 2, \ldots, n)$ which means that $\Theta_n = \tilde{P}_{\nu^*} \in \mathrm{SwAut}(G)$. Therefore, A commutes with Θ_n and it is also a circulant matrix since they share the same basis of eigenvectors.

Now for the converse, suppose that G is switching isomorphic to a circulant matrix. Then, it is possible to write A as $A = \tilde{P}^\dagger C \tilde{P}$ for some circulant matrix C and monomial matrix $\tilde{P}$. The previous theorem showed that $\mathrm{SwAut}(G)$ is cyclic of order n and Cameron showed that, in such cases, the order of the group divides n. We saw that any circulant matrix is a polynomial in Θ_n, then we can write $C = f(\Theta_n)$ for some polynomial $f(x)$. Consider the monomial matrix $Q = \tilde{P}^\dagger \Theta_n \tilde{P}$ and notice that

$$A = \tilde{P}^\dagger f(\Theta_n)\tilde{P} = f(\tilde{P}^\dagger \Theta_n \tilde{P}) = f(Q), \tag{3.150}$$

where it was used the fact that $\tilde{P}$ is unitary. This shows that A and Q commutes, since A is a polynomial in Q. Then $Q \in \mathrm{SwAut}(G)$ and Q has order n since Θ_n has order n. So, $\mathrm{SwAut}(G)$ has order n due to the fact that one of its elements has order n. □

Cameron *et al.* [81] conjectured in their work that K_2 and K_3 are the only oriented graph with UPST. This was proved in a recent work by Acuaviva *et al.* [1] and the following theorems are the results from their work.

First, we will see how bounds to the eigenvalues of UPST graphs limits the maximum number of edges they can have. We will start with the following lemma:

Lemma 3.7.1 ([1]). *Let G be an oriented graph with universal perfect state transfer. If any two vertices of G are strongly cospectral, then the eigenvalues of A are all simple and its matrix of eigenvectors is flat, i.e. all of its entries have the same magnitude.*

Proof. We saw in Lemma 3.3.4 that there are complex scalar α_r of norm one such that

$$E_r |a\rangle = \alpha_r E_r |b\rangle . \tag{3.151}$$

Therefore each column of E_r is a scalar multiple of the column $E_r |a\rangle$, since all vertices are strongly cospectral, so $\mathrm{rank}(E_r) = 1$. Notice that

$$|\langle a| E_r |a\rangle| = |\alpha_r||\langle a| E_r |b\rangle| = |\langle a| E_r |b\rangle|, \tag{3.152}$$

then, since $|\alpha_r| = 1$, each row of E_r is flat. Since E_r is Hermitian, it itself is flat. □

Then we have the following lemma that will bound the minimum distance of eigenvalues for graphs oriented with i.

Lemma 3.7.2 ([1]). *Let G be an oriented graph and A its adjacency matrix. A will be a skew-symmetric $n \times n$ matrix and let σ denote the minimum distance between two eigenvalues of A. Then*

$$\sigma^2 \leq \frac{12}{n+1}. \tag{3.153}$$

Proof. Assume that $\lambda_1, \ldots, \lambda_n$ are the eigenvalues of A in non-increasing order. Remember that these eigenvalues are purely imaginary. Equivalently iA is Hermitian and its eigenvalues are real, we set $\lambda_j = i\theta_j$.

If

$$M = A \otimes I - I \otimes A, \tag{3.154}$$

then the eigenvalues of M are the numbers

$$i(\theta_j - \theta_k),\ 1 \leq j, k \leq n. \tag{3.155}$$

Now

$$M^2 = A^2 \otimes I + I \otimes A^2 - 2A \otimes A, \tag{3.156}$$

and, if m is the number of edges in the graph underlying A, then

$$\sum_{j,k=1}^{n} (\theta_j - \theta_k)^2 = -\operatorname{Tr}\big(M^2\big) = 2n \operatorname{Tr}\big(-A^2\big) = 2n \operatorname{Tr}\big(AA^T\big) = 4nm, \tag{3.157}$$

where it was used that A is skew-symmetric and AA^T counts the number of edges of G. Since $\theta_j - \theta_k \geq (j-k)\sigma$, we have

$$\sum_{j,k=1}^{n} (\theta_j - \theta_k)^2 \geq \sigma^2 \sum_{j,k=1}^{n} (j-k)^2. \tag{3.158}$$

We can write the summation on the right side as

$$\sum_{j,k=1}^{n} (r-s)^2 = \sum_{j,k=1}^{n} j^2 + \sum_{j,k=1}^{n} k^2 - 2\sum_{j,k=1}^{n} jk \tag{3.159}$$

$$= 2n \sum_{j=1}^{n} j^2 - 2\left(\sum_{j=1}^{n} j\right)^2. \tag{3.160}$$

Notice that

$$\sum_{j=1}^{n} j^2 = \frac{n(n+1)(2n+1)}{6}, \tag{3.161}$$

then

$$\sum_{j,k=1}^{n} (r-s)^2 = \frac{n^2(n^2-1)}{6}. \tag{3.162}$$

Since $m \leq n(n-1)/2$, it gives that

$$\sigma^2 \frac{n^2(n^2-1)}{6} \leq 4nm \leq 2n^2(n-1). \tag{3.163}$$

This gives the stated bound. □

Lemma 3.7.2 allowed them to conclude a result that bounds the number of vertices for universal perfect state transfer.

Corollary 3.7.1 ([1]). *If we have universal perfect state transfer on the oriented graph G, then $|V(X)| \leq 11$. Additionally, if $n \geq 6$, then G has integer eigenvalues.*

Proof. The first result comes as a direct result of the above lemma. As we saw before, the eigenvalues of G must be in $\mathbb{Z}\sqrt{\Delta}$, then $\sigma^2 \geq \Delta \geq 1$. However, for $n \geq 6$, the previous lemma tells us $\sigma^2 < 2$, which leads to $\Delta = 1$. □

Now, we are ready for the main theorem:

Theorem 3.8 ([1]). *The oriented K_2 and K_3 are the only oriented graphs admitting universal perfect state transfer.*

Proof. If a graph G with n vertices has UPST, then its underlying graph is k-regular for some integer k. As we saw before, let $\theta_0 < \cdots < \theta_j$ be the eigenvalues associated with the Hermitian matrix H of the oriented graph, then $\theta_i \in \mathcal{Z}\sqrt{\Delta}$ for some positive square-free integer Δ. The characteristic polynomial of H must be equal to the characteristic polynomial of its underlying graph over $\mathbb{Z}_2$ and, additionally, since H is skew-symmetric, then

$$\theta_r = -\theta_{n-r-1} \; \forall r = 1, \ldots, n. \tag{3.164}$$

After remembering all those results, we are ready for an exhaustive search for all graphs with less than 12 vertices.

When $n = 4, 5$, the only regular graphs are K_n and C_n. An inspection of the spectrum of those graphs makes it clear that they do not satisfy the above criteria.

When we analyse $n \geq 6$, then, from the previous result, we notice that

$$\frac{n^2 - 1}{12} \leq k \leq n - 1. \tag{3.165}$$

All that is left is to check graphs from 6 vertices to 11 that satisfy all of those criteria. The above bounds gives us the following possibilities Each entry of k-th power of the

n	6	7	8	9	10	11
k	3,4,5	4,6	6,7	8	9	10

adjacency matrix, $(H^k)_{ij}$, counts the number of walks between vertex i and j. So, the diagonals elements of H^2 counts the number of neighbours in the graph. This leads to the following, when considering that H is skew-symmetric, for $\mathrm{Tr}(H^2)$:

$$nk = 2 \sum_{r=1}^{\lfloor \frac{n+1}{2} \rfloor} \theta_r^2. \tag{3.166}$$

Direct computation returns an integral value for this relation only for the following cases

n	k	underlying graph	spectrum of iH
11	10	K_{11}	$0, \pm i, \pm 2i, \pm 3i, \pm 4i, \pm 5i$
7	6	K_7	$0, \pm i, \pm 2i, \pm 4i$
7	4	$\bar{C}_7$	$0, \pm i, \pm 2i, \pm 3i$

It is possible to check that the characteristic polynomial of the underlying graph is not equal to the characteristic polynomial constructed with the above eigenvalues over $\mathbb{Z}_2$. Therefore, there isn't a graph with UPST for $n \geq 4$. □

Chapter 4

Quantum walks on oriented graphs

4.1 Introduction

In the previous chapter, two different models of quantum walks were presented with some of their applications. We saw how discrete-time quantum walks are connected to Grover's algorithm and how continuous-time quantum walks allow the transfer of a state from one vertex to another. The addition of orientation created new and interesting phenomena that were unachievable in undirected graphs. In order to increase the current knowledge about oriented graphs and continuous-time quantum walks, this chapter will be devoted to presenting our original results related to it.

First, we will present our first result: how to efficiently simulate continuous-time quantum walks of circulant graphs in quantum computers [56]. As we saw, the simulation of quantum walks is one of the challenges related to quantum computing and we propose a method that only requires two quantum Fourier transforms and a diagonal unitary.

The following result is a physically realizable Hamiltonian with subspaces that are adjacency matrices of oriented graphs. The result is similar to the undirected case that we saw previously. Phenomena associated with orientation are not only related to UPST, but we also have zero-transfer, which is a lack of probability of finding the walker in a specific vertex of some graphs. This characteristic was discovered in cycle graphs with some orientations and, seeking to shed light on why it occurs, we tackle the problem from an algebraic graph theory perspective. This allows us to make a connection between the occurrence of zero transfer and the degeneracy of the Hamiltonian subspaces.

As we saw previously, a wavefunction in quantum walks spreads quadratically faster than its correspondent random walk. However, a known result in the literature, shows that the diffusion rate of the wavefunction can be cubically faster for some initial conditions. Our results show that this can also be obtained for certain orientations.

4.2 Quantum walks simulation in a superconductor quantum computer

Our first result will be presented in this section and it is related to the simulation of continuous-time quantum walks in superconductor computers [56]. We aim to answer the following question: how can algebraic graph theory assist in the simulation of quantum walks? Usually, quantum walks require a lot of multi-controlled qubit gates that create a lot of noise in current noisy devices. Here, we will see that continuous-time quantum walks in circulant graphs can be done efficiently with the assistance of the quantum Fourier transform.

4.2.1 Quantum Fourier Transform

The quantum Fourier transform is an implementation of the discrete Fourier transform over amplitudes of quantum states. It is a subroutine for many quantum algorithms like Shor's factoring and quantum phase estimation.

This transform can be described as the following operation over an orthonormal basis $\{|0\rangle, |1\rangle, \cdots, |N-1\rangle\}$,

$$U_{QFT}(|j\rangle) = \frac{1}{\sqrt{N}} \sum_{k=0}^{N-1} e^{\frac{2\pi ijk}{N}} |k\rangle. \tag{4.1}$$

This can be rewritten as a product

$$U_{QFT}(|j_1, \ldots, j_n\rangle) = \frac{(|0\rangle + e^{2\pi i 0.j_n} |1\rangle) \cdots (|0\rangle + e^{2\pi i 0.j_{n-1}j_n} |1\rangle)}{2^{\frac{N}{2}}}, \tag{4.2}$$

where $[0.j_1 \ldots j_n]$ is the fractional binary notation defined as

$$[0.j_1 \ldots j_n] = \sum_{k=1}^{m} j_k 2^{-k}. \tag{4.3}$$

This is a very useful representation because it makes constructing an efficient circuit much more simple, as well as proving that the quantum Fourier transform is unitary. However, the circuit implementation of the QFT requires $O(n^2)$ phase-shift gates. This can be contrasted with the classical implementation of a fast-Fourier transform that has complexity $O(n2^n)$ where n is the number of qubits.

For applications that do not require precise calculations of the Fourier transform, the phase-shift operations between the most distant qubits can be omitted while maintaining reasonable accuracy [24]. More specifically, given a certain positive integer threshold m, the approximate quantum Fourier transform (AQFT) circuit is generated by removing gates that perform rotations R_p, whenever $m > p$, from the original quantum Fourier transform circuit, as is shown in figure 4.1. The output states can be defined as

$$|y_i\rangle = \begin{cases} \frac{1}{\sqrt{2}}(|0\rangle + e^{2\pi i(0.j_i \cdots j_n)} |1\rangle\,, & n-m < i \leq n \\ \frac{1}{\sqrt{2}}(|0\rangle + e^{2\pi i(0.j_i \cdots j_{i+m-1})} |1\rangle\,, & 1 < i \leq n-m \end{cases}. \tag{4.4}$$

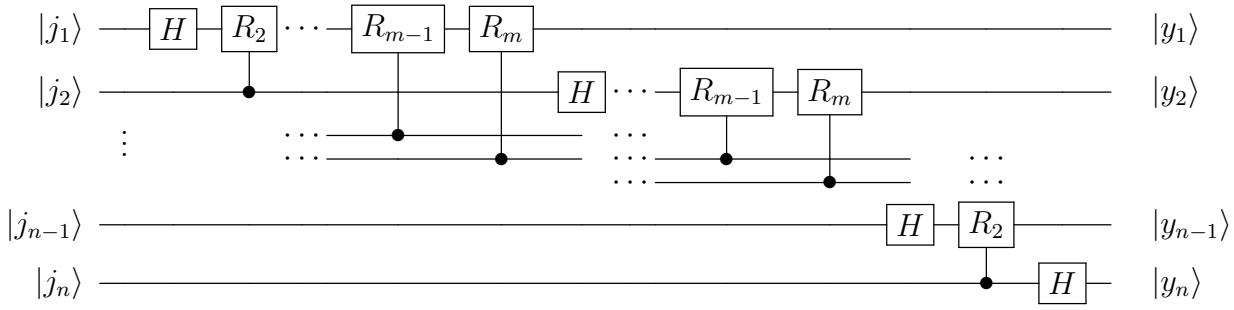

Figure 4.1: AQFT Quantum Circuit

4.2.2 Circulant graphs and the Quantum Fourier Transform

Given a graph G and its underlying adjacency matrix A, as we saw, we can describe a CTQW by the equation

$$|\psi(t)\rangle = e^{-iAt} |\psi(0)\rangle\,, \tag{4.5}$$

where A is assuming the role of the Hamiltonian [33]. Throughout this work, the circulant class of graphs will be considered again. Remember that this kind of graph is defined by a circulant matrix, such that

$$A = \begin{bmatrix} c_0 & c_{N-1} & \cdots & c_2 & c_1 \\ c_1 & c_0 & c_{N-1} & & c_2 \\ \vdots & c_1 & c_0 & \ddots & \vdots \\ c_{N-2} & & \ddots & \ddots & c_{N-1} \\ c_{N-1} & c_{N-2} & \cdots & c_1 & c_0 \end{bmatrix}. \tag{4.6}$$

Considering a simple graph, the adjacency matrix in (4.6) should have some constraints: firstly, $c_0 = 0$ by the absence of self-loops; secondly, the matrix must be symmetric, meaning that $c_{n-j} = c_j$.

To construct the quantum circuit, notice that the circulant matrix is diagonalizable by the Fourier transform, such that the eigenvalues are

$$\lambda_p = c_0 + \sum_{q=1}^{N} c_{N-q}\omega^{pq}. \tag{4.7}$$

where $\omega = e^{2i\pi/N}$. We can then construct an operator which diagonalizes the circulant graph and we can define the unitary operator for the CTQW as

$$U = U_{QFT}^{\dagger} e^{i\Lambda t} U_{QFT} \tag{4.8}$$

where U_{QFT} will be the unitary associated with the QFT, and

$$e^{i\Lambda t} = \sum_{j} e^{i\lambda_j t} |j\rangle \langle j| \tag{4.9}$$

is a diagonal operator which is implemented using multiplexors [88, 84]. We aim to show that even with AQFT, this efficient way of implementing a quantum walk already yields fidelities very similar to the ideal probability distribution.

4.2.3 Simulation in a Quantum Computer

First, we construct our circuits, as is shown in figure 4.2.

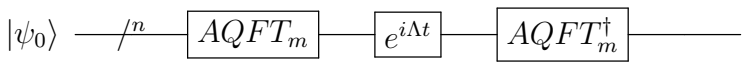

Figure 4.2: Circuit for the continuous-time quantum walk.

The Qiskit[1] package is then used to submit our jobs to IBM's *Toronto* backend. To construct this circuit, we use two features in the package. The first one is a function that constructs AQFT by inputting the number of qubits, n, and approximation degree. The second one is a unitary diagonal matrix constructor that allows the creation of diagonal gates in the circuit. Notice that the exponential gate dictates the time evolution of the system and only discrete times can be simulated. Since the Hamiltonian used for the simulation is a simple adjacency matrix of a graph, we believe that there isn't a phase

[1]One of the most used software development kits for quantum computing that was developed by IBM. IBM Montreal, which is now a decommissioned quantum computer, was used to create the data showed here.

transition in the quantum walk and the dynamics of the walk will be the same for every time t.

Each experiment is performed 10 times, with 3000 shots each, to extract substantial statistical data, using the confidence interval of 95%. We calculate the average fidelity between the ideal distribution $p(x,t)$ and the experimental $q(x,t)$ using the following norm:

$$F(p,q) = \frac{1}{10}\sum_{i=1}^{10}\sum_{x=0}^{N-1}\sqrt{p(x,t)q(x,t)} \tag{4.10}$$

where x is the vertex and t time, so we can compare to previous work [92]. This norm creates a way to measure the distance between two probability distributions and goes from 0 to 1. The 0 fidelity corresponds to two completely different probability distributions while 1 occurs when they are equal probability distributions.

We selected a considerable number of graphs, as is shown in figure 4.3, to observe how the effects of the AQFT differ. For instance, the graph G_1 is generated by setting c_1 and c_{n-1} to 1, and the rest of the elements to 0, and this corresponds to a cycle graph. On the other hand, graph G_2 with $N = 8$ can be described by column vector $[0,1,1,0,0,0,1,1]^T$. In this way, we can systematically construct circulant graphs varying from sparse to dense.

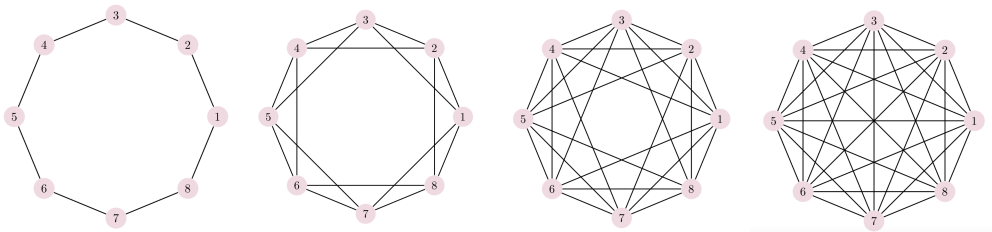

(a) G_1 (b) G_2 (c) G_3 (d) G_4

Figure 4.3: Circulant graphs G_k for $N = 8$ elements.

Figure 4.4 shows the probability distributions for the CTQW on the graph G_2, for $N = 8$ elements. The blue bar represents the quantum walk on the aer simulator, which is not a real quantum computer but an ideal simulator offered by the Qiskit package. The remaining bar plots were obtained by running the circuit on the Toronto backend, where we can see the error introduced by noise.

For the smaller $N = 4$ case, two non-isomorphic circulant graphs are possible to construct. G_1 corresponds to the cycle graph, and G_2 to the complete graph. Table 4.1 shows the achieved average fidelities, which were calculated with (4.10). Our result for the complete graph slightly outperforms Qiang's et al work [92], where they obtained a fidelity of 0.967 ± 0.003.

In the $N = 8$ case, table 4.2 shows that state fidelity is greater as graph connectivity increases, and as m increases. This is due to the fact that a greater m results in a more precise circuit due to the approximation.

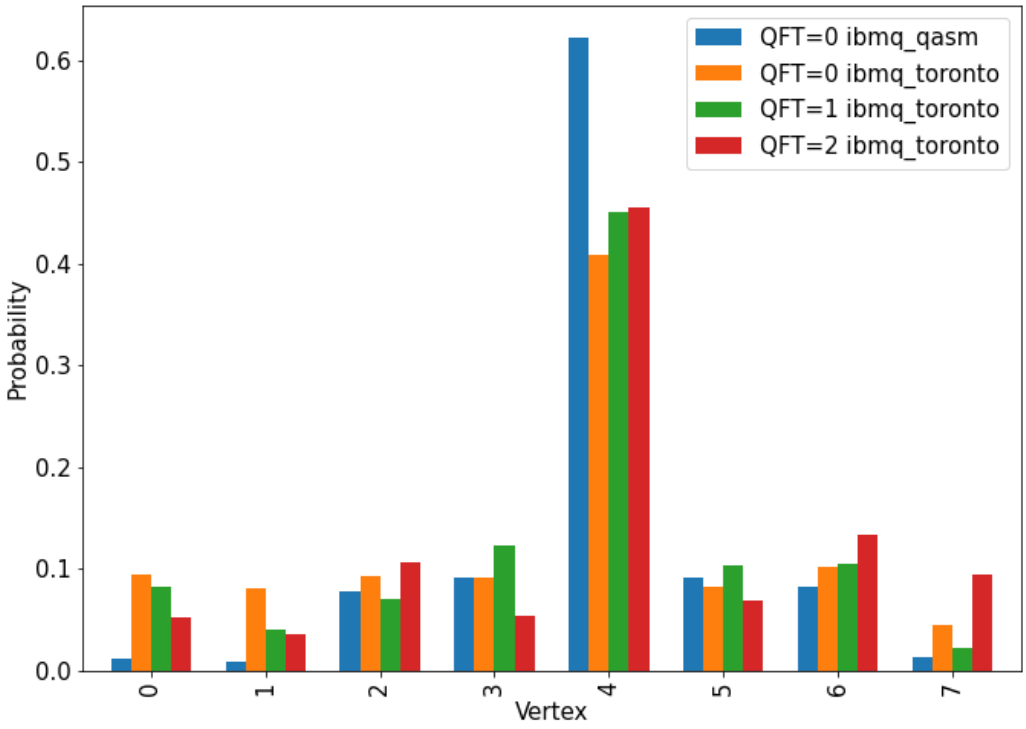

Figure 4.4: Continuous-time quantum walk for N=8 elements, with time=1 and initial condition $|\psi(0)\rangle = |4\rangle$.

m\G	G_1	G_2
0	0.98 ± 0.01	0.99 ± 0.01
1	0.98 ± 0.02	0.993 ± 0.006

Table 4.1: Fidelity of quantum state with $N = 4$, backend *Toronto*, and $t = 1$.

m\G	G_1	G_2	G_3	G_4
0	0.80 ± 0.01	0.92 ± 0.02	0.968 ± 0.007	0.965 ± 0.006
1	0.894 ± 0.007	0.95 ± 0.01	0.98 ± 0.01	0.973 ± 0.008
2	0.852 ± 0.009	0.955 ± 0.004	0.985 ± 0.003	0.990 ± 0.002

Table 4.2: Fidelity of quantum state with $N = 8$, backend *Toronto*, and $t = 1$.

Finally we consider the case where $N = 16$ is in table 4.3. Here, the behavior is similar to the previous case up to graph G_5, meaning that higher graph connectivity and larger m will result in higher fidelity. However, graphs G_6, G_7 and G_8 even though are highly connected and have relatively low depth, present lower fidelity. This is due to the fact that the probability distribution of the dynamic of the walk on these structures is highly concentrated in a small number of vertices, which means they are more susceptible to noise introduced by NISQ computers, specially readout errors due to bias. Nonetheless, the increase of m still has a positive impact on the fidelity of these circuits, as expected

since it gets closer to the real implementation of a QFT.

m\G	G1	G2	G3	G4	G5	G6	G7	G8
0	0.47 ± 0.03	0.61 ± 0.02	0.78 ± 0.02	0.86 ± 0.01	0.86 ± 0.01	0.70 ± 0.04	0.54 ± 0.03	0.49 ± 0.04
1	0.50 ± 0.03	0.63 ± 0.03	0.79 ± 0.03	0.87 ± 0.02	0.85 ± 0.03	0.70 ± 0.03	0.55 ± 0.05	0.50 ± 0.04
2	0.55 ± 0.03	0.71 ± 0.03	0.83 ± 0.02	0.90 ± 0.01	0.89 ± 0.02	0.75 ± 0.02	0.62 ± 0.04	0.59 ± 0.06
3	0.60 ± 0.03	0.70 ± 0.02	0.85 ± 0.01	0.92 ± 0.01	0.91 ± 0.01	0.80 ± 0.03	0.71 ± 0.04	0.69 ± 0.04

Table 4.3: Fidelity of quantum state with $N = 16$, backend *Toronto*, and $t = 1$.

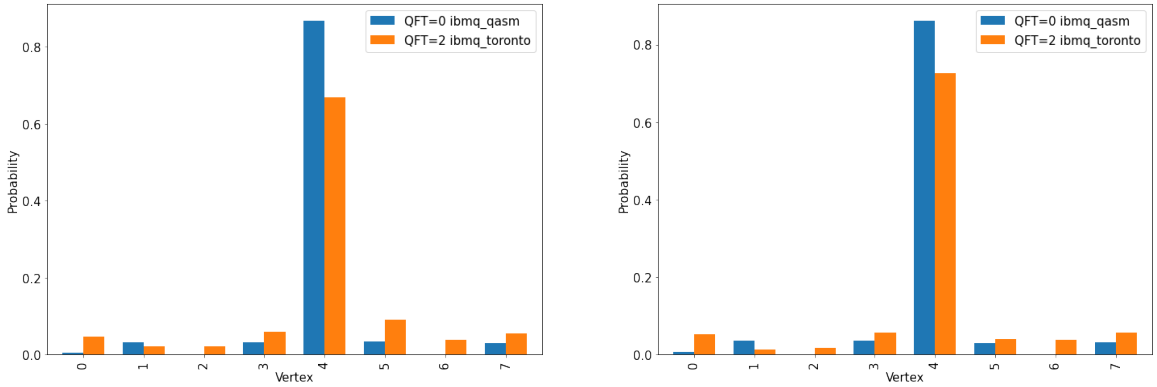

(a) $v_1 = [0, 1, 0, 0, 0, 0, 0, 1]^T$ (b) $v_2 = [0, 1, 1, 0, 1, 0, 1, 1]^T$

Figure 4.5: Pretty good state transfer for different circulant graphs defined by v.

We implemented pretty good state transfer (PGST) which is a transport phenomenon similar to PST. However, PGST occurs between vertex i and j if, for any $\epsilon > 0$, there exists a time τ_ϵ such that

$$|U(\tau_\epsilon)_{ij}| > 1 - \epsilon. \tag{4.11}$$

It was proved by Pal *et al.* [49] that PGST occurs in some classes of circulant graphs at $\tau_\epsilon = 2\pi n$, where n is a positive integer. One of those classes is cycles with 2^k vertices (C_{2^k}), where $k \geq 3$, and the other is the union $C_{2^k} \cup G(2^k)$, with $G(2^k)$ being circulant graphs with connection set given by gcd-sets of $\mathbb{Z}_{2^k}$. We chose one graph of each class, $v_1 = [0, 1, 0, 0, 0, 0, 0, 1]^T$ and $v_2 = [0, 1, 1, 0, 1, 0, 1, 1]^T$, and we obtained a fidelity of 0.93 ± 0.01 for v_1 and 0.906 ± 0.009 for v_2. Figure 4.5 shows the comparison between the simulated model in blue and the experimental result in orange.

4.3 Hamiltonians and graphs

In section 3.5.1, we presented a known result of how natural it is to use an adjacency matrix of graphs to describe a physical realizable Hamiltonian. Since the previous results

were for undirected graphs, we proved that the same happens for oriented graphs [76]. Following, we will see which Hamiltonian has subspaces described by oriented graphs as long as the orientations are complex numbers of absolute value equal to 1. This theorem follows the same steps of section 3.5.1 and it is proved similarly. These graphs are called complex unit gain graphs [79] in the literature.

In the next theorem, we will prove a result similar to the one obtained for the result in section 3.5.1, however for a Hamiltonian that can be associated with a complex unit gain graph. In physics, this Hamiltonian is associated with the Rashba effect [65, 61, 55] and a better understand of it implies a better understanding of spin-orbit couplings in semi-conductors. This effect appears when there is an external magnetic fied that induces a split in the conduction band of certain types of semiconductors.

Theorem 4.1. *The H_{xy} Hamiltonian is defined as*

$$H_\alpha = \frac{1}{2}\sum_{ij\in E(G)} \cos\alpha(X_iX_j + Y_iY_j) + \sin\alpha(X_iY_j - X_iY_j), \tag{4.12}$$

where $E(G)$ is the edge set of the graph, X and Y are Pauli matrices. The Hamiltonian is a block matrix where with each one being a k-excitation subspace. Also, the 1-subpace is described by the adjacency matrix of a unit gain graph.

Proof. Let $S \subseteq \{1,\dots,n\}$ and $\{|0\rangle, |1\rangle\}$ be the standard basis for $\mathbb{C}^2$. Define

$$|f_S\rangle = |i_1\rangle \otimes |i_2\rangle \otimes \dots |i_n\rangle, \tag{4.13}$$

where $i_r = 1$ if $r \in S$. For simplicity, we will say that

$$h_1 = \frac{\cos\alpha}{2}\sum_{ij\in A(G)} (X_iX_j + Y_iY_j), \tag{4.14}$$

$$h_2 = \frac{\sin\alpha}{2}\sum_{ij\in A(G)} (X_iY_j - X_iY_j). \tag{4.15}$$

Notice that

$$X_iX_j\,|f_S\rangle = \left|f_{S\oplus\{i,j\}}\right\rangle, \tag{4.16}$$

$$Y_iY_j\,|f_S\rangle = -(-1)^{|S\cap\{i,j\}|}\left|f_{S\oplus\{i,j\}}\right\rangle, \tag{4.17}$$

$$X_iY_j\,|f_S\rangle = i(-1)^{|S\cap\{j\}|}\left|f_{S\oplus\{i,j\}}\right\rangle, \tag{4.18}$$

where $S \oplus T$ is the symmetric difference of sets. Using that on the Hamiltonian above,

$$\begin{aligned} h_1\,|f_S\rangle &= \frac{\cos\alpha}{2}\left(1-(-1)^{|S\cap\{i,j\}|}\right)\left|f_{S\oplus\{i,j\}}\right\rangle \\ &= \begin{cases} \cos\alpha\left|f_{S\oplus\{i,j\}}\right\rangle, & \text{if } |S\cap\{i,j\}| = 1; \\ 0, & \text{otherwise} \end{cases}, \end{aligned} \tag{4.19}$$

and

$$h_2 \left|f_S\right\rangle = \frac{\sin\alpha}{2}\left(i(-1)^{|S\cap\{j\}|} - i(-1)^{|S\cap\{i\}|}\right)\left|f_{S\oplus\{i,j\}}\right\rangle$$
$$= \begin{cases} i\sin\alpha\left|f_{S\oplus\{i,j\}}\right\rangle, \text{ if } |S\cap\{i\}| = 1; \\ -i\sin\alpha\left|f_{S\oplus\{i,j\}}\right\rangle, \text{ if } |S\cap\{j\}| = 1; \\ 0, \text{ otherwise} \end{cases}. \tag{4.20}$$

As a consequence,

$$H_\alpha \left|f_S\right\rangle = \begin{cases} \sum_{ij\in E(G)}(\cos\alpha + i\sin\alpha)\left|f_{S\oplus\{i,j\}}\right\rangle, \text{ if } |S\cap\{i\}| = 1; \\ \sum_{ij\in E(G)}(\cos\alpha - i\sin\alpha)\left|f_{S\oplus\{i,j\}}\right\rangle, \text{ if } |S\cap\{j\}| = 1; \\ 0, \text{ otherwise} \end{cases}$$
$$= \begin{cases} \sum_{ij\in E(G)} e^{i\alpha}\left|f_{S\oplus\{i,j\}}\right\rangle, \text{ if } |S\cap\{i\}| = 1; \\ \sum_{ij\in E(G)} e^{-i\alpha}\left|f_{S\oplus\{i,j\}}\right\rangle, \text{ if } |S\cap\{j\}| = 1; \\ 0, \text{ otherwise} \end{cases} \tag{4.21}$$

which shows that the Hamiltonian H_α maps the k-subspace to itself. □

Similarly to the previous result, this shows that adjacency matrices of graphs arise naturally as subspaces of physical realizable Hamiltonians. Therefore, this connection justifies the study of adjacency matrices of graphs, from a physical perspective, due to the insights about 1-excitation subspaces.

From now on, we will assume that all of our Hamiltonians are written as

$$H_\alpha = e^{i\alpha}B + e^{-i\alpha}B^T, \tag{4.22}$$

for some matrix B that is responsible for the outgoing arcs while $\alpha \in \mathbb{R}$ will give the orientation. Notice that α does not need to be equal for every vertex, but it will be stated whenever they are not all equal.

4.4 Oriented finite and infinite path graph

This section will be devoted to our results on oriented path graphs [77]. As we will see, orientation can be used to change the rate at which the wavefunction spreads in infinite line graphs. First, we will see a quick review of Bessel functions. We will see the definitions that are more useful for our results and the properties that will be used in the future. A similar phenomenon can be obtained for undirected graphs when the initial conditions are non-local and it is a known result from the literature.

4.4.1 Bessel functions

Bessel functions of the first kind, $J_n(x)$, are solutions to Bessel's differential equations and have numerous representations and relations. They are widely used in physics since they are a solution to important partial differential equations related to heat dissipation. The first definition is related to the integral of cosines and is given by

$$J_n(x) = \frac{1}{\pi}\int_0^{\pi} \cos\left(n\tau - x\sin\tau\right)d\tau = \frac{1}{2\pi}\int_{-\pi}^{\pi} e^{i(n\tau - x\sin\tau)}d\tau. \tag{4.23}$$

The convergence radius is infinity for all Bessel functions [62] and it has an oscillatory behavior that will be evident in the dynamics of the infinite line.

Throughout this chapter, we will need some properties from the Bessel equations. One of them is a different way to define the Bessel functions:

$$\tilde{J}_n(x) = i^n J_n(x), \tag{4.24}$$

and it will be very present in our demonstrations. Also, the following recurrence relations will be crucial to understand some of the results

$$J_{n+1}(x) + J_{n-1}(x) = \frac{2n}{x}J_n(x), \tag{4.25}$$

and

$$J_{n+1}(x) - J_{n-1}(x) = 2J_n^{'}(x), \tag{4.26}$$

Finally, we will also need

$$J_{-n}(x) = (-1)^n J_n(x). \tag{4.27}$$

The connection between line graphs and Bessel functions is known in other contexts [5, 45, 90, 18]. However, the connection between the Bessel functions and unitary gain graphs is not present in the literature. That is what we are going to analyze in the next section.

4.4.2 Survival probability on finite path graphs

One way to associate the spread of the wavefunction through a graph is by analyzing the survival probability. Define $v \in \mathbb{Z}^+$ then we can define the survival probability as

$$P_v(t) = \sum_{k=-v}^{v} P_k(t), \tag{4.28}$$

where $P_k(t)$ is the mean probability of finding the walker on vertex k[66]. In short, we are defining a box containing vertices from $-p$ to p and verifying how likely it is for the walker to be inside it. It is shown that in classical random walks, $P_s(t)$ decays with $t^{-\frac{1}{2}}$ while for discrete-time quantum walks with the initial condition centered in one vertex it decays with t^{-1}[38]. We aim to show a result by Abal *et al.*[38], in this section, that decaying time on the line can be improved if we consider non-local initial conditions. We start by defining our Hilbert space composed of $\mathcal{H} = \mathcal{H}_c \otimes \mathcal{H}_p$, where $\mathcal{H}_c$ is associated with the orthonormal vectors $\{|R\rangle, |L\rangle\}$ and $\mathcal{H}_p$ with the characteristic vectors of the graph $\{|x\rangle\}$. Then, we are ready for the following theorem by Romanelli *et al.*:

Theorem 4.2 ([10])**.** *Let $\mathcal{H} = \mathcal{H}_c \otimes \mathcal{H}_p$ be the Hilbert space associated with discrete-time quantum walk. Define the initial state given by*

$$\left|\Psi^{\pm}\right\rangle = \sum_{x=-\infty}^{\infty} (a_x |L\rangle + b_x |R\rangle) \otimes (|x\rangle), \tag{4.29}$$

with the time evolution operator given by

$$U = \left[\sum_{x=-\infty}^{\infty} |x+1\rangle\langle x| \otimes |R\rangle\langle R| + |x-1\rangle\langle x| \otimes |L\rangle\langle L| \right] \cdot (I_p \otimes H), \tag{4.30}$$

where I_p is the identity in $\mathcal{H}_p$. Then, the survival probability at time t will be

$$P_x(t) = \sum_{y,y'} (-1)^{y+y'} \left(a_y(0) a^*_{y'}(0) + b_y(0) b^*_{y'}(0)\right) J_{x-y}(t/\sqrt{2}) J_{x-y'}(t/\sqrt{2}), \tag{4.31}$$

where $J_x(t)$ is the first-order Bessel functions. □

Consider now the initial condition given by

$$\left|\Psi^{\pm}\right\rangle = \frac{1}{2}(|L\rangle + i\,|R\rangle) \otimes (|-k\rangle \pm |k\rangle), \tag{4.32}$$

for $k \in \mathbb{Z}^+$. Then, by the above theorem, the survival probability becomes

$$P^{\pm}_x(t) = \frac{1}{2}[J_{x+k}(t/\sqrt{2}) \pm J_{x-k}(t/\sqrt{2})]^2. \tag{4.33}$$

A striking difference arises when the limit $t >> 1$ is analyzed. The survival probability for the state $|\Psi^+\rangle$ can be approximated as

$$P^{+}_x(t) = \frac{1}{2}[J_{x+k}(t/\sqrt{2}) + J_{x-k}(t/\sqrt{2})]^2 = 2x^2 \left[\frac{\sqrt{2} J_x(t/\sqrt{2})}{t}\right]^2 \frac{1}{t^3}. \tag{4.34}$$

While the state $|\Psi^-\rangle$ results in

$$P^{-}_x(t) = \frac{1}{2}[J_{x+k}(t/\sqrt{2}) - J_{x-k}(t/\sqrt{2})]^2 = 2\left[\frac{x\sqrt{2} J_x(t/\sqrt{2})}{t} - J_{x-1}(t/\sqrt{2})\right]^2 \frac{1}{t}. \tag{4.35}$$

Notice how the initial condition changes the speed of the decaying with $|\Psi^+\rangle$ showing an enhanced speed, as the author called it, compared to the other initial conditions. Figure 4.6 shows the survival probability for the two initial conditions and gives a visual comparison between them. It also gives a shred of visual evidence that one initial condition spreads way faster than the other.

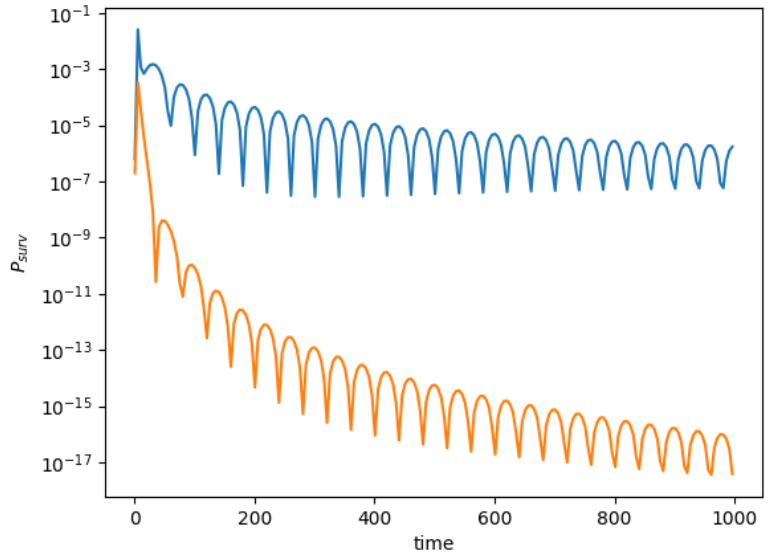

Figure 4.6: Figure showing the survival probability of $|\Psi^+\rangle$ (orange) and $|\Psi^-\rangle$ (blue line). The graph shows with clarity how the initial conditions change the diffusion speed of the wavefunction.

4.4.3 Infinite line and Bessel functions

We saw how Bessel functions can describe the evolution in time of infinite path graphs on discrete-time quantum walks. Here, we will see a result by Bessen[18] that shows a connection between Bessel functions and continuous-time quantum walks in line graphs. Define G as the line graph with $N = R - L$ vertices where L is the leftmost vertex and R the rightmost. Then, our state after the time of evolution can be defined as

$$|\psi(t)\rangle = \sum_{x=L}^{R} \psi(x,t)\,|x\rangle\,, \tag{4.36}$$

where $|x\rangle$ is the caractheristic vector of vertex x. As usual, the time evolution will be given by

$$|\psi(t)\rangle = e^{iAt}\,|\psi(0)\rangle\,, \tag{4.37}$$

where A is the $(N-1)\times(N-1)$ adjacency matrix of the graph defined as

$$A = \begin{bmatrix} 0 & 1 & & & \\ 1 & 0 & 1 & & \\ & \ddots & \ddots & \ddots & \\ & & 1 & 0 & 1 \\ & & & q & 0 \end{bmatrix}. \tag{4.38}$$

As we will see, there is a strict connection between $\psi(x,t)$ and Bessel functions of the first kind.

Theorem 4.3 ([18]). *Let $J_n(t)$ be the n-th Bessel function of first kind and set $\tilde{J}_n(t) = i^n J_n(t)$. Then, the continuous-time quantum walk of the line with initial condition $|\psi(0)\rangle = |x_0\rangle$, $R = \infty$, and $L = \infty$ has the wavefunction $\psi(x,t)$ defined as*

$$\psi(x,t) = \tilde{J}_{|x-x_0|}(2t). \tag{4.39}$$

Proof. The orthogonal and normalized eigenvectors for the adjacency matrix are given by

$$|\psi_k\rangle = \sqrt{\frac{2}{N}} \sum_{x=L+1}^{R-1} \sin\frac{k\pi(x-L)}{N} |x\rangle \tag{4.40}$$

for $k = 1, \ldots, N-1$ and eigenvalues given by $2\cos\frac{k\pi}{N}$. Therefore the wavefunction associated with the state after time evolution will be

$$\psi(x,t) = \frac{2}{N}\sum_{k=1}^{N-1} \sin\frac{\pi k(x-L)}{N} e^{it2\cos\frac{k\pi}{N}} \sum_{y=L+1}^{R-1} \sin\frac{\pi k(y-L)}{N}\psi(y,0). \tag{4.41}$$

Putting the vertex x_0 as the initial condition is the same as defining $\psi(x,0) = \delta_{x,x_0}$. Then, the equation above becomes

$$\psi(x,t) = \frac{2}{N}\sum_{k=1}^{N-1} \sin\frac{k\pi(x-L)}{N} \sin\frac{k\pi(x_0-L)}{N} e^{it2\cos\frac{k\pi}{N}} \tag{4.42}$$

$$= \frac{1}{N}\sum_{k=1}^{N-1} \cos\frac{k\pi(x-x_0)}{N} e^{it2\cos\frac{k\pi}{N} - \frac{1}{N}} \sum_{k=1}^{N-1} \cos\frac{k\pi(x+x_0-2L)}{N} e^{it2\cos\frac{k\pi}{N}}. \tag{4.43}$$

Notice that the terms for $k = 0$ and $k = N$ are equal to two zeros and they can be added without loss of generality. Therefore

$$\psi(x,t) = \frac{1}{N}\sum_{k=0}^{N} \cos\frac{k\pi(x-x_0)}{N} e^{it2\cos\frac{k\pi}{N}} - \frac{1}{N}\sum_{k=0}^{N} \cos\frac{k\pi(x+x_0-2L)}{N} e^{it2\cos\frac{k\pi}{N}}. \tag{4.44}$$

In an interval $[a,b]$ for a function $f(x)$, the Newton-Cotes quadrature can be defined as[9]

$$\int_a^b f(y)dy \approx \sum_{i=0}^{n} w_i f(y_i). \tag{4.45}$$

Notice that for our case, we can assume our interval to be $[0,1]$ and our $w_i = 1$ for all i and the function $f(k/N) = \cos\frac{k\pi(x-x_0)}{N} e^{it2\cos\frac{k\pi}{N}}$. We can rewrite the wavefunction as

$$\psi(x,t) = \frac{1}{N}\int_0^1 \cos\pi(x-x_0) w e^{it2\cos w\pi} dw - \frac{1}{N}\int_0^1 \cos\pi(x+x_0-2L) w e^{it2\cos w\pi} dw \pm \epsilon(x,x_0,t,N), \tag{4.46}$$

where $\epsilon(x, x_0, t, N)$ is the error associated with the approximation. The Newton-Cotes quadrature has approximation errors bounded by

$$\left|\frac{1}{N}\left(\frac{1}{2}f(0)+\frac{1}{2}f(0)+\sum_{k=1}^{N-1}f(k/N)\right)-\int_0^1 f(y)dy\right|\leq\mathcal{O}\left(\frac{1}{N^2}\|f''(y)\|_\infty\right), \tag{4.47}$$

where the norm is the supremum of the second derivative of $f(y)$ in the interval $[0,1]$. The value of this norm will be

$$\|\frac{\partial^2}{\partial w^2}\cos\alpha w e^{i\beta\cos w}\|_\infty\leq(\alpha+\beta)^2+\beta \tag{4.48}$$

with $\alpha,\beta>0$. Therefore, the error associated with the approximation for this case will be

$$\epsilon(x,x_0,t,N)=\mathcal{O}\left(\frac{(x-x_0+2t)^2+(x+x_0-2L+2t)^2}{N^2}\right). \tag{4.49}$$

Remembering the previous definition of $\tilde{J}_n(y)$ we can rewrite the wavefunction $\psi(x,t)$ as a sum of Bessel functions:

$$\psi(x,t)=\tilde{J}_{x-x_0}(2t)+\tilde{J}_{x-x_0+2L}(2t)+\epsilon(x,x_0,t,N). \tag{4.50}$$

When we set $R, L\to\infty$ then the approximation is exact and the wavefunction becomes

$$\psi(x,t)=\tilde{J}_{x-x_0}(2t). \tag{4.51}$$

□

Although the above result is enough to understand our results, Bessen also proved other associations between the Bessel functions and wavefunctions with different boundary conditions:

- For $L\in\mathbb{Z}$, $R\to\infty$, and $\psi(L,0)=0$ then

$$\psi(x,t)=\tilde{J}_{x-x_0}(2t)+\tilde{J}_{x-x_0+2L}(2t). \tag{4.52}$$

- For $R, L\in\mathbb{Z}$, $L<R$, and $\psi(R,0)=\psi(L,0)=0$:

$$\psi(x,t)=\sum_{n=-\infty}^{\infty}(-1)^n\tilde{J}_{x-x_n}(2t) \tag{4.53}$$

with

$$x_n=\begin{cases}L-(x_{-n-1}-L) & n<0,\\ R+(R-x_{-n+1}) & n>0\end{cases}. \tag{4.54}$$

- For $R, L\in\mathbb{Z}$, $L<R$, and $\psi(R,0)=\psi(L,0)$

$$\psi(x,t)=\sum_{n=-\infty}^{\infty}\tilde{J}_{x-y_n}(2t) \tag{4.55}$$

with

$$y_n=nN+x_0. \tag{4.56}$$

Figure 4.7 shows the probability distribution for the different cases.

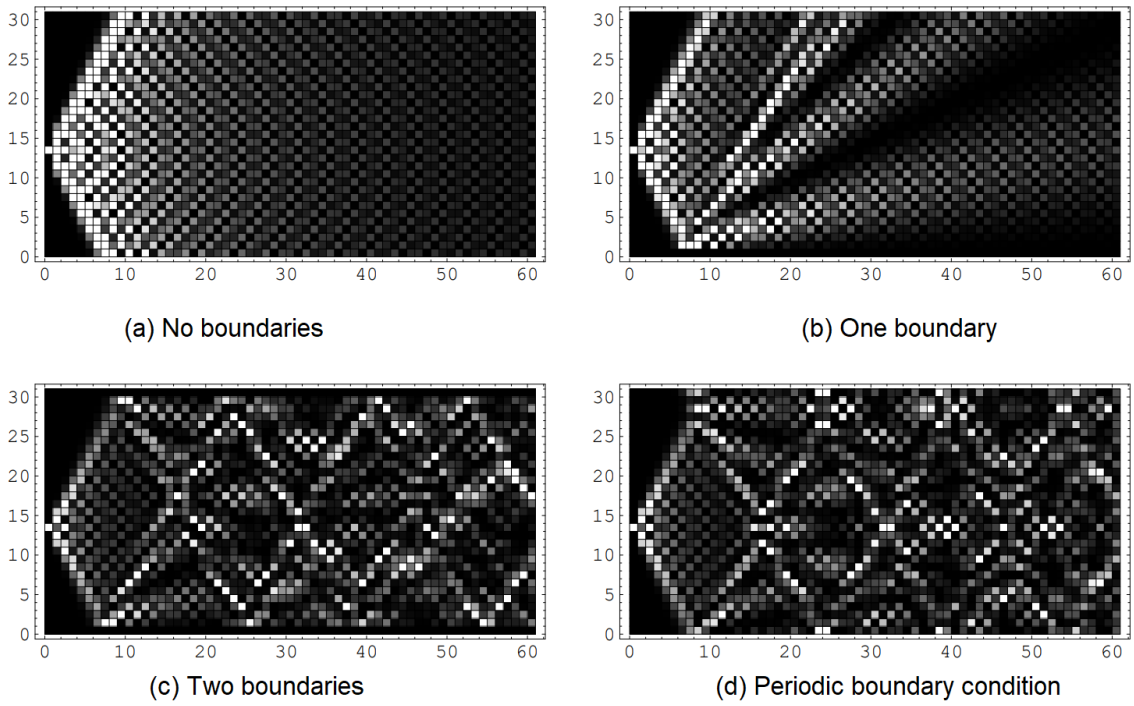

Figure 4.7: Figure showing the probability distribution for the path graph with different boundary conditions. The initial vertex $x_0 = 13$, $L = 0$, and $R = 30$ with a precision of 10^{-5}. Source: Bessen [18]

4.4.4 Oriented trees

As we saw, orientation plays a part in different new phenomena. An interesting question that we answered was: are there any types of graphs whose orientation does not change the dynamics of the CTQW? As we will see, this is the case for the dynamics of oriented trees. A special case arises for finite path graphs that will be crucial for future results about cycle graphs.

First, we prove the following lemma related to an orientation on trees:

Lemma 4.3.1. *Let H_α be the adjacency matrix of an oriented tree T on n vertices, where each arc (a, b) has received weight $e^{i\alpha(a,b)}$ and arcs (b, a) with weights equal to $e^{-i\alpha(a,b)}$. Then, there is a diagonal matrix D, that obeys $D^\dagger D = I$, so that*

$$D^\dagger H_\alpha D = H_0, \tag{4.57}$$

where H_0 is the adjacency matrix of an undirected underlying tree.

Proof. The proof goes by induction on the number of vertices. The base case for a tree on 2 vertices is trivial. Assume a is a leaf of T, connected to b (say by an arc (a, b)). Let E be the $(n-1) \times (n-1)$ diagonal matrix that gives $E^\dagger H_\alpha(T-a)E = H_0(T-a)$. Let

D be obtained from E upon appending one diagonal entry corresponding to vertex a of T, so that

$$D_{aa} = E_{bb} \cdot e^{-i\alpha(a,b)}.$$

It is immediate to verify that $|D_{aa}| = 1$, and that $D^\dagger H_\alpha(T) D = H_0(T)$. □

The above lemma leads us to the following corollary:

Corollary 4.3.1. *Let the initial state be restricted to a single excitation space, H_α the Hamiltonian of a finite oriented path graph, and S a diagonal matrix that obeys $S^\dagger S = I$ and*

$$S^\dagger H_\alpha S = H, \tag{4.58}$$

where H is the Hamiltonian of a finite undirected path graph. Then, the walk dynamics is equal for both H_α and H. □

This will be a crucial corollary for one of our future results related to transport properties in cycles.

4.4.5 Infinite oriented path graphs

Consider the spin model on the infinite line [15]. The Hamiltonian in such cases will be given by

$$H_\alpha = \sum_{x=-\infty}^{+\infty} e^{i\alpha} |x+1\rangle\langle x| + e^{-i\alpha} |x\rangle\langle x+1|, \tag{4.59}$$

where $|x\rangle$ is the characteristic vector of the vertex x with 1 in the x-th position and 0 everywhere else.

Figure 4.8 shows the dynamics of an infinite path graph with the initial state given by

$$|\psi(0)\rangle = \frac{1}{\sqrt{2}}(|0\rangle + |1\rangle). \tag{4.60}$$

It is clear how the addition of orientation changes the walk dynamics. When $\alpha = 0$, we see that the walk is symmetric around the origin and that the probability is equal for vertex a or $-a$. However, we can see that we get a skewed walk to one side or the other whenever there is an orientation. Notice that for $\alpha = \pi/2$, the probability rises on the right side, while, for $\alpha = -\pi/2$, the probability rises on the left side. Notice that the initial condition plays a crucial role here. Suppose that instead of $|\psi(0)\rangle$, we had $|0\rangle$ as the initial condition. Then, the dynamics would always be symmetric.

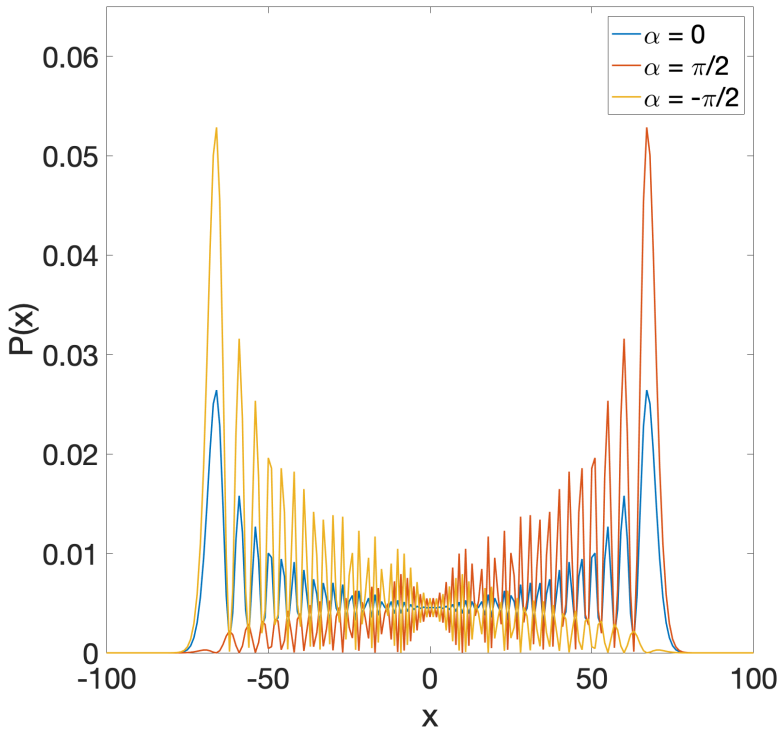

Figure 4.8: Figure showing the dynamics for an infinite path graph with three different values of orientation 0, $\pi/2$, and $-\pi/2$.

After this brief intuition of the dynamics in infinite path graphs, we are ready to see that the time evolution is closely related to Bessel functions, similar to the undirected case.

Adjacency matrices of path graphs are a special case of Toeplitz matrices. The first step in our results is to get the spectral decomposition of those matrices and it is a known result shown by Trench[87]:

Lemma 4.3.2 ([87]). *Define a band Toeplitz matrix of dimension* $(n-1)\times(n-1)$, T_k, *with* $k < n$,

$$\begin{bmatrix} 0 & \dots & a_k & & \\ \vdots & \ddots & & \ddots & \\ a_{-k} & & \ddots & & \ddots \\ & \ddots & & \ddots & a_k \\ & & & a_{-k} & \dots & 0 \end{bmatrix}. \tag{4.61}$$

If $k = 1$ *and* $a_k = e^{i\alpha} = a_{-k}^*$, *where* $\alpha \in \mathbb{R}$, *then its eigenvalues will be given by*

$$\lambda_k = 2\cos\left(\frac{k\pi}{n}\right) \qquad k = 1, \dots, n-1 \tag{4.62}$$

and the corresponding eigenvectors will be

$$|\psi_k\rangle = \sqrt{\frac{2}{n}} \sum_{x=L+1}^{R-1} e^{-i\alpha x} \sin\left(\frac{k\pi x}{n}\right) |x\rangle \tag{4.63}$$

□

The adjacency matrix of a path graph can be described by a Toeplitz matrix like the one above with $k = 1$ and, with this knowledge, the main theorem follows

Theorem 4.4. *Let $J_n(t)$ denote the n-th Bessel function of the first kind and $\tilde{J}_n(z) = i^n J_n(z)$. The continuous-time quantum walks for an infinite line and start point $|\psi(0)\rangle = |x_0\rangle$ has the coefficients:*

$$\psi(x,t) = e^{-i\alpha(x-x_0)} \tilde{J}_{x-x_0}(2t) \tag{4.64}$$

Proof. The coefficients $\psi(x,t)$ will be given by

$$\langle x|\psi(t)\rangle = e^{itT_1} \langle x|\psi(0)\rangle .$$

From lemma 4.3.2 we can use the spectral decomposition of T_1 to obtain

$$\psi(x,t) = \frac{2}{n} \sum_{k=1}^{n-1} e^{-i\alpha x} \sin\left(\frac{k\pi(x-L)}{n}\right) e^{it2\cos\left(\frac{k\pi}{n}\right)} \sum_{y=L+1}^{R-1} e^{-i\alpha y} \sin\left(\frac{k\pi(y-L)}{n}\right) \psi(y,0).$$

Set $\psi(y,0) = \delta_{x,x_0}$, then

$$\begin{aligned}\psi(x,t) =& \frac{e^{-i\alpha(x-x_0)}}{n} \left(\sum_{k=1}^{n-1} e^{-it2\cos\left(\frac{k\pi}{n}\right)} \cos\left(\frac{k\pi(x-x_0)}{n}\right) - \right. \\ & \left. - \sum_{k=1}^{n-1} e^{-it2\cos\left(\frac{k\pi}{n}\right)} \cos\left(\frac{k\pi(x+x_0-2L)}{n}\right) \right)\end{aligned}$$

Notice that the terms with $k = 0$ and $k = n$ vanish, hence we can add them to the sums without loss of generality. After the addition, the sum can be changed to an integral by using Newton-Cotes quadrature. The error of the approximation, $\epsilon(x, x_0, t, n)$, is

$$\epsilon(x, x_0, t, n) \leq \mathcal{O}\left(\frac{1}{N^2} \|f''(x)\|_\infty\right),$$

where $\|f(x)\|_\infty$ is the supremum of $f(x)$. Since we are in the interval $[0, 1]$, the supremum will always be bounded since the function $f''(x)$ will only have complex exponentials and cosines. The coefficients can now be rewritten as

$$\begin{aligned}\psi(x,t) =& e^{-i\alpha(x-x_0)} \left(\int_0^1 \cos\big(\pi(x-x_0)\phi\big) e^{i2t\cos\pi\phi} d\phi - \right. \\ & \left. - \int_0^1 \cos\big(\pi(x+x_0-2L)\phi\big) e^{i2t\cos\pi\phi} d\phi \right) + \\ & + \epsilon(x, x_0, t, n).\end{aligned}$$

Using 4.24 we get that

$$\psi(x,t) = e^{-\alpha(x-x_0)}\left[\tilde{J}_{x-x_0}(2t) - \tilde{J}_{x+x_0-2L}(2t)\right] + \epsilon(x,x_0,t,n). \tag{4.65}$$

By setting $R \to \infty$ and $L \to -\infty$ we see that the error terms go to zero while one of the Bessel functions goes to zero too. We finally get to our result:

$$\psi(x,t) = e^{-i\alpha(x-x_0)}\tilde{J}_{x-x_0}(2t). \tag{4.66}$$

□

4.4.6 Survival probability on infinite oriented path graphs

Recalling the definition of survival probability as the mean probability of finding the walker in a certain location after some time t. The symmetric position range of $[k_0, k_1]$ on the line will have it defined as

$$P_{[k_0,k_1]}(t) = \sum_{i=k_0}^{k_1} P_i(t). \tag{4.67}$$

An initial condition such that $P_{[k_0,k_1]}(0) = 1$, we can evaluate the decay rate of the survival probability, which indicates how fast the walker leaves the specified range of positions. In a classical random walk the decay rate scales with $t^{-\frac{1}{2}}$, and, typically, with t^{-1} in a quantum walk. However, as we saw the result of Abal *et al.* [38], certain non-local initial conditions can further increase this decay rate, where the survival probability decreases with t^{-3}. One of our results shows that the same phenomena can be obtained with oriented graphs and with the proper selection of α.

Lemma 4.4.1. *Define a non-localized initial condition for a continuous-time quantum walk on an infinite and oriented path graph as*

$$|\psi(0)\rangle = \cos(\theta)\,|-k\rangle + e^{i\gamma}\sin(\theta)\,|k\rangle\,, \tag{4.68}$$

where $k \in \mathbb{Z}$, $\theta \in [0, 2\pi)$, and $\gamma \in \mathbb{R}$. Then, the wavefunction $\psi(x,t)$ associated with the time evolution of the quantum walk will be

$$\psi(x,t) = \cos(\theta)e^{-i\alpha(x+k)}\tilde{J}_{x+k}(2t) + e^{i\gamma}\sin\theta e^{-i\alpha(x-k)}\tilde{J}_{x-k}(2t), \tag{4.69}$$

which leads to the general equation for the probability associated with this initial condition

$$\begin{aligned} P_k(x,t) &= \psi(x,t)\psi(x,t)^* \\ &= \cos^2(\theta)J^2_{x+k}(2t) + \sin^2(\theta)J^2_{x-k}(2t) \\ &\quad + 2(-1)^k\cos(2\alpha k+\gamma)\cos(\theta)\sin(\theta)J_{x+k}(2t)J_{x-k}(2t). \end{aligned} \tag{4.70}$$

Proof. Notice that

$$\psi(x,t) = \langle x|\psi(t)\rangle = \sum_{x=-\infty}^{\infty} \psi'(y,t)\,\langle x|\psi(0)\rangle\,, \tag{4.71}$$

and the first result follows immediately from theorem 4.4. The result for the survival probability can be easily obtained using trigonometric relations. □

This choice of initial condition was motivated by the increased interest in experimental physics with the superposition of the walker states [75] in discrete-time quantum walks.

We are now ready for the main theorem

Theorem 4.5. *Let G be an infinite oriented graph with arcs having orientation $e^{-i\alpha}$ and $e^{i\alpha}$. Let the initial condition be defined as*

$$|\psi(0)\rangle = \cos(\theta)\,|-k\rangle + e^{i\gamma}\sin(\theta)\,|k\rangle\,. \tag{4.72}$$

Then, for $\theta = \pi/4$, the survival probability will decay with $1/t^3$ for α equals to

$$\alpha = \begin{cases} \dfrac{2\pi v - \gamma}{2k}, \textit{ even } k, \\ \dfrac{\pi + 2\pi v - \gamma}{2k}, \textit{ odd } k, \end{cases}, \tag{4.73}$$

and it will decay with $1/t$ for α equals to

$$\alpha = \begin{cases} \dfrac{2\pi v - \gamma}{2k}, \textit{ even } k, \\ \dfrac{\pi + 2\pi v - \gamma}{2k}, \textit{ odd } k, \end{cases}. \tag{4.74}$$

Proof. Although we decided to choose a box of size 1 for the survival probability, the expression for a bigger box could be obtained from equation (4.70). The enhanced decay rate can then be analytically obtained from equation (4.70) by considering

$$(-1)^k\cos(2\alpha k + \gamma) = 1, \tag{4.75}$$

and the value of α will be

$$\alpha = \begin{cases} \dfrac{2\pi v - \gamma}{2k}, \text{even } k, \\ \dfrac{\pi + 2\pi v - \gamma}{2k}, \text{ odd } k, \end{cases} \tag{4.76}$$

where $v \in \mathbb{Z}$. The probability will be, after some algebraic manipulation, as follows

$$P_k(x,t) = \left[\cos\theta J_{x+k}(2t) + \sin\theta J_{x-k}(2t)\right]^2. \tag{4.77}$$

Considering a value of $k = 1$ and $\theta = \frac{\pi}{4}$

$$P_1(x,t) = \frac{1}{2}\left[J_{x+1}(2t) + J_{x-1}(2t)\right]^2 = 2x^2\left[\frac{J_x(2t)}{2t}\right]^2 \sim \frac{1}{t^3}, \tag{4.78}$$

thus confirming these parameters do indeed lead to the probability of finding the walker in the survival region decreasing with an enhanced rate.

Analogously, we can recover the normal decay rate by changing the value of α to

$$\alpha = \begin{cases} \dfrac{2\pi v - \gamma}{2k}, \text{odd } k, \\ \dfrac{\pi + 2\pi v - \gamma}{2k}, \text{ even } k. \end{cases} \tag{4.79}$$

The associated probability will then be

$$P_k(x,t) = \left[\cos\theta J_{x+k}(2t) - \sin\theta J_{x-k}(2t)\right]^2. \tag{4.80}$$

Once more, if we take a value of $k = 1$ and $\theta = \frac{\pi}{4}$

$$P_1(x,t) = \frac{1}{2}\left[J_{x+1}(2t) - J_{x-1}(2t)\right]^2 = 2\left[\frac{xJ_x(2t)}{2t} - J_{x-1}(2t)\right]^2 \sim \frac{1}{t}, \tag{4.81}$$

and we recover the normal decay rate of the quantum walk.

□

Considering a value of $k = 1$ and $\theta = \frac{\pi}{4}$, figure 4.9 shows how the survival probability decays over time. For a value of $\alpha = \frac{\pi}{2}$ the enhanced decay rate is observed, whereas other values of α display a normal decay rate. The code used to plot the figures can be found in the `GitHub`[2] repository.

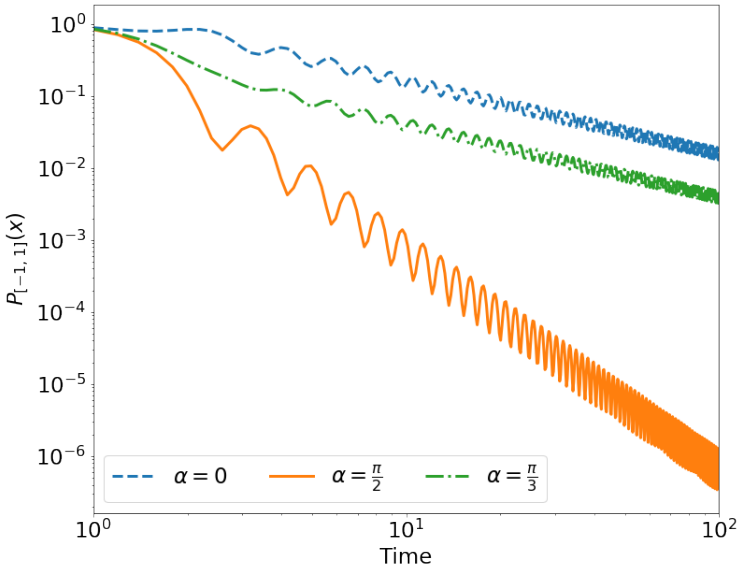

Figure 4.9: Evolution of the survival probability on a oriented infinite line, for $\theta = \frac{\pi}{4}$, $\gamma = 0$, and $\alpha = 0, \frac{\pi}{2}, \frac{\pi}{3}$.

This difference in behavior is explained by an interference effect influenced, in part, by the relative phase of the initial state. Introducing direction to the line graph also affects

[2] https://github.com/JaimePSantos/QWAK

this interference effect, and we can reproduce enhanced and normal decay rates for the given initial condition by choosing the appropriate value of α, regardless of the parity of k. Then, no nodes admit localization since the decay rate of the right-hand side of every vertex is O(1/t).

4.5 Zero transfer

We will start with the definition of zero transfer: suppose we have a graph G. There is zero transfer from vertex a to b, if

$$|\langle b| U(t) |a\rangle| = 0, \tag{4.82}$$

for all t. Zero transfer is a complete suppression of information transport between two vertices and it is only possible in quantum walks modeled by oriented graphs.

Notice that if we had an undirected connected graph, it would be impossible to obtain such a phenomenon. The intuition behind that affirmation is that the time evolution operator decomposes as the sum of powers of the adjacency matrix. Since $(A^k)_{ij}$ counts the number of walks of length k from vertex i to j, it is impossible, for undirected graphs, that we get a walker never visiting a vertex for all time t.

The phenomenon was first proposed by Zimborás *et al.* [96] while studying quantum walks with orientation (also called chiral quantum walk by them). They show that zero transfer occurs for the even cycle, similar to our result. However, our result is for a different set of orientations while focusing on the algebraic properties of the graph.

Sett *et al.* [13] while working with oriented graphs gave a physical justification for zero transfer. They proposed that this phenomenon can be an indirect measure of decoherence in a system. Although we will not dive into open quantum systems, the reasoning behind their justification is simple. We defined the phenomena to occur in closed systems, however, when the system starts to interact with an environment, it will lose its quantum aspect and the transfer probability will increase as the decoherence increases.

Unfortunately, we lack a detailed characterization of zero transfer as the one for perfect state transfer. Therefore we will show when the phenomenon occurs for even cycles and its connection with the adjacency matrix eigenvalues.

4.5.1 Chebyshev polynomials

Chebyshev polynomials are a set of orthogonal polynomials that can be of the first kind, written as $T_n(x)$, or the second kind, written as $U_n(X)$. They are related to sine and cosines function with the first kind being the solution to the Chebyshev differential equations[53]:

$$(1-x^2)\frac{d^2y}{dx^2} - x\frac{dy}{dx} + \alpha^2 y = 0 \tag{4.83}$$

for $|x| < 1$. The polynomial of the first kind is defined as

$$T_n(cos\theta) = cos(n\theta) \tag{4.84}$$

and the second kind as

$$U_n(\cos\theta)\sin\theta = \sin((n+1)\theta). \tag{4.85}$$

Among many properties, they also have a recurrence relation given by

$$T_{n+1}(x) = 2xT_n(x) - T_{n-1}(x), \tag{4.86}$$

$$U_{n+1}(x) = 2xU_n(x) - U_{n-1}(x). \tag{4.87}$$

As we will see, they are closely related to the characteristic polynomials of path graphs and it is one of many applications. This connection will allow us to prove some results of zero transfer in oriented even cycles. To do that, we will first define a recurrence relation that connects polynomials of the first kind with polynomials of the second kind:

$$T_n(x) = \frac{1}{2}\Big(U_n(x) - U_{n-2}(x)\Big), \tag{4.88}$$

$$T_{2n}(x) = 2T_n^2(x) - 1. \tag{4.89}$$

4.5.2 Zero transfer in even cycles

Let C_{2k}^{α} denote the adjacency matrix for a cycle with $2k$ vertices. We will show an expression for its characteristic polynomial and its connection to the characteristic polynomial of the undirected cycle. Before we dive into the results, define a sesquivalent subgraph of a graph G as regular subgraphs with degree 1 or 2, i.e. singles vertices or cycles. A theorem of Harary [51] states that

Theorem 4.6 ([51]). *Let G be a simple graph, and $\mathcal{H}$ be the set of all sesquivalent subgraphs of G. Then,*

$$\phi_G = \sum_{H \in \mathcal{H}} (-1)^{e(H)} (-2)^{c(H)} x^{v(H)}, \tag{4.90}$$

where ϕ_G is the characteristic polynomial of G, $e(H)$ is the number of edges, $v(H)$ the number of isolated vertices, and $c(H)$ the number of cycles.

A known fact about tridiagonal matrices is the following lemma

Lemma 4.6.1. *Let T be a tridiagonal matrix given by*

$$T = \begin{pmatrix} a_1 & b_1 & & & \\ c_1 & a_2 & b_2 & & \\ & c_2 & \ddots & \ddots & \\ & & \ddots & \ddots & b_{n-1} \\ & & & c_{n-1} & a_n \end{pmatrix}, \tag{4.91}$$

Let f_{n-i} be the determinant of T with the last i columns and rows removed. Then the determinant of T is given by

$$f_n = a_n f_{n-1} - c_{n-1} b_{n-1} f_{n-2}, \tag{4.92}$$

where $f_{-1} = 0$ and $f_0 = 1$.

As a corollary of the previous lemma

Corollary 4.6.1. *Let T be a tridiagonal matrix of size $n \times n$ with 0 in the diagonal and 1 in every other non-zero entry, then its determinant is given by*

$$f_n = \begin{cases} (-1)^p & \text{if } n = 2p \text{ and } p \text{ is an integer,} \\ 0 & \text{otherwise} \end{cases}. \tag{4.93}$$

Proof. Since $a_k = 0$ and $c_k = b_k = 1$ for all k, we get that

$$f_n = -f_{n-2}. \tag{4.94}$$

Knowing that $f_{-1} = 0$ and $f_0 = 1$ it is easy to see that

$$\begin{aligned} f_1 &= -f_{-1} = 0, \\ f_2 &= -f_0 = -1, \\ f_3 &= -f_1 = 0, \\ f_4 &= -f_2 = 1, \\ f_5 &= -f_3 = 0, \\ f_6 &= -f_4 = -1, \end{aligned}$$

and so on. □

Now, we are ready to prove the following theorem

Theorem 4.7. *Let C_{2k}^{α} be the adjacency matrix of the oriented cycle graph with $2k$ vertices. Half of its arcs have orientation $e^{i\frac{\pi}{k}}$ from arcs going from i to $i+1$ and orientation $e^{-i\frac{\pi}{k}}$ from arcs going from $i+1$ to i, while the other half is undirected. Then, its characteristic polynomial, $\phi_{C_{2k}^{\alpha}}$ is given by*

$$\phi_{C_{2k}^{\alpha}} = \phi_{C_{2k}} + 4, \tag{4.95}$$

where $\phi_{C_{2k}}$ is the characteristic polynomial of an undirected cycle with $2k$ vertices. Additionally, $\phi_{C_{2k}^{\alpha}}$ can be factored as

$$\phi_{C_{2k}^{\alpha}} = 4T_k^2(x/2), \tag{4.96}$$

where $T_n(x)$ is the Chebyshev polynomial of the first kind.

Proof. The Leibniz formula for the determinant gives that

$$\phi_{H_\alpha} = \sum_{\sigma}(-1)^{\mathbf{sgn}(\sigma)}\prod_{i=1}^{2k}(xI - H_\alpha)_{i\sigma(i)}, \tag{4.97}$$

where the sum corresponds to all permutations σ of the set $\{1, 2, \ldots, 2m\}$. Notice that the permutation will only give a non-zero entry of $(xI - H_\alpha)$ if it maps i to a neighbor. Therefore, we can rewrite

$$\phi_{H_\alpha} = \sum_{D\subseteq V(G)} x^{|D|}(-1)^{n-|D|}\det(H_\alpha \setminus D), \tag{4.98}$$

where the sum runs over all subsets D of the vertices of the graph, and $(H_\alpha \setminus D)$ denotes the matrix H_α with rows and columns corresponding to D removed.

It is easy to see those subgraphs obtained for $|D| < n$ are all paths or multiple disconnected paths where some edges might have been weighted. As we saw on Lemma 4.3.1, all these possibly oriented paths are similar (via a diagonal matrix) to their undirected unweighted counterparts. Therefore

$$\phi_{H_\alpha} = \phi_H - \det(H) + \det(H_\alpha). \tag{4.99}$$

To compute the determinant of H_α, it suffices to observe the following decomposition, which follows the Laplace expansion (see for instance [41]):

$$\begin{aligned}\det(H_\alpha) = &-(H_\alpha)_{12}(H_\alpha)_{21}\det((H_\alpha)\setminus\{1,2\})\\ &+(-1)^{n+1}\cdot 2\cdot\prod_{j=1}^{n}(H_\alpha)_{j\,j+1}\\ &-(H_\alpha)_{1n}(H_\alpha)_{n1}\det((H_\alpha)\setminus\{1,n\})\end{aligned} \tag{4.100}$$

From the given weights, Lemma 4.3.1 and from 4.6.1, we have

$$(H_\alpha)_{12}(H_\alpha)_{21} = (H_\alpha)_{1n}(H_\alpha)_{n1} = 1,$$
$$\det((H_\alpha) \setminus \{1,2\}) = \det((H_\alpha) \setminus \{1,n\}) = (-1)^m,$$
$$\prod_j (H_\alpha)_{j\,j+1} = -1.$$

If instead, we were computing the determinant of H, the only difference would have been that $\prod_j (H)_{j\,j+1} = 1$. Therefore

$$\phi_{H_\alpha} = \phi_H + 4. \tag{4.101}$$

Also following from (4.100), we have

$$\phi_H = \phi_{P_n} - \phi_{P_{n-2}} - 2, \tag{4.102}$$

where ϕ_{P_n} is the characteristic polynomial of the adjacency matrix of the path graph with $n = 2m$ vertices, hence, from 4.6.1, we have

$$\det(H) = \begin{cases} 0 & \text{if } m \text{ is even,} \\ -4 & \text{if } m \text{ is odd} \end{cases}. \tag{4.103}$$

Also, ϕ_{P_n} can be defined in terms of the Chebyshev polynomials as

$$\phi_{P_n} = U_n(x/2). \tag{4.104}$$

Using that in the expression for ϕ_{H_α} and the properties presented in the definition of the Chebyshev polynomials we have

$$\phi_{H_\alpha} = (2T_m(x/2))^2. \tag{4.105}$$

□

As a corollary to the previous theorem, it is possible to show that there is zero transfer from any vertex to its antipodal vertex.

Corollary 4.7.1. *Let C^α_{2k} be the adjacency matrix of a cycle graph with $2k$ vertices and weights $e^{\pm i\frac{\pi}{k}}$ in half of its arcs while the other half is undirected. Then, there is zero transfer for any time t between the vertex 0 and its antipodal vertex k.*

Proof. Take a vertex a, and consider its indicator vector $|a\rangle$. The minimal polynomial of H_α on $|a\rangle$ is the monic polynomial $p(x)$ of the smallest degree so that $p(H_\alpha)\,|a\rangle = 0$. It is well known that $p(x)$ divides the minimal polynomial of the matrix H_α, and this latter polynomial has a degree equal to the number of distinct eigenvalues of H_α. From Theorem

4.7, this number is at most m. Therefore, $H_\alpha^\ell |a\rangle$, for $\ell \geq m$, is a linear combination of $H_\alpha^k |a\rangle$ for $0 \leq k \leq m-1$. Because the combinatorial distance between a and $(a+m)$ is m, it follows that $\langle a+m| H_\alpha^k |a\rangle = 0$ for all $0 \leq k \leq m-1$, and therefore $\langle a+m| H_\alpha^\ell |a\rangle = 0$ for all $\ell \geq 0$. This immediately implies that for all idempotents E_r in the spectral decomposition of H_α, this corresponding entry related to a and $(a+m)$ is 0, and therefore

$$\left|\langle a+m| e^{itH_\alpha} |a\rangle\right|^2 = \left|\sum_r e^{it\theta_r} \langle a+m| E_r |a\rangle\right|^2 = 0. \tag{4.106}$$

□

Chapter 5

Conclusion

We started this work aiming to tackle four different problems related to quantum mechanics and graph theory:

1. It is known that noisy quantum computers cannot efficiently simulate quantum walks due to the number of multi-controlled gates required. Is it possible to use algebraic graph theory to make the simulation more efficient?

2. Are there graphs for which the addition of orientation does not change the quantum system's dynamics?

3. Even though the weights have modulus 1, can the addition of orientation be enough to change the velocity in which the information is spread through the graph?

4. Can algebraic graph theory explain known phenomena in the literature and offer new perspectives to phenomena closely related to the addition of orientation?

The investigation of the first question led us to circulant matrices and their spectral decomposition with Fourier matrices. We saw that this allowed for an implementation of the continuous-time quantum walk by using the QFT algorithm which can be efficiently implemented by NISQ devices with few qubits. To show this, we used one of IBM's QPUs to simulate the quantum walk and we compared it to its ideal results. We were able to show that the results coincide in spite of errors associated to NISQ devices. We were also able to obtain good results with an approximate version of the QFT algorithms. An open question remaining from this work is whether there are other graphs with similar symmetries such that their spectral decomposition can be easily implemented in NISQ devices. This would make continuous-time quantum walk a lot easier for current devices and would make it possible to tackle problems associated with quantum walks.

The second question led us to explore how the dynamics of a quantum walk can be altered by the addition of orientation. We were able to derive a result showing how trees are unaffected by orientation. In those graphs, it is always possible to find a linear transformation using a unitary diagonal matrix that sends the adjacency matrix of the oriented tree to the adjacency matrix of the tree without orientation. As a consequence, the operator associated with the time evolution of continuous-time quantum walks in

oriented trees just creates a global phase compared to the time of evolution of undirected trees. A follow up question would be if there are other graphs that share similarities with oriented tree and have a transformation that associates the oriented adjacency matrix with the undirected adjacency matrix.

The third question created the scenario for the study of the differences between infinite graphs and finite graphs. Our results showed that some types of orientation allowed us to change the velocity that information is spread in the graph. Some orientations showed that information spread with $1/t^2$ while others with $1/t^3$. This was similar to known results in the literature for infinite graphs. However, their results were also present in path graphs while we showed that orientation does not change the dynamics of trees. This creates a striking result showing that there is a disconnection between the result for finite and infinite graphs when orientation is considered. A usual trick recurrent in the literature is to extrapolate results found in finite graphs to infinite graphs and, as a consequence of this result, the trick must be made with care for oriented graphs.

Zero transfer was the main phenomenon of interest to answer the final question. We were able to see that its occurrence in oriented cycle graphs was associated with the degeneracy of the eigenvalues of the graph's adjacency matrix due to the addition of orientation. We expanded the knowledge about the phenomenon and might have paved a way to a possible general characterisation. A follow up project would be to find other graphs with zero transfer and, possibly, achieve a general characterisation.

Bibliography

[1] A. Acuaviva, A. Chan, S. Eldridge, C. Godsil, M. How-Chun-Lun, C. Tamon, E. Wright, X. Zhang. State transfer in complex quantum walks. arXiv:2301.01473 (2023).

[2] A. Ambainis, E. Bach, A. Nayak, A. Vishwanath, J. Watrous. One-dimensional quantum walk. Proceedings of the thirty-third annual ACM symposium on Theory of computing, 37-49 (2001).

[3] A. Ambainis, J. Kempe, A. Rivosh. Coins make quantum walks faster. Proceedings of the 16th Annual ACM-SIAM Symposium on Discrete Algorithms SODA '05, 1099-1108 (2005).

[4] A. I. Lvovsky, M. G. Raymer. Continuous-variable optical quantum-state tomography. Reviews of Modern Physics **81** (1), 299-332 (2009).

[5] A. M. C. Souza, R. F. S. Andrade. Fast and slow dynamics for classical and quantum walks on mean-field small world networks. Scientific Reports **9**, 19143 (2019).

[6] A. M. Childs, E. Farhi, S. Gutmann . An example of the difference between quantum and classical random walks. Quantum Information Processing **1**, 35-43 (2002).

[7] A. Peruzzo, M. Lobino, J. C. F. Matthews, N. Matsuda, A. Politi, K. Poulios, X. Zhou, Y. Lahini, N. Ismail, K. W¨orhoff, Y. Bromberg, Y. Silberberg, M. G. Thompson, J. L. O'Brien. Quantum walks of correlated photons. Science **329**, 1500-1503 (2010).

[8] A. Politi, J. C. F. Matthews, J. L. O'Brien. Shor's quantum factoring algorithm on a photonic chip. Science **325**, 1221 (2009).

[9] A. Quarteroni, R. Sacco, F. Saleri. Numerical mathematics. Springer (2006).

[10] A. Romanelli, A.C. Sicardi Schifino, R. Siri, G. Abal, A. Auyuanet, R. Donangelo. Quantum random walk on the line as a markovian process. Physica A: Statistical Mechanics and its Applications **338**, 395-405 (2004).

[11] A. S. Holevo. The capacity of quantum channel with general signal states. IEEE Transactions on Information Theory **44**, 269-273 (1973).

[12] A. Schreiber, K. N. Cassemiro, V. Potoček, A. Gábris, P. J. Mosley, E. Andersson, I. Jex, C. Silberhorn. Photons walking the line: A quantum walk with adjustable coin operations. Physical Review Letters **104**, 050502 (2010).

[13] A. Sett, H. Pan, P. E. Falloon, J. B. Wang. Zero transfer in continuous-time quantum walks. Quantum Information Processing **18**, 159 (2019).

[14] B. Do, M. L. Stohler, S. Balasubramanian, D. S. Elliott, C. Eash, E. Fischbach, M. A. Fischbach, A. Mills, B. Zwickl. Experimental realization of a quantum quincunx by use of linear optical elements. JOSA B **22**, 499 (2005).

[15] B. Tödtli, M. Laner, J. Semenov, B. Paoli, M. Blattner, J. Kunegis. Continuous-time quantum walks on directed bipartite graphs. Physical Review A **94**, 052338 (2016).

[16] S. M. Barnett. Quantum information. Oxford University Press (2009).

[17] P. Benioff. The computer as a physical system: A microscopic quantum mechanical hamiltonian model of computers as represented by turing machines. Journal of Statistical Physics volume **22**, 563-591 (1980).

[18] A. J. Bessen. Distributions of continuous-time quantum walks. arXiv:quant-ph/0609128 (2006).

[19] C. A. Ryan, M. Laforest, J. C. Boileau, R. Laflamme. Experimental implementation of a discrete-time quantum random walk on an nmr quantum-information processor. Physical Review A **72**, 062317 (2005).

[20] C. Godsil, G. Royle. Algebraic graph theory. Springer (2001).

[21] C. H. Bennett, S. J. Wiesner. Communication via one- and two-particle operators on einstein-podolsky-rosen states. Physical Review Letters **69** (20), 2881-2884 (1992).

[22] A. Chefles. Quantum state discrimination. Contemporary Physics **41**, 401-424 (2000).

[23] A. M. Childs. Universal computation by quantum walk. Physical Review Letters **102**, 180501 (2009).

[24] D. Coppersmith. An approximate fourier transform useful in quantum factoring. arXiv:quant-ph/0201067 (1994).

[25] G. Coutinho. Quantum state transfer in graphs. PhD thesis, University of Waterloo (2014).

[26] D. Aharonov, A. Ambainis, J. Kempe, U. Vazirani. Quantum walks on graph. Proceedings of the thirty-third annual ACM symposium on Theory of computing, 50-59 (2001).

[27] D. Aldous, J. A. Fill. Reversible markov chains and random walks on graphs. University of California, Berkeley unfinished monograph (2014).

[28] D. Bouwmeester, I. Marzoli, G. P. Karman, W. Schleich, J. P. Woerdman. Optical galton board. Physical Review A **61**, 013410 (1999).

[29] D. Deutsch, R. Jozsa. Rapid solution of problems by quantum computation. Proceedings of the Royal Society of London A. **439**,553-558 (1907).

[30] D. Dieks. Communication by epr devices. Physics Letters A **92**, 271-272 (1982).

[31] D. N. Christodoulides, F. Lederer, Y. Silberberg. Discretizing light behaviour in linear and nonlinear waveguide lattices. Nature **424**, 817-823 (2003).

[32] E. Connelly, N. Grammel, M. Kraut, L. Serazo, C. Tamon. Universality in perfect state transfer. Linear Algebra and its Applications **531**, 516-532 (2017).

[33] E. Farhi, S. Gutmann. Quantum computation and decision trees. Physical Review A **58**, 915.

[34] E. Lieb, T. Schultz, D. Mattis. Two soluble models of an antiferromagnetic chain. Annals of Physics **16**, 407-466 (1961).

[35] F. Acasiete, F. P. Agostini, J. Khatibi Moqadam, R. Portugal. Implementation of quantum walks on ibm quantum computers. Quantum Information Processing **19**, 12 (2020).

[36] F. Magniez, M. Santha, M. Szegedy. Quantum algorithms for the triangle problem. SIAM Journal on Computing **102**, 413-424 (2007).

[37] F. Xia, J. Liu, H. Nie, Y. Fu, L. Wan, X. Kong. Random walks: A review of algorithms and applications. IEEE Transactions on Emerging Topics in Computational Intelligence **4**, 2 (2020) .

[38] G. Abal, R. Donangelo, A. Romanelli, R. Siri. Effects of non-local initial conditions in the quantum walk on the line. Physica A: Statistical Mechanics and its Applications **371**(1), 1-4 (2006).

[39] G. Coutinho, C. Godsil. Graph spectra and continous quantum walks. Unpublished book (2021).

[40] G. S. Engel, T. R. Calhoun, E. L. Read, T. Ahn, T. Mančal, Y. Cheng, R. E. Blankenship, G. R. Fleming. Evidence for wavelike energy transfer through quantum coherence in photosynthetic systems. Nature **446**, 782–786 (2007).

[41] C. Godsil. *Algebraic combinatorics*. Chapman and Hall/CRC, 1993.

[42] C. Godsil. When can perfect state transfer occur? Electronic Journal of Linear Algebra **23**, 877-890 (2012).

[43] C. Godsil. Periodic graphs. The Electronic Journal of Combinatorics **18**, 23 (2011).

[44] J. Gordon. Quantum effects in communications systems. Proceedings of the IRE **50** (9), 1898-1908 (1962).

[45] A. D. Gottlieb. Convergence of continuous-time quantum walks on the line. Physical Review E **72**, 047102 (2005).

[46] L. K. Grover. A fast quantum mechanical algorithm for database search. Proceedings of the twenty-eighth annual ACM symposium on Theory of Computing STOC '96, 212-219 (1996).

[47] H. B. Perets, Y. Lahini, F. Pozzi, M. Sorel, R. Morandotti, Y. Silberberg. Realization of quantum walks with negligible decoherence in waveguide lattices. Physical Review Letters **100**, 170506 (2008).

[48] H. Barnum, C. M. Caves, C. A. Fuchs, R. Jozsa, B. Schumacher. Noncommuting mixed states cannot be broadcast. Physical Review Letters **76** (15), 2818-2821 (1996).

[49] H. Pal and B. Bhattacharjya. Pretty good state transfer on circulant graphs. The Electronic Journal of Combinatorics **24**, 2 (2017).

[50] H. Schmitz, R. Matjeschk, Ch. Schneider, J. Glueckert, M. Enderlein, T. Huber, T. Schaetz. Quantum walk of a trapped ion in phase space. Physical Review Letters **103**, 090504 (2009).

[51] F. Harary. The determinant of the adjacency matrix of a graph. SIAM Review **4**, 202-210 (1962).

[52] C. W. Helstrom. Quantum detection and estimation theory. Springer (1976).

[53] J. C. Mason, D. C. Handscomb. Chebyshev polynomials. CRC Press (2002.

[54] J. D. Whitifield, C. A. Rodríguez-Rosario, A. Aspuru-Guzik. Quantum stochastic walks: A generalization of classical random walks and quantum walks. Physical Review A **81**, 022323 (2010).

[55] J. Qi, X. Li, Q. Niu, J. Feng. Giant and tunable valley degeneracy splitting in mote$_2$. Physical Review B **92**, 121403 (2015).

[56] J. Santos, B. Chagas, R. Chaves. Quantum walks in a superconducting quantum computer. Workshop de Comunicação e Computação Quântica (WQUANTUM) **1**, 25-30 (2021).

[57] K. Pearson. The problem of the random walk. Nature **72**, 294 (1905).

[58] J. Kempe. Discrete quantum walks hit exponentially faster. Probability Theory and Related Fields **133**, 215-235 (2005).

[59] J. Kempe. Quantum random walks: an introductory overview. Contemporary Physics **44** (4), 307-327 (2003).

[60] L. Henriet, L. Beguin, A. Signoles, T. Lahaye, A. Browaeys, G. Reymond, C. Jurczak. Quantum computing with neutral atoms. Quantum **4**, 327 (2020).

[61] L. W. Molenkamp, G. Schmidt, G. E. W. Bauer. Rashba hamiltonian and electron transport. Physical Review B **64**, 121202 (2001).

[62] N. N. Lebedev. Special functions and their applications. *Dover Publications*, 1972.

[63] M. A. Nielsen, I. L. Chuang. Quantum computation and quantum information. Cambridge University Press (2000).

[64] M. Christandl, N. Datta, A. Ekert, A. J. Landahl. Perfect state transfer in quantum spin networks. Physical Review Letters **92**, 187902 (2004).

[65] M. Gmitra, J. Fabian. Graphene on transition-metal dichalcogenides: A platform for proximity spin-orbit physics and optospintronics. Physical Review B **92**, 155403 (2015).

[66] M. Gönülol, E. Aydıner, Y. Shikano, Ö. Müstecaplıoglu. Survival probability in a one-dimensional quantum walk on a trapped lattice. New Journal of Physics **13**, 033037 (2011).

[67] M. Karski , L. Forster, J. Choi, A. Steffen, W. Alt, D. Meschede, A. Widera. Quantum walk in position space with single optically trapped atoms. Physical Review Letters **103**, 090504 (2009).

[68] M. Mohseni, P. Rebentrost, S. Lloyd, A. Aspuru-Guzik. Environment-assisted quantum walks in photosynthetic energy transfer. Journal of Chemical Physiscs **129**, 174106 (2008).

[69] M. Mohseni, P. Rebentrost, S. Lloyd, A. Aspuru-Guzik. Environment-assisted quantum walks in photosynthetic energy transfer. Journal of Chemical Physiscs **129**, 174106 (2008).

[70] A. Montanaro. Quantum speedup of monte carlo methods. Proceedings of the Royal Society A [471, 20150301 (2015).

[71] N. Shenvi, J. Kempe, K. B. Whaley. Quantum random-walk search algorithm. Physical Review A **67**(5), 052307 (2003).

[72] P. K. Pathak, G. S. Agarwal. Quantum random walk of two photons in separable and entangled states. Physical Review A **75**, 032351 (2007).

[73] P. L. Knight, E.o Roldán, J. E. Sipe. Quantum walk on the line as an interference phenomenon. Physical Review A **68**, 020301(R) (2003).

[74] R. Portugal. Quantum walks and search algorithms. Springer (2013).

[75] Q. Su, Y. Zhang, L. Yu, J. Zhou, J. Jin, X. Xu, S. Xiong, Q. Xu, Z. Sun, K. Chen, F. Nori, C. Yang. Experimental demonstration of quantum walks with initial superposition states. npj Quantum Information **5**. 40 (2019).

[76] R. Chaves, B. Chagas, G. Coutinho. Why and how to add direction to a quantum walk. Quantum Information Processing **22** (1), 41 (2023).

[77] R. Chaves, J. Santos, B. Chagas. Transport properties in directed quantum walks on the line. Quantum Information Processing **22**, 144 (2023).

[78] R. Feynman, R. B. Leighton, M. Sands. The feynman lectures on physics. Hachette Book Group (1963).

[79] N. Reff. Spectral properties of complex unit gain graphs. Linear Algebra and its Applications **436**, 3165-3176 (2012).

[80] S. B. Kotsiantis. Decision trees: a recent overview. Artificial Intelligence Review **39**, 261-283 (2013).

[81] S. Cameron, S. Fehrenbach, L. Granger, O. Hennigh, S. Shrestha, C. Tamon. Universal state transfer on graphs. Linear Algebra and its Applications **455**, 115-142 (2014).

[82] S. Lato, C. Godsil. Perfect state transfer on oriented graphs. Linear Algebra and its Applications **604**, 278-292 (2020).

[83] S. M. Barnett, S. Croke. Quantum state discrimination. Advances in Optics and Photonics **1**, 238-278 (2009).

[84] I. L. Markov S. S. Bullock. Smaller circuits for arbitrary n-qubit diagonal computations. Quantum Information and Computation **4**, 27-47 (2004).

[85] T. Monz, D. Nigg, E. A. Martinez, M. F. Brandl, P. Schindler, R. Rines, S. X. Wang, I. L. Chuang, R. Blatt. Realization of a scalable shor algorithm. Science **351**, 1068-1070 (2016).

[86] T. Toffoli. Reversible computing. Automata, Languages and Programming, ICALP (1980).

[87] W. F. Trench. On the eigenvalue problem for toeplitz band matrices. Linear Algebra and its Applications **64**, 199-214 (1985).

[88] V. V. Shende, S. S. Bullock, I. L. Markov. Synthesis of quantum-logic circuits. IEEE Transactions on Computer-Aided Design of Integrated Circuits and Systems **25**, 1000-1010 (2006).

[89] W. Wootters, W. Zurek. Single quantum cannot be cloned. Nature **299**, 802-803 (1982).

[90] Y. Wang. Simulating stochastic diffusions by quantum walks. Proceedings of the ASME 2013 International Design Engineering Technical Conferences and Computers and Information in Engineering Conference **3B**, V03BT03A053 (2013).

[91] T. G. Wong. Grover search with lackadaisical quantum walks. Journal of Physics A: Mathematical and Theoretical **48**, 435304 (2015).

[92] X. Qiang, T. Loke, A. Montanaro, K. Aungskunsiri, X. Zhou, J. L O'Brien, J. B Wang, J. C. F. Matthews. Efficient quantum walk on a quantum processor. Nature Communications **7**, 11511 (2016).

[93] Y. Aharanov, L. Davidovich, N. Zagury. Quantum random walks. Physical Review A **48**, 1687-1690 (1993).

[94] Y. Aharonov, L. Davidovich, N. Zagury. Quantum random walks. Physical Review A **48**, 1687 (1993).

[95] Y. Nakamura, Y. A. Pashkin, J. S. Tsai. Coherent control of macroscopic quantum states in a single-cooper-pair box. Nature **398**, 786-788 (1999).

[96] Z. Zimborás, M. Faccin, Z. Kádár, J. Whitfield, B. Lanyon, J. Biamonte. Quantum transport enhancement by time-reversal symmetry breaking. Scientific Reports **3**, 2361 (2013).